Multi-scale 4D imaging of fault zone environments

Yehuda Ben-Zion, University of Southern California
with A. Allam, D. Zigone, G. Hillers, M. Campillo, P. Roux, Z. Peng, M. Lewis, C. Wu and others

Frequency	**Mhz-kHz**	**10000-100Hz**	**250-0.0001Hz**	**10Hz-1Hz**	**1-0.01Hz**
Domain	Laboratory acoustics	Underwater acoustics	**Crustal seismic imaging**	Seismic imaging	Seismology-large scale
Applications	NDT Monitoring	Tomography Source detection	**Structure of shallow layers Geotechnical applications, land slides, fault zones** **Monitoring** **Earthquake processes, FZ rheology, dynamic stress fields –> seismic hazard**	Natural resources Natural hazards Monitoring	Structure of the Earth, Earthquake risk zonation, Monitoring
Wave type	Acoustic/elastic waves	Acoustic waves	**Elastic waves (nonlinearities), strong attenuation (e.g., Q~10), strong heterogeneities**	Elastic waves	Elastic waves

Outline

- Introduction
- Observational results based on multiple signals and techniques
- Conclusions and future prospects

Multi-scale 4D imaging of fault zone environments

Why image fault zones?

- Derivation of earthquake source properties.
- Evolutionary processes on long (tectonic) and short (e.g., precursory) timescales.
- Static/dynamic stress fields (e.g. from internal structure).
- Brittle rock rheology (e.g. from observing & monitoring rock damage).
- FZs control crustal fluid flow: hydrology, oil, sub-surface storage, etc.
- Elements of FZ structure (bimaterial interfaces and damage zones) can control future (and reflect past) earthquake rupture properties.

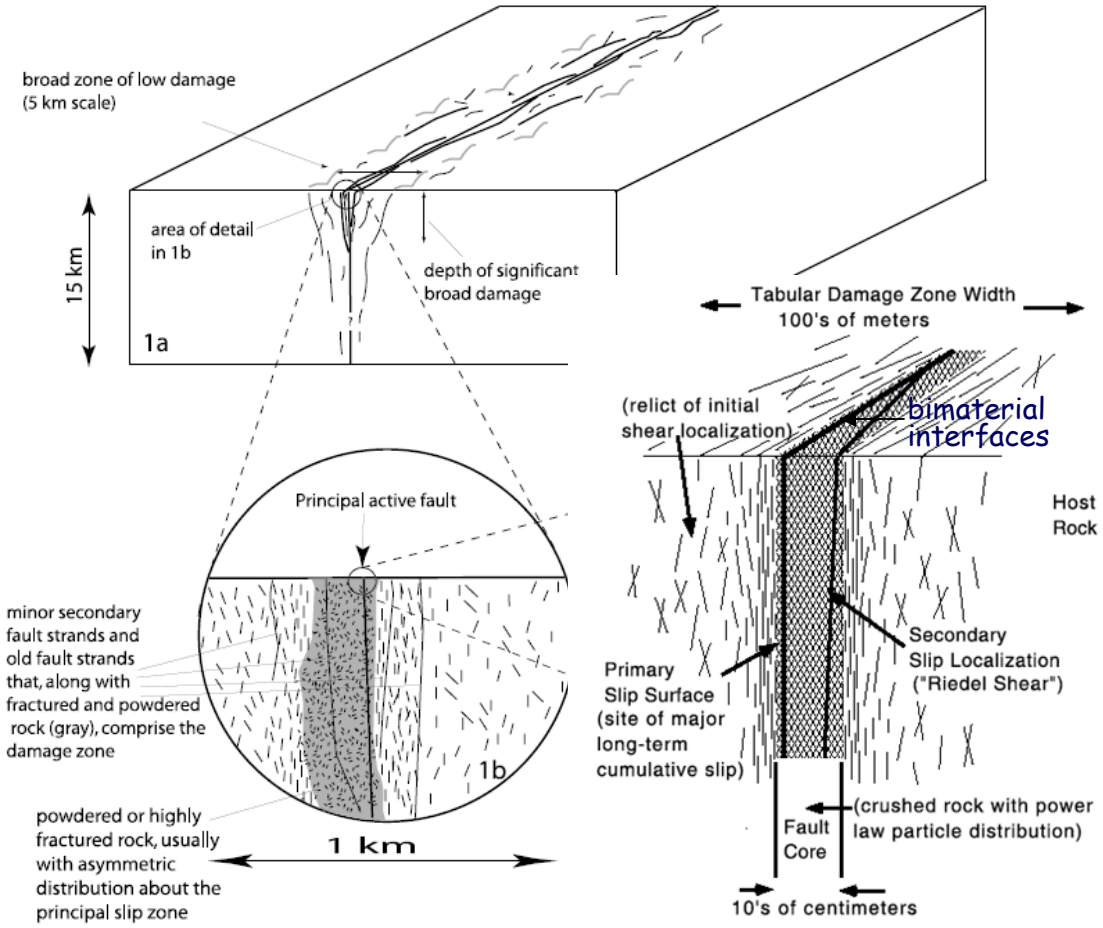

Ben-Zion and Sammis (2003)
Rockwell and Ben-Zion (2007)

Aside: Dynamic rupture on a bimaterial interface

1957 rupture, Gobi-Altai fault, Mongolia

S. Marco (pers. comm.)

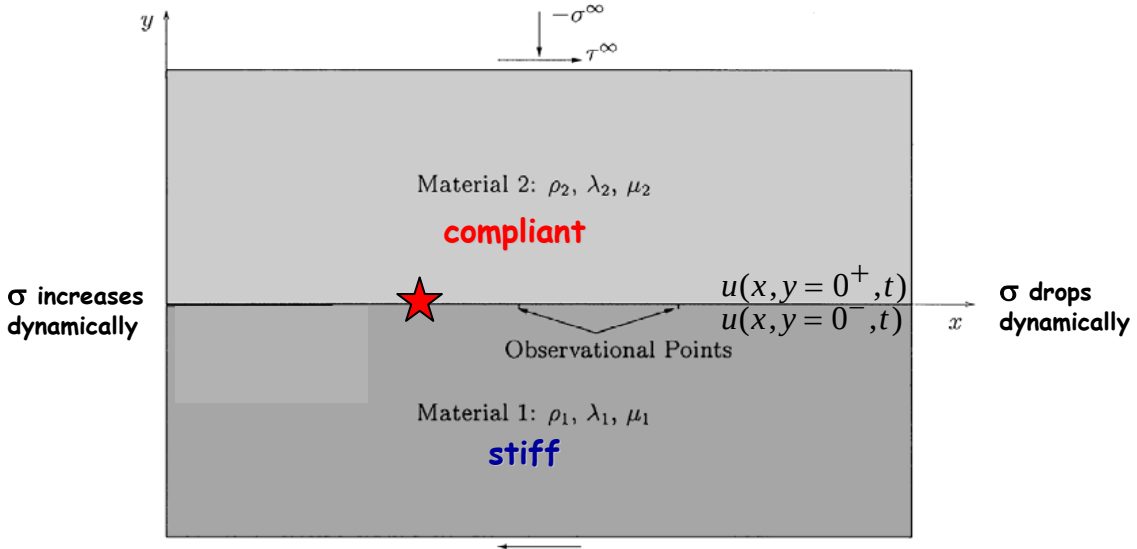

Andrews & Ben-Zion (1997)

Weertman (1980): 2D analytical solution for steady state mode II slip pulse on a frictional bimaterial interface

In-plane slip: δ = u+ − u-

Moving coordinate system: $\xi = x - ct$

Dislocation density: $B(\xi) = -d\delta/d\xi$

Dynamic shear stress: $\tau(\xi) = \tau^\infty + \frac{\bar{\mu}(c,\Delta\beta)}{\pi}\int_{-\infty}^{\infty}\frac{B(\xi')}{\xi-\xi'}d\xi'$

Dynamic normal stress: $\sigma(\xi) = \sigma^\infty - \mu^*(c,\Delta\beta)B(\xi)$

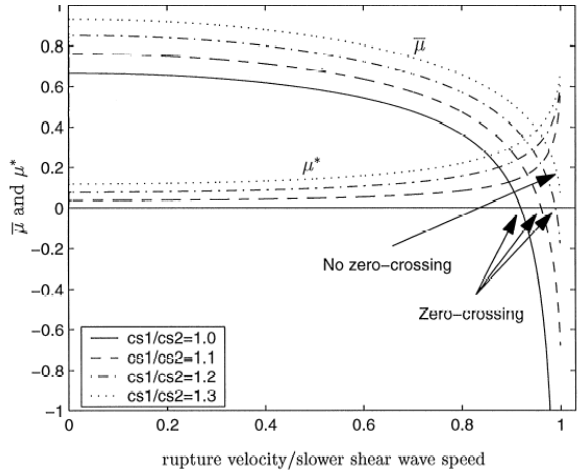

- In a homogeneous solid $\mu^* = 0$; there is no coupling between slip and σ.
- For subsonic rupture on a bimaterial interface in the direction of motion of the compliant solid, $\mu^* > 0$ and σ drops dynamically (producing local dilation).
- In the opposite direction, $\mu^* < 0$ and σ increases dynamically (local compression).

Wrinkle-like rupture on a bimaterial interface (Andrews and Ben-Zion, 1997)

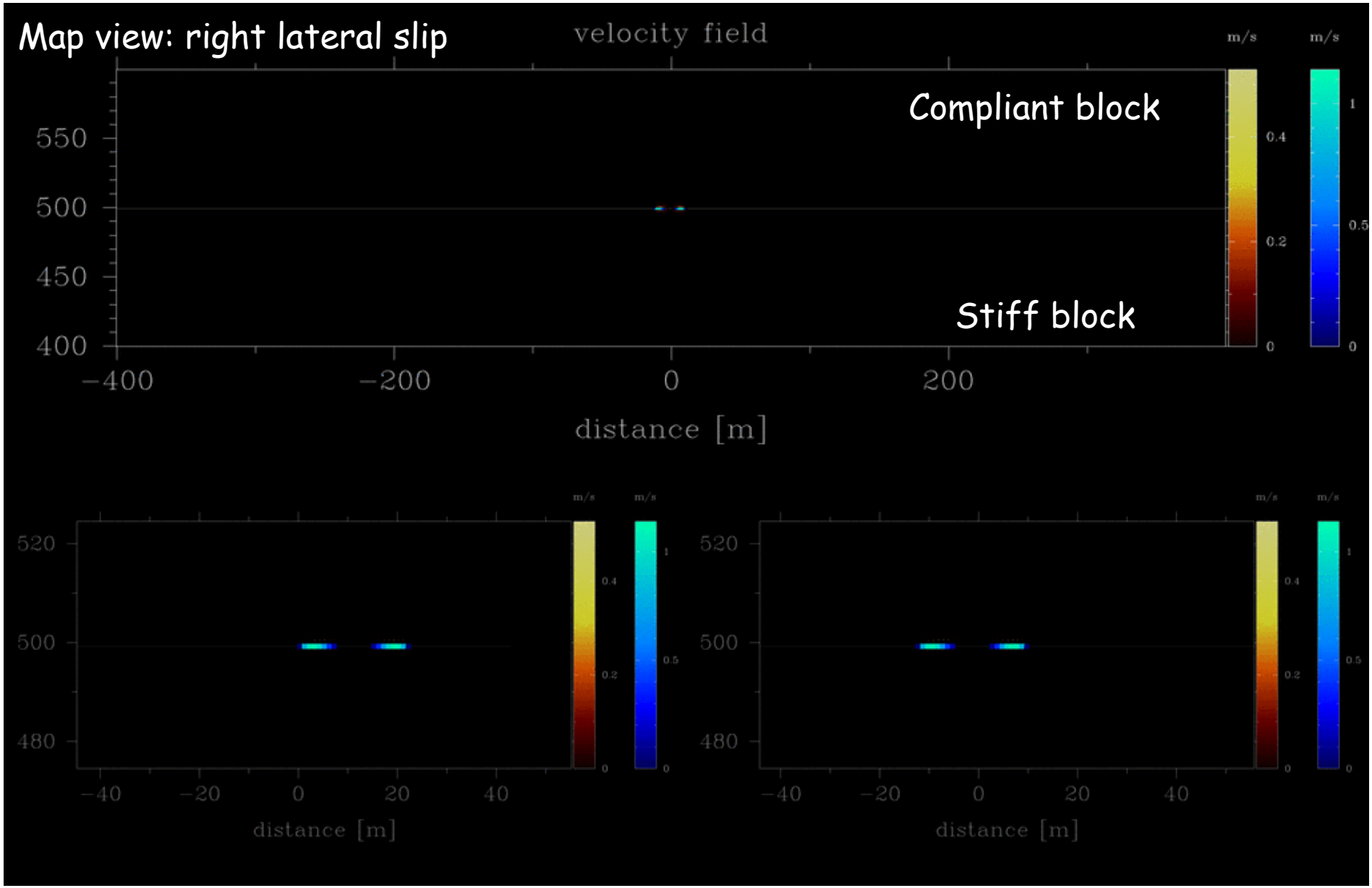

Wrinkle-like rupture on a bimaterial interface

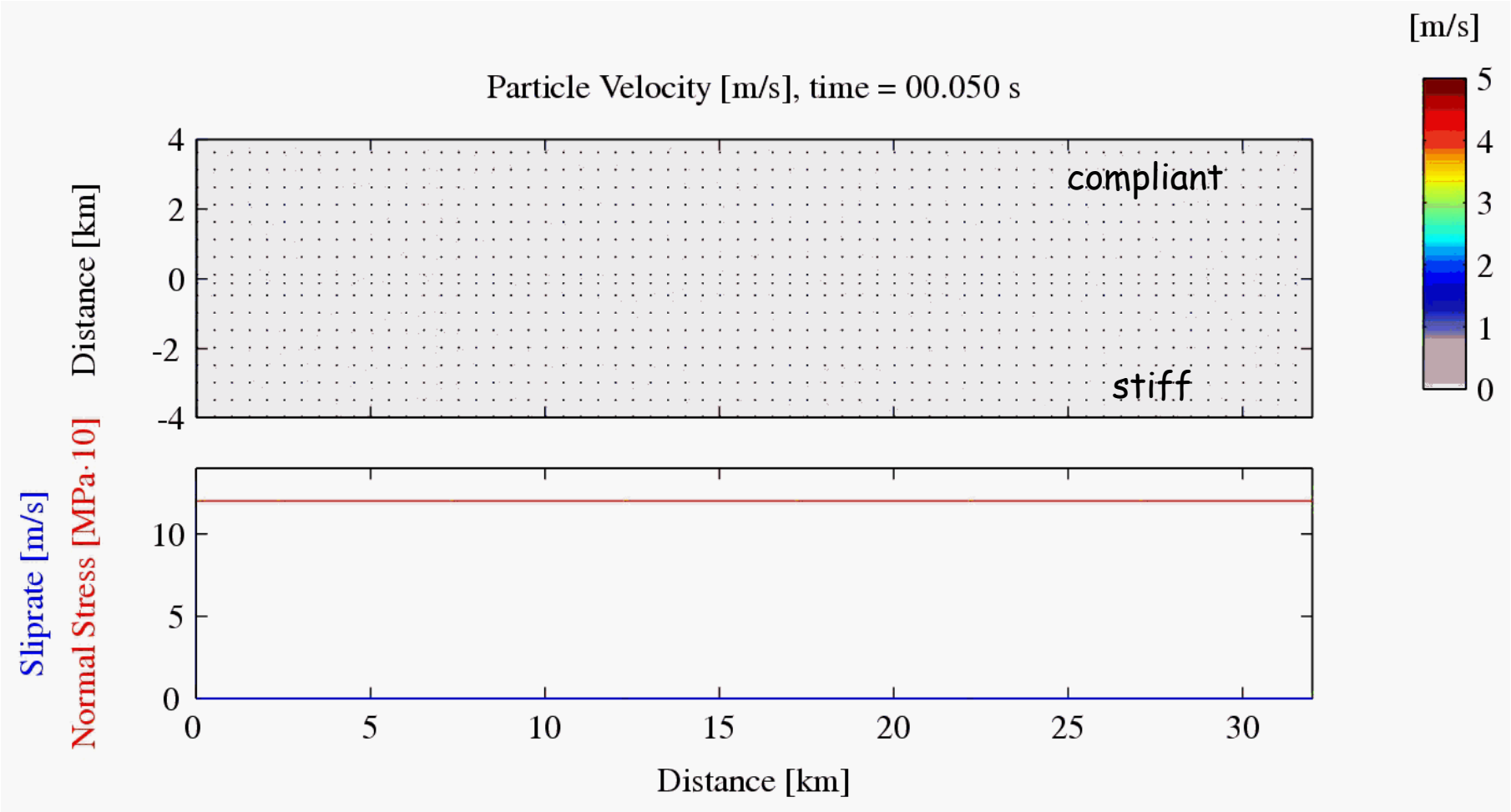

Wrinkle-like rupture pulse

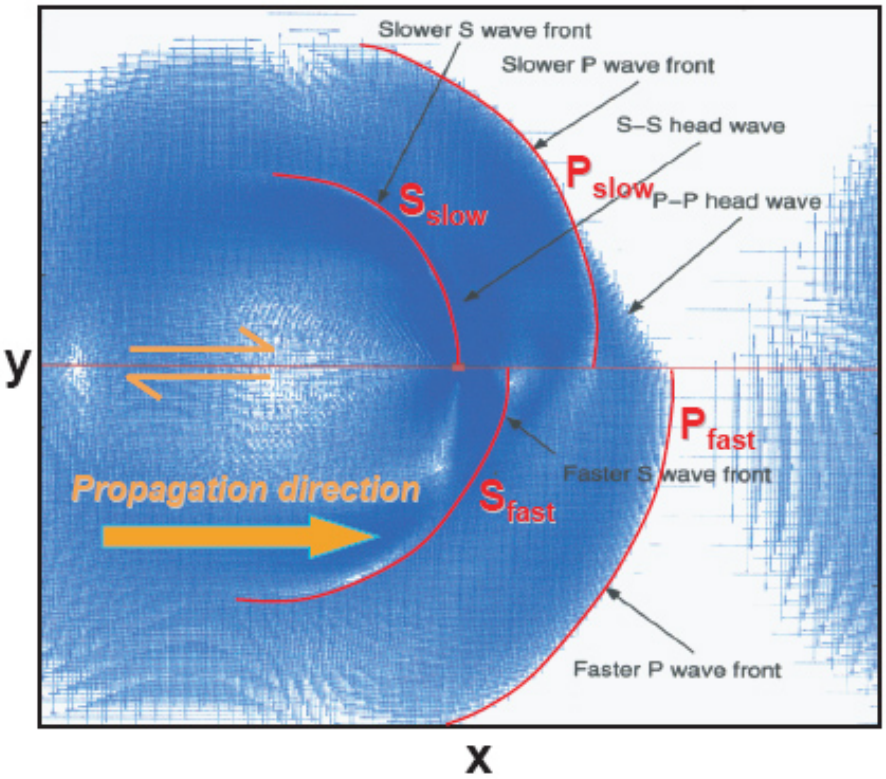

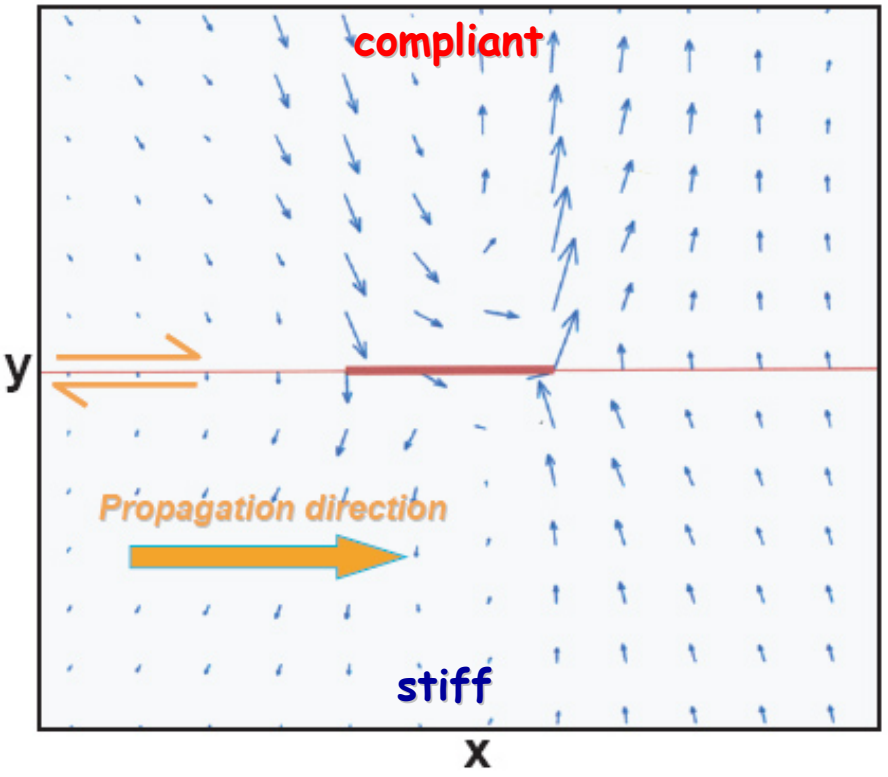

Andrews and Ben-Zion, 1997; Ben-Zion and Andrews, 1998; Cochard and Rice, 2000; Ben-Zion, 2001; Ben-Zion and Huang, 2002, Shi and Ben-Zion, 2006, Ampuero and Ben-Zion, 2008; Brietzke et al., 2009

Rupture Directivity and Ground Motion

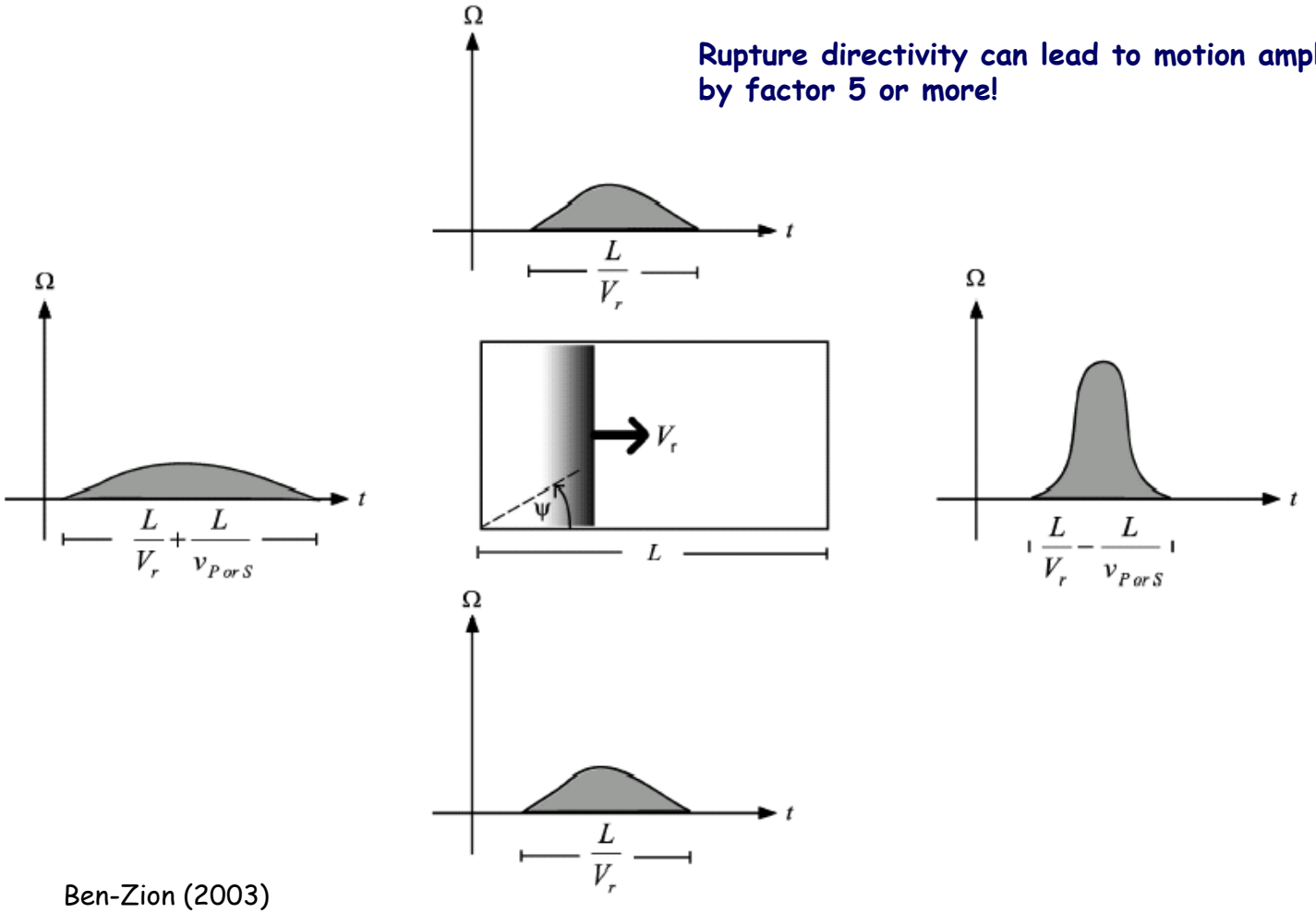

Rupture directivity can lead to motion amplification by factor 5 or more!

Ben-Zion (2003)

TeraShake simulations of M7.7 earthquake on Southernmost San Andreas (Olsen et al. 2006)

Rupture Directivity and Ground Motion

Rupture directivity can lead to motion amplification by factor 5 or more

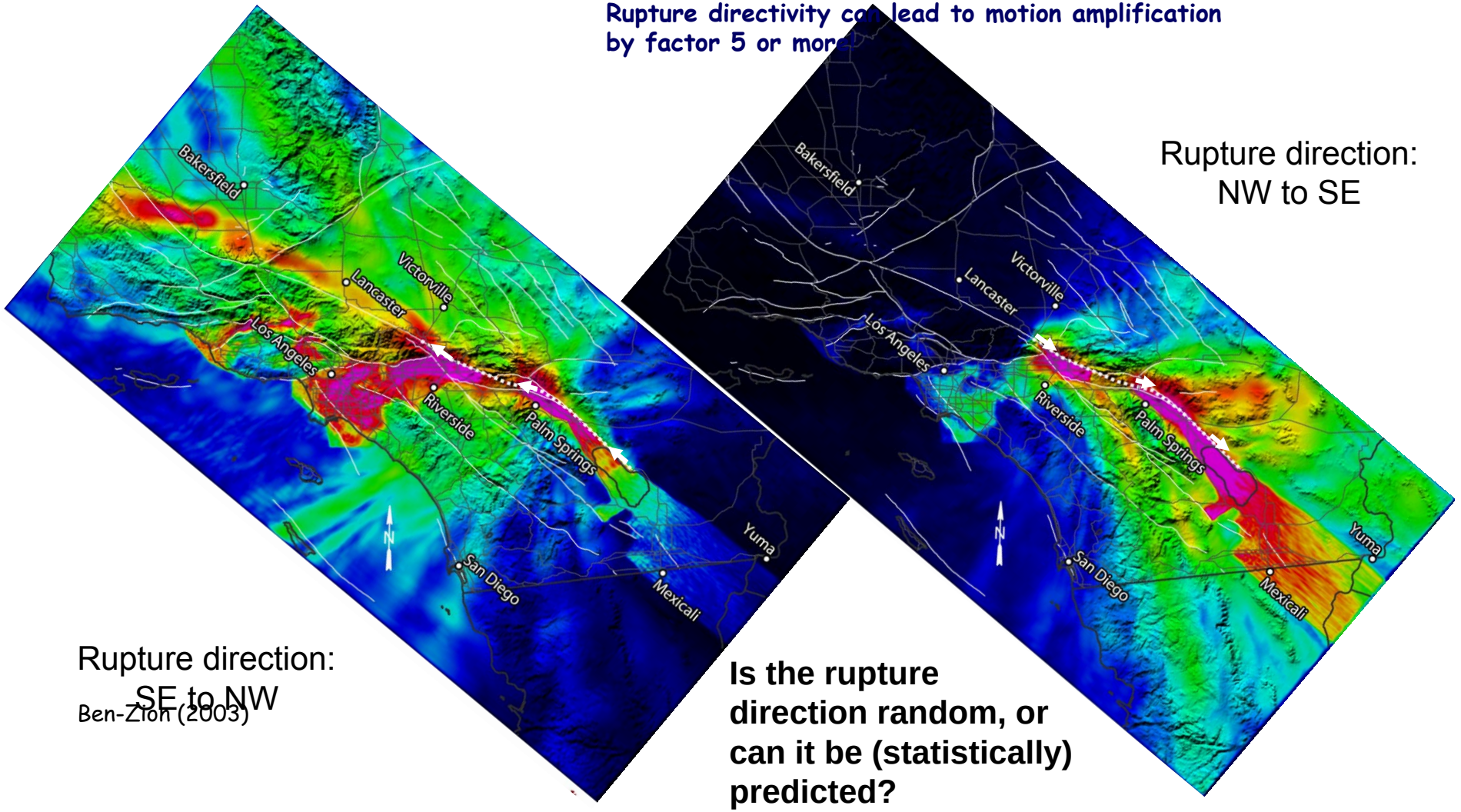

Rupture direction:
NW to SE

Rupture direction:
SE to NW

Ben-Zion (2003)

Is the rupture direction random, or can it be (statistically) predicted?

TeraShake simulations of M7.7 earthquake on Southernmost San Andreas (Olsen et al. 2006)

Seismic Imaging: Data Sources

weaker damage falling ~log(x) from center of fault
strong variations along strike and with depth

Ambient Noise

- Weak diffuse waveforms (typical frequencies < 1 hz)
- Available in all space-time domains (not masked by earthquake waveforms)
- Considerable stacking needed
- Time resolution relatively low (e.g. > 1 day)
- Space resolution > 10-100m
- High sensitivity to shallow structure
- Good for imaging fault zones in interseismic periods (and other environments)

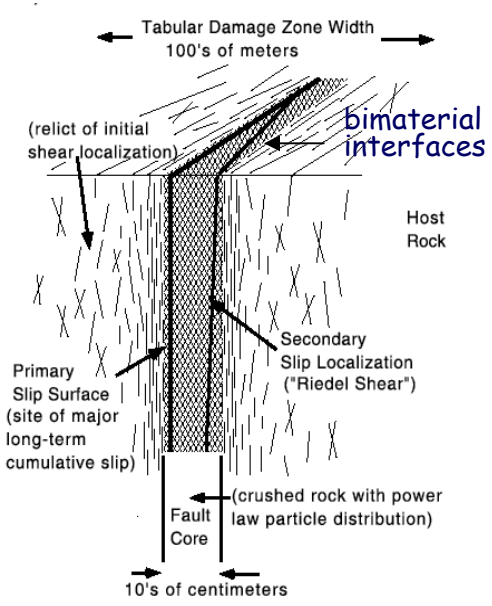

Earthquake Seismograms

- Correlated waveforms (with Green function up to e.g. 10-100Hz)
- Available close in space-time to earthquakes/faults (aftershock rates: $dN/dt \sim 1/t^p$; foreshocks)
- Stacking helps but not essential
- Time resolution limited by event rates (~1 sec with aftershocks)
- Space resolution down to an interface
- High sensitivity to seismogenic zone
- Good for imaging active fault zones close to large E/q. times

Analyzing seismograms with earthquake and noise signals combines the best from both

Imaging Techniques

- **Modeling travel times**

-Infinitely thin rays & Snell's law. Simple, wide applicability

-Use/get limited information

-Reduction of cell size increases the number of empty cells (holes in the image)

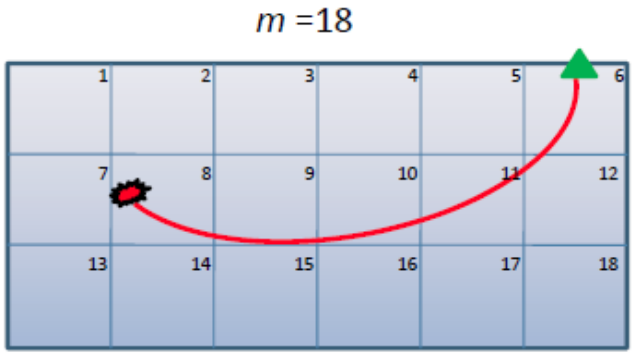

Shearer 2009

- **Modeling waveforms**

-Finite size wave fronts. More involved but use/get more information.

-Empty cells not a problem.

Highest nominal resolution $\lambda/2$

Can get (much) higher resolution using waves generated by / propagate along interfaces (e.g., fault zone head waves)

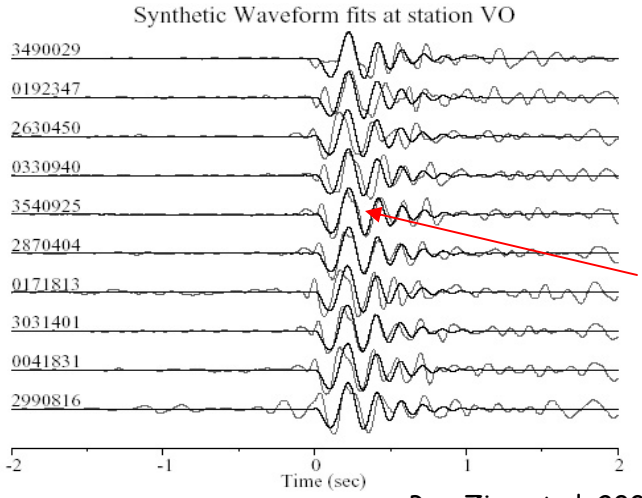

Ben-Zion et al. 2003

Following slides – Seismic imaging

- **Results from the San Jacinto, San Andreas, Hayward, and North Anatolian faults**
- **Earthquake travel time tomography**
- **Ambient seismic noise imaging**
- **Travel time and waveform analyses of fault zone (guided) head and trapped waves**
- **High resolution temporal changes of seismic velocities based on earthquake data**

Seismic Velocity Structures in the Southern California Plate Boundary Environment from Double-difference Tomography (Allam and Ben-Zion, GJI, 2012)

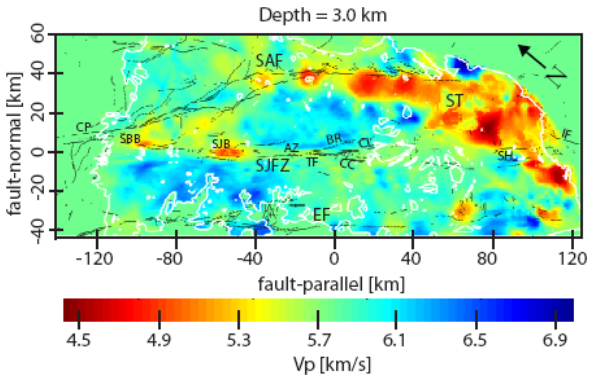

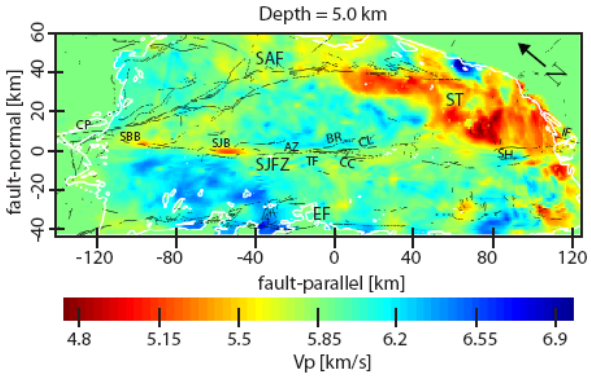

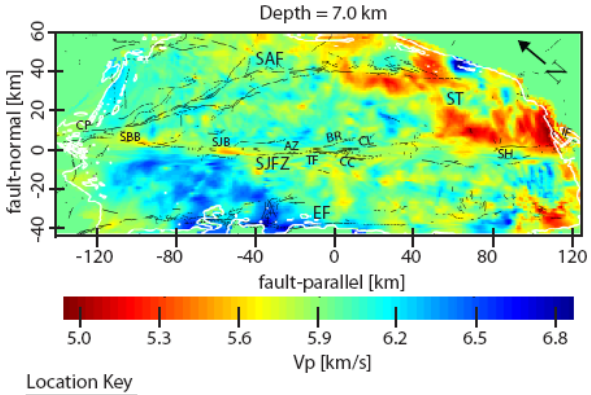

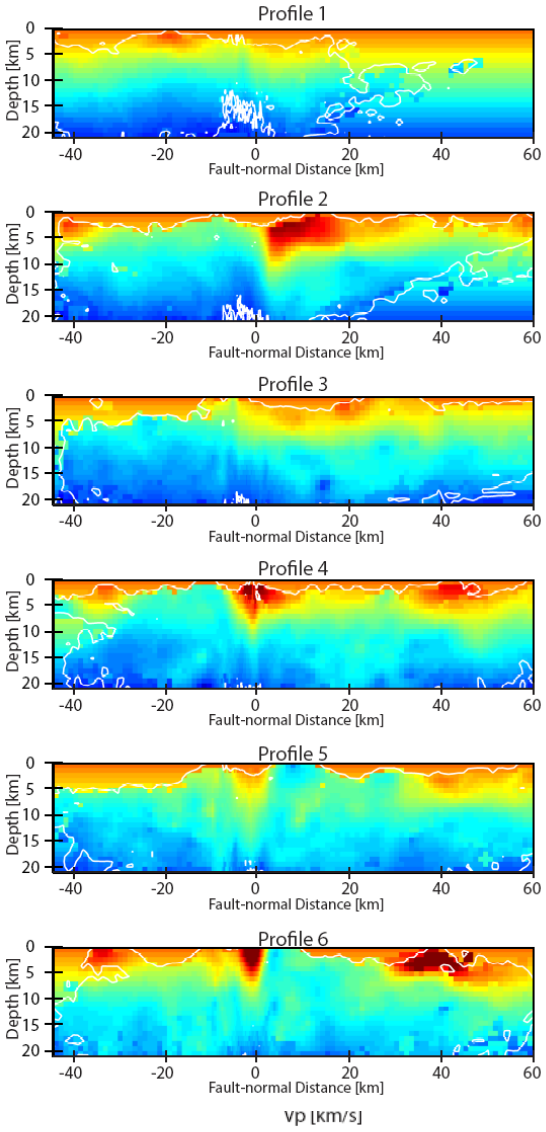

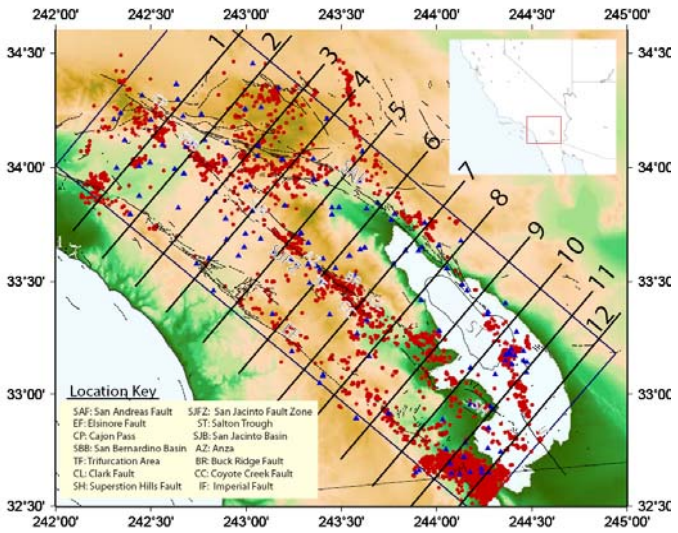

Location Key

SAF: San Andreas Fault SJFZ: San Jacinto Fault Zone EF: Elsinore Fault ST: Salton Trough CP: Cajon Pass SBB: San Bernardino Basin
SJB: San Jacinto Basin AZ: Anza TF: Trifurcation Area BR: Buck Ridge Fault CL: Clark Fault
CC: Coyote Creek Fault SH: Superstion Hills Fault IF: Imperial Fault

- 5493 earthquakes (2000-2011)
- 139 stations
- 360,000 *P*- and *S* arrival times
- grid cell size: 1km
- white contours > 10 rays/cell

central section

- Prominent generally in top 5 km

- Follow overall "flower" shape with depth

- Larger reductions of Vs (up to 40% in top 3-5 km) than Vp

Velocity contrasts along sections of the SJFZ

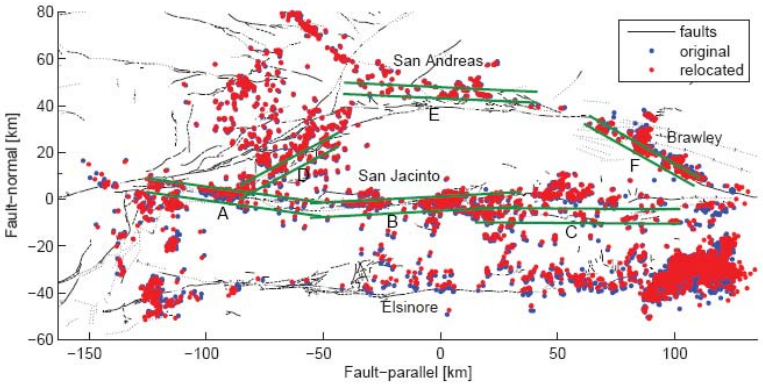

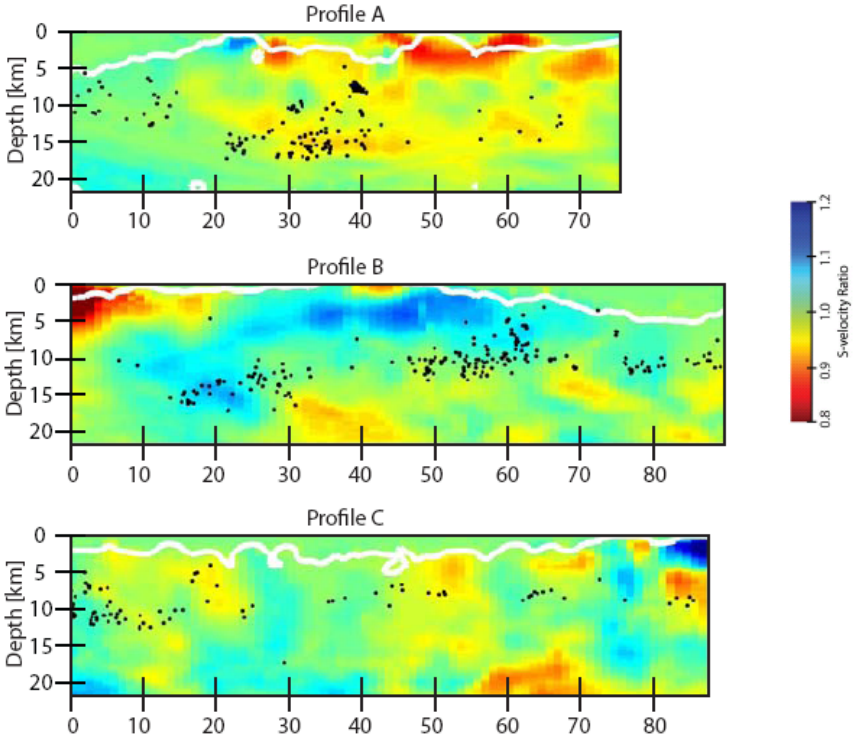

Profile B along the central SJFZ has significant velocity contrast (up to 20%) with NE side fast.

Profile C from the trifurcation to the SE has smaller and less persistent contrast.

Profile A from Cajon pass to the San-Jacinto basin has mild contrast with reversed polarity (slow NE)

Comments:

- **Higher resolution (250m^3 cells) TomoDD for the trifurcation areas** (Allam, Ben-Zion, Kurzon, Vernon)
- **Good resolution between 3-15 km; poor in top 3 km.**
- **Ambient noise imaging can resolve the structures in top 3 km (coming next)**
- **Fault zone head and trapped waves provide highest resolution of bimaterial interfaces and damage zones (coming later)**

Noise based Imaging of Southern California Plate Boundary area

Dimitri Zigone, Yehuda Ben-Zion, Michel Campillo

with contributions from X. Briand, G. Hillers, P. Boué, L. Sthely, P. Roux, X. Liu

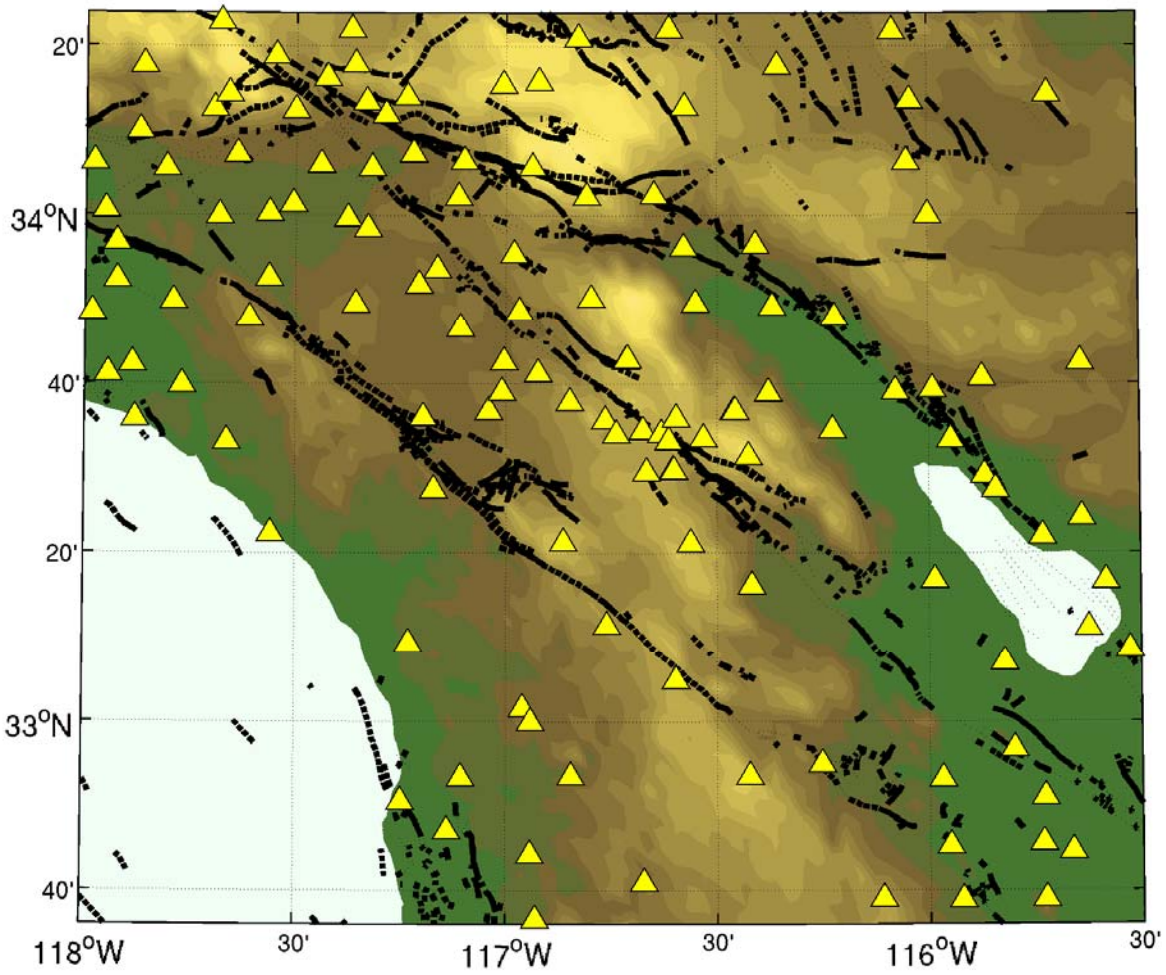

140 Stations

1 year of data
2012

Both 3 components (66%) and short period (33%) sensors

Cross-correlations : processing

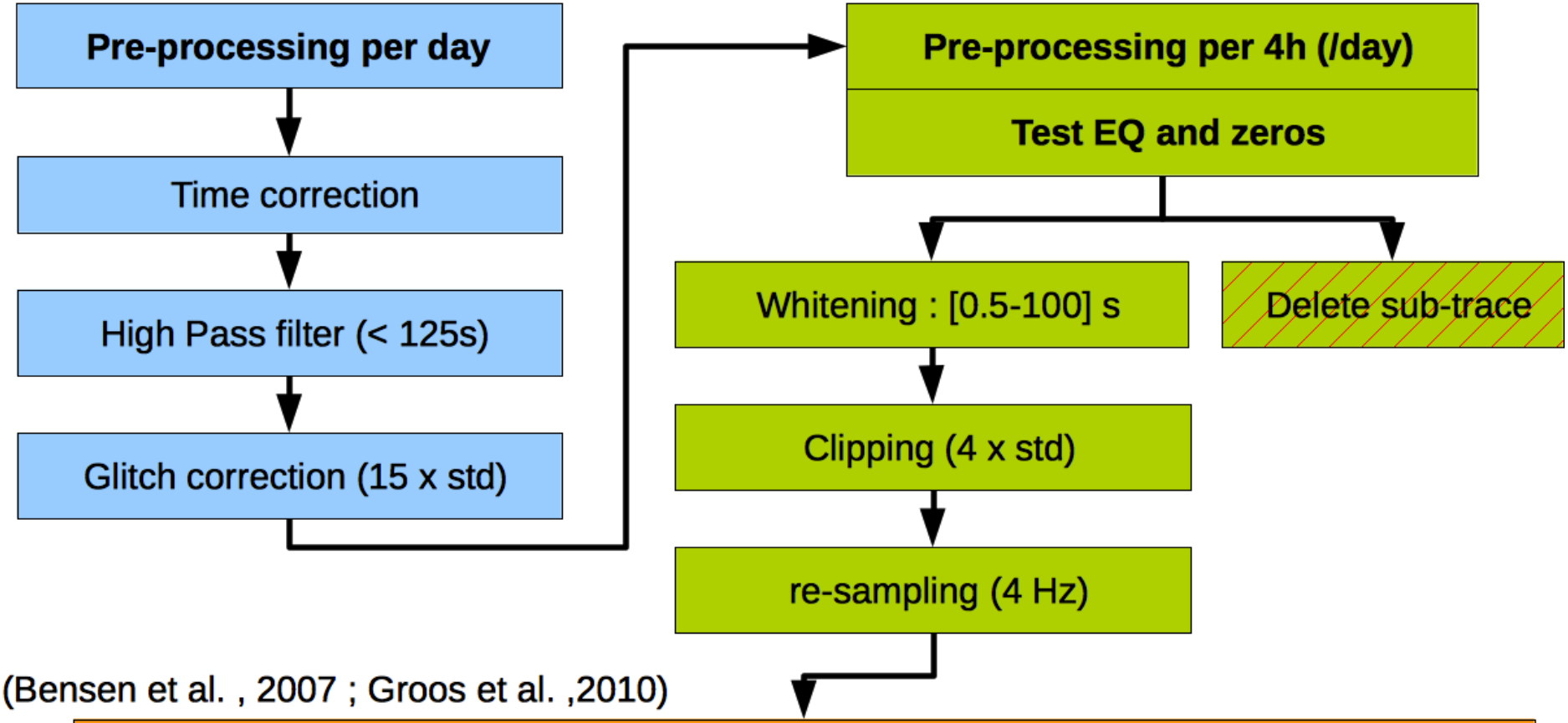

(Bensen et al. , 2007 ; Groos et al. ,2010)

Correlations per 4h (stacked per day)

9 components
Maxlag = 300 s

$$[C_{AB}(t)]_{ij} = \frac{\int_0^T S_{A,i}(\tau)\, S_{B,j}(t+\tau)\, \mathrm{d}\tau}{\sqrt{\int_0^T S_{A,i}^2(\tau)\, \mathrm{d}\tau \int_0^T S_{B,j}^2(\tau)\, \mathrm{d}\tau}}$$

Surface Waves Green's functions and Velocity Measurements

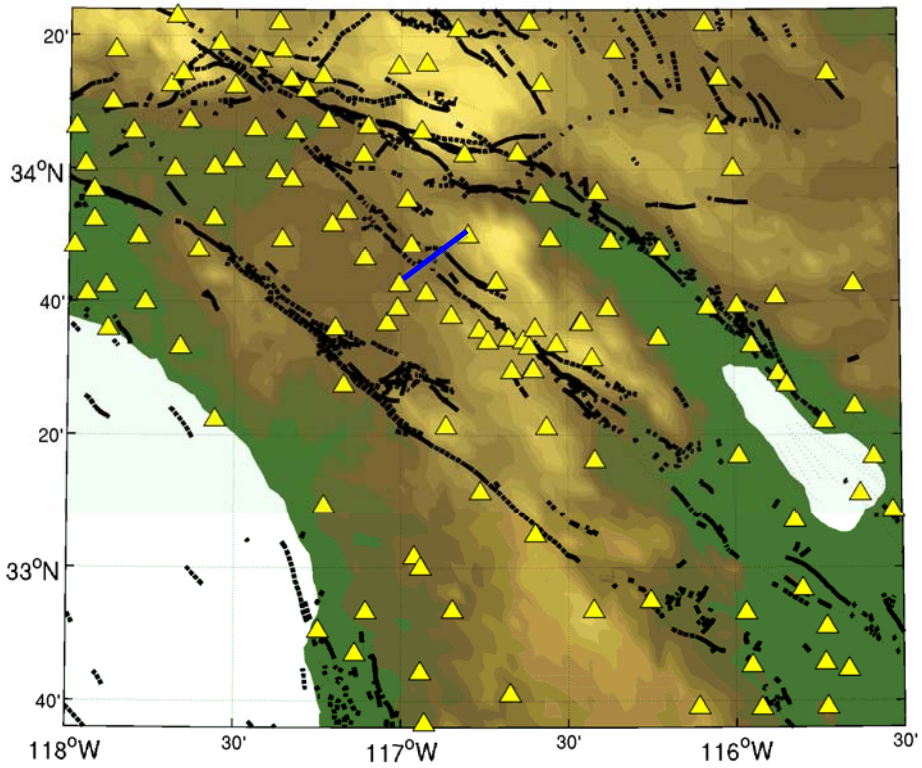

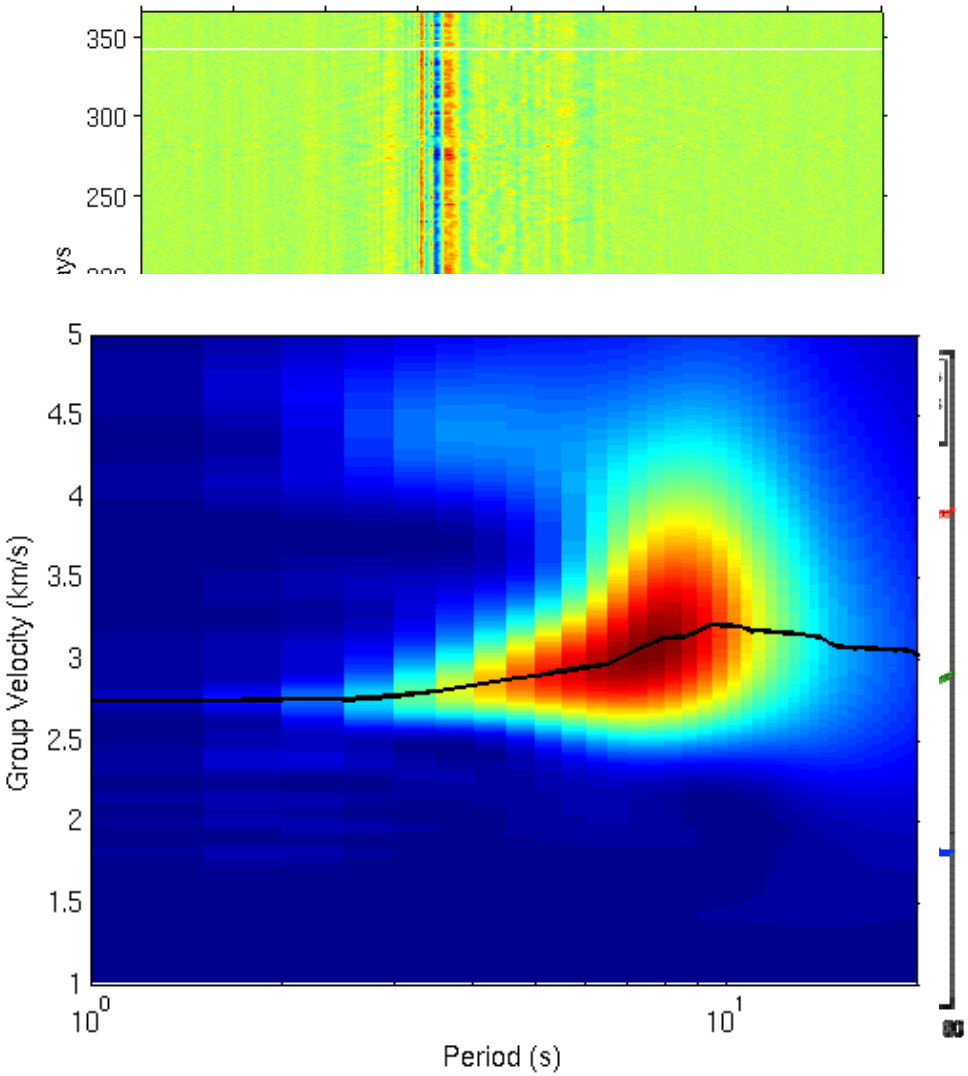

Frequency time analysis (Levshin et al, 1989)

6734 paths with SNR>10

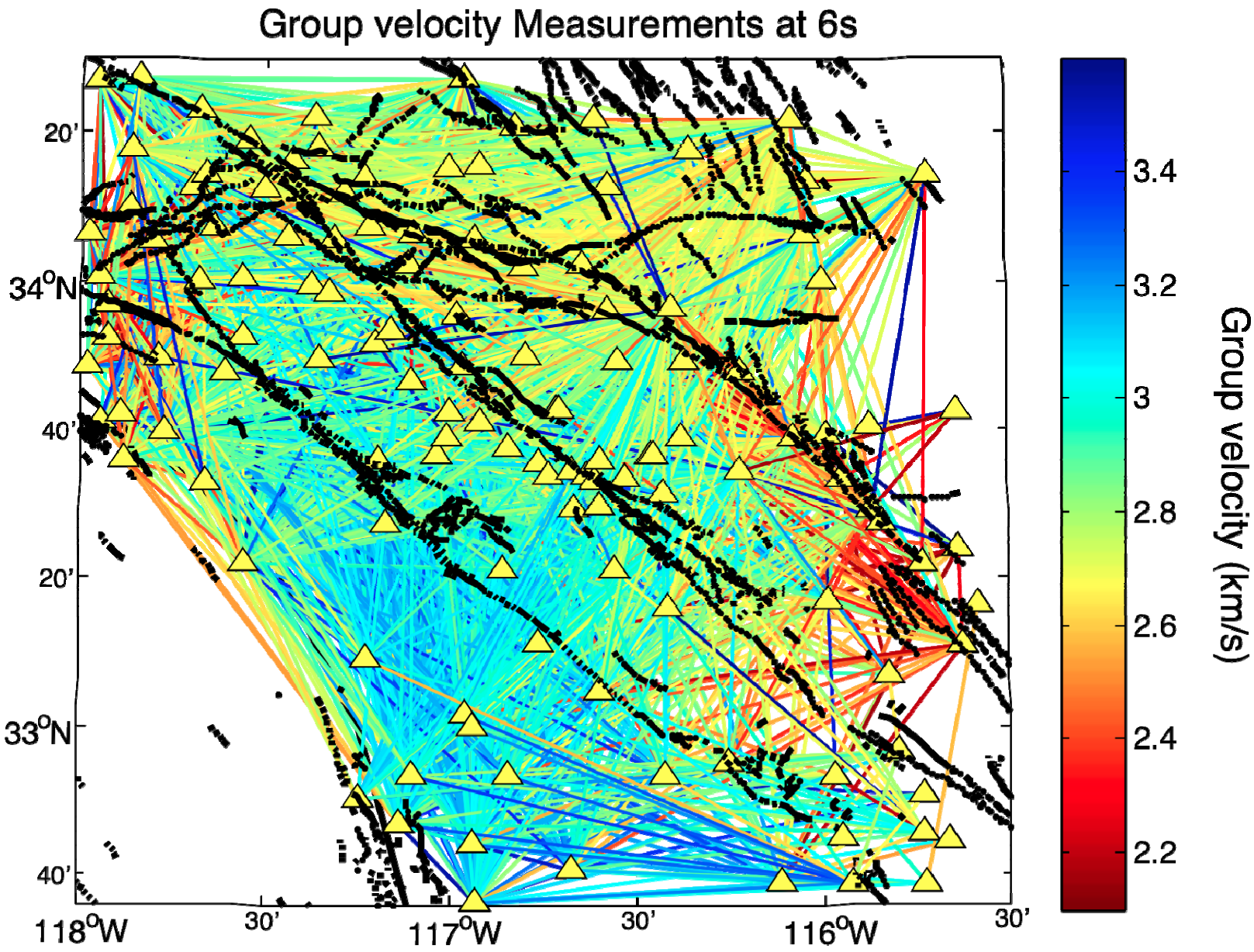

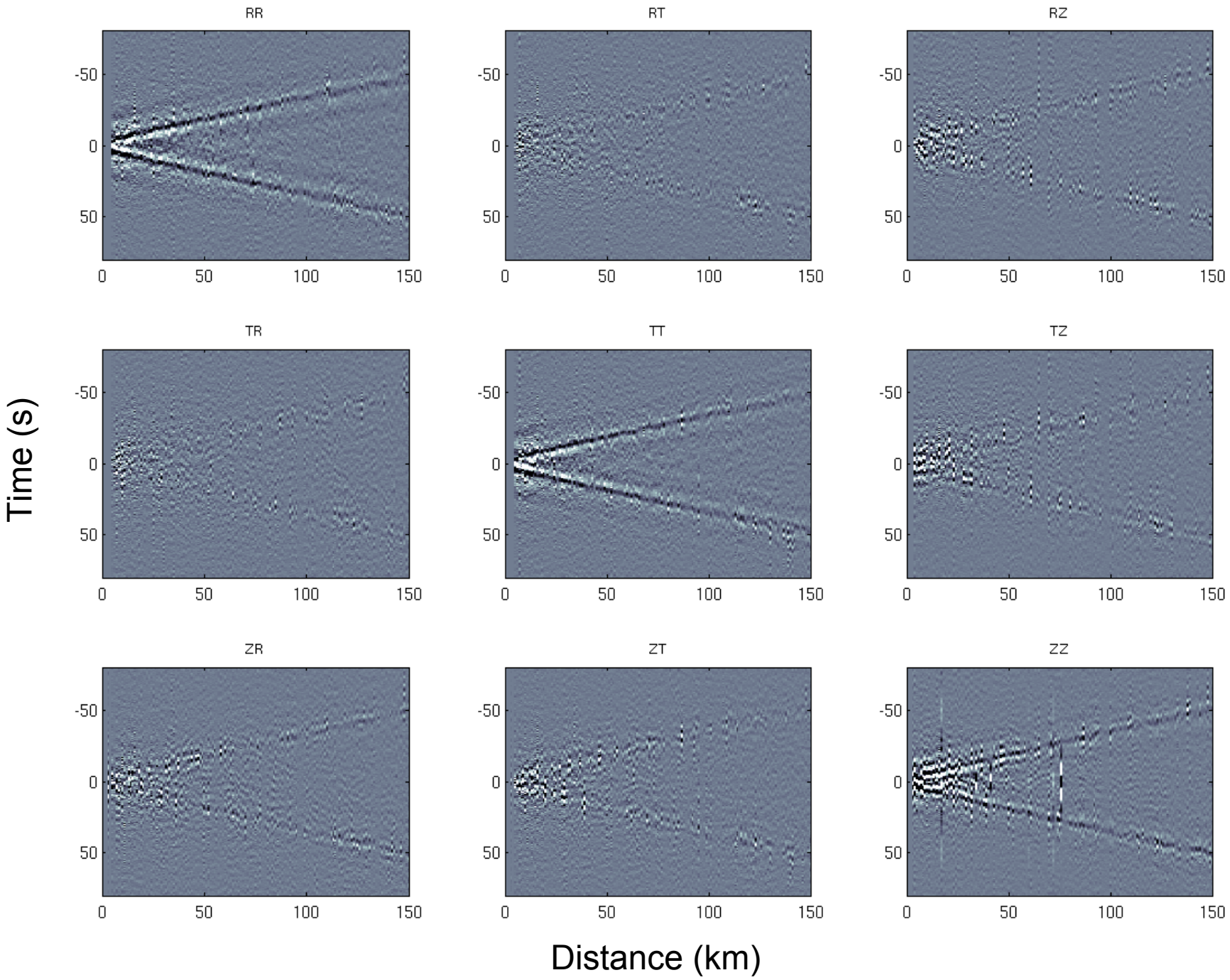
RR
RT
RZ
TR
TT
TZ
ZR
ZT
ZZ
-50
0
50
0
50
100
150
Time (s)
Distance (km)

Group Velocity Maps

- Inversion of velocity measurements from dispersion curves;
- use only cells with >3 data
- Barmin et al. (2001) procedure; 1.5 km grid

Number of paths per cell (used for weight)

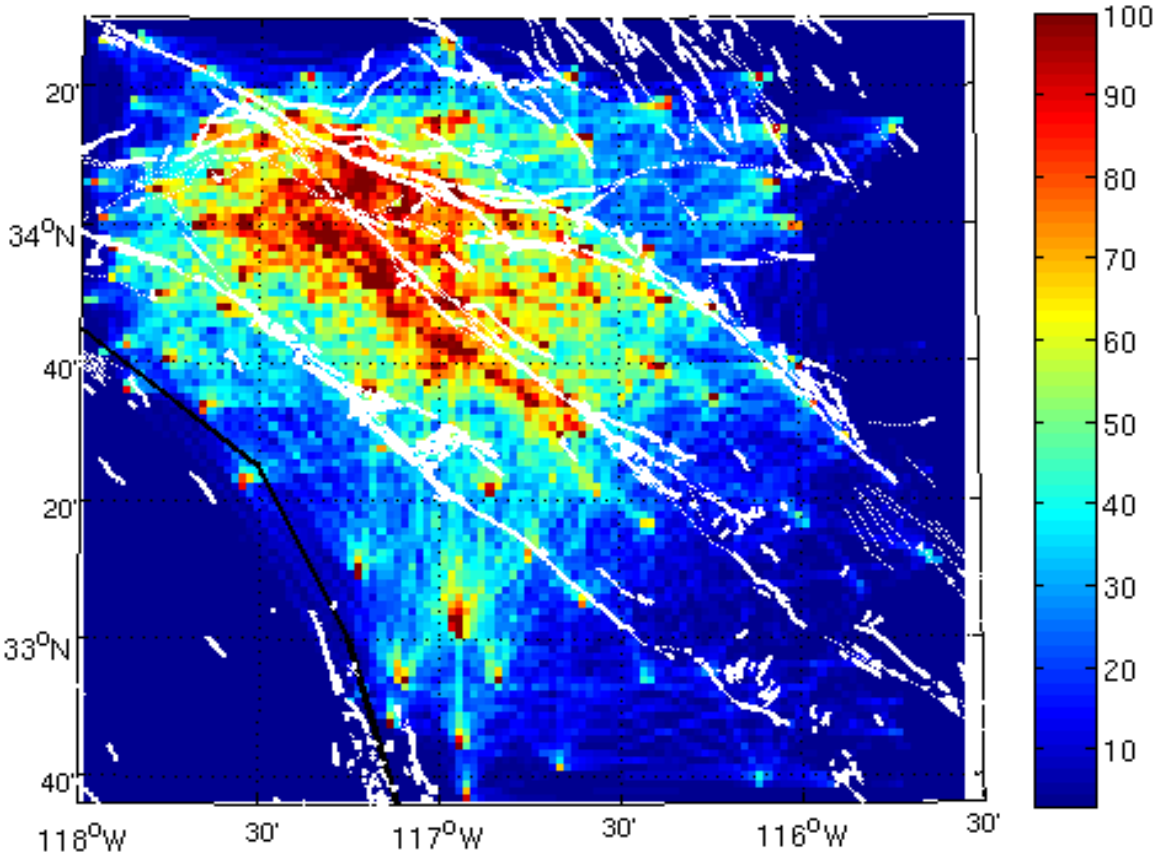

Rayleigh

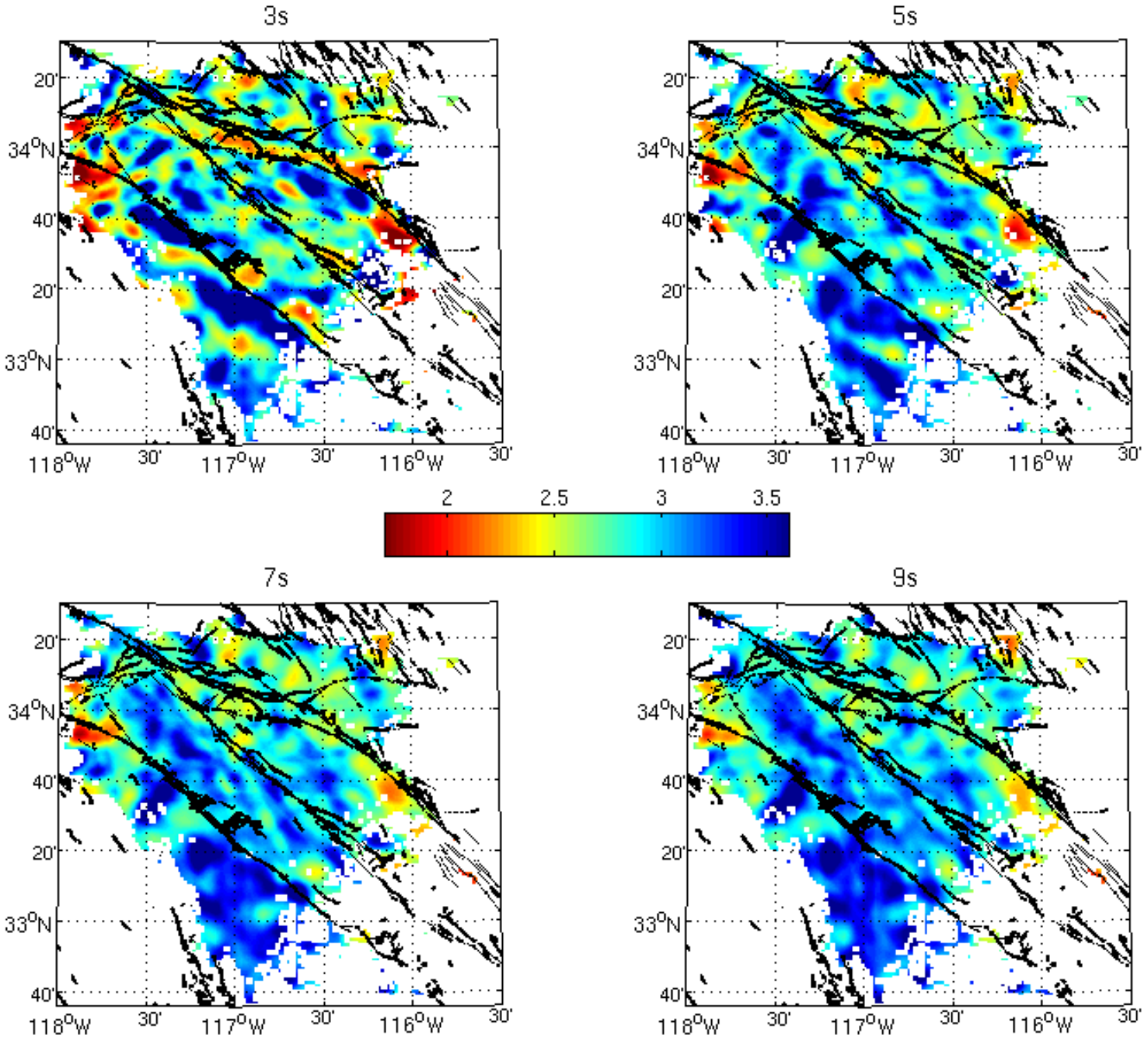

Love

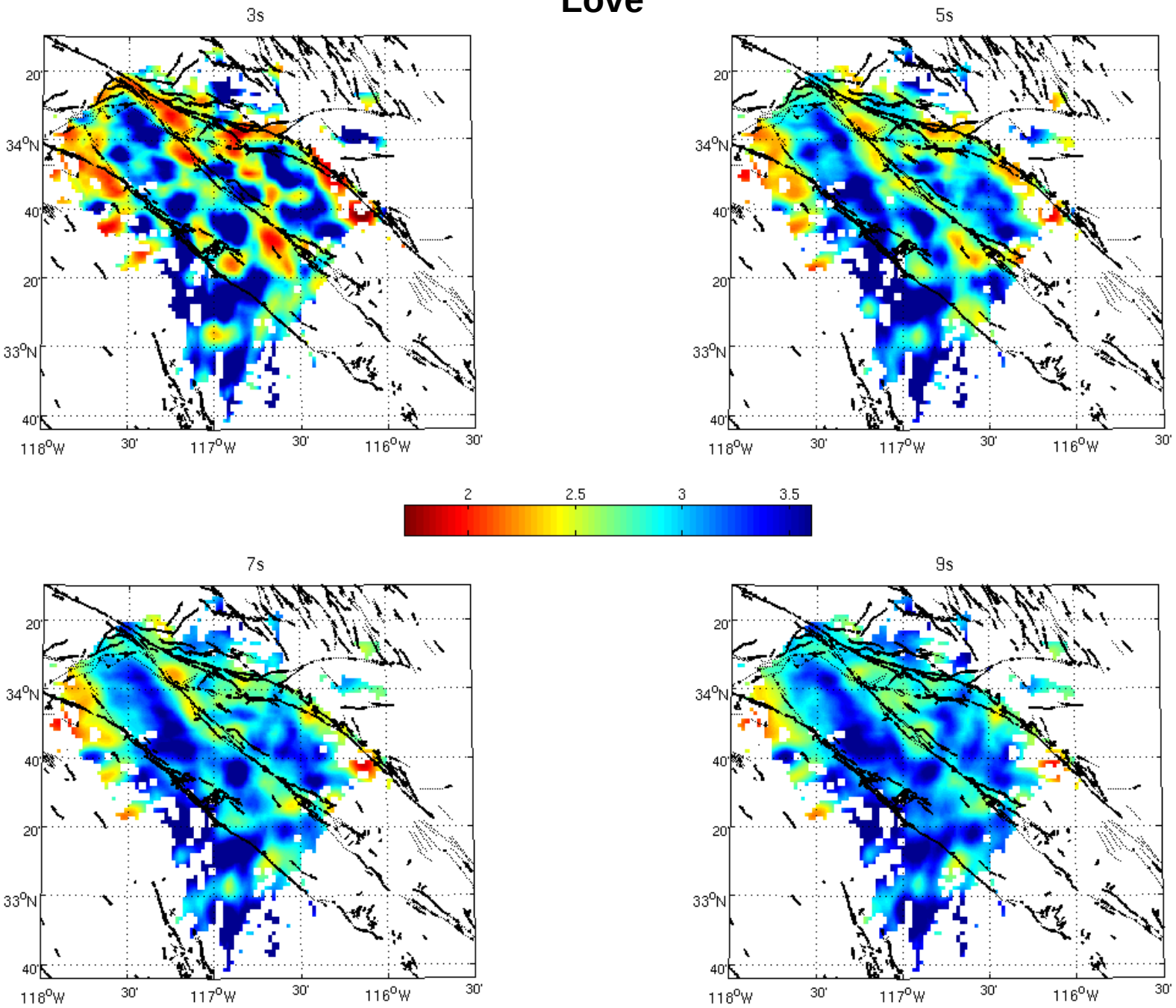

Inversion of Vs

- Linearized Inversion of Hermann and Ammon (2002)
  - 3 main steps:
    - Average dispersion curves for cells with more than 10 paths
    - Inversion of the average dispersion starting from the Allam and Ben-Zion (2012) velocity model
    - Inversion for velocity model for each cell

Average Model from Rayleigh

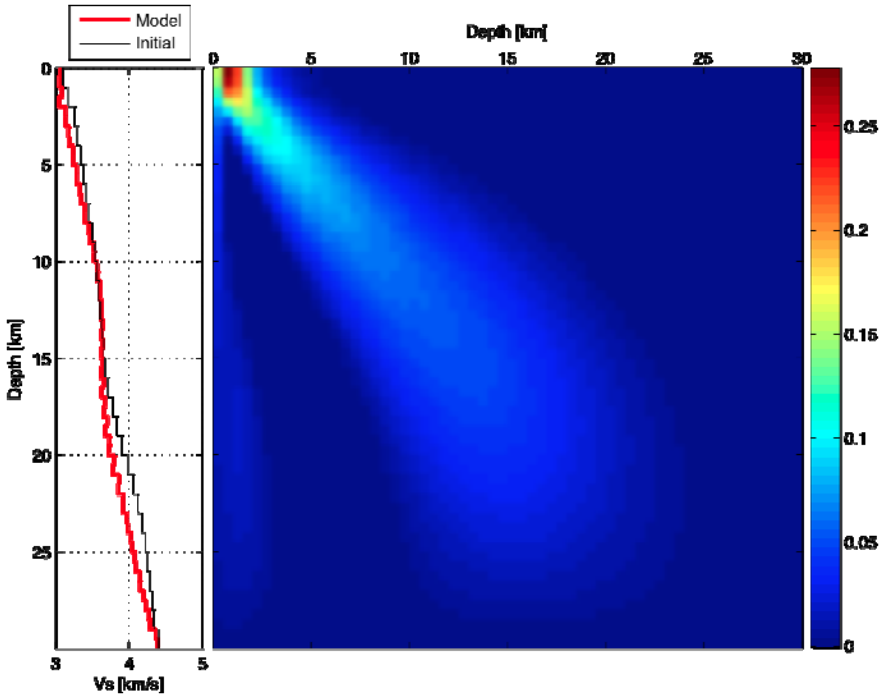

Average Model from Love

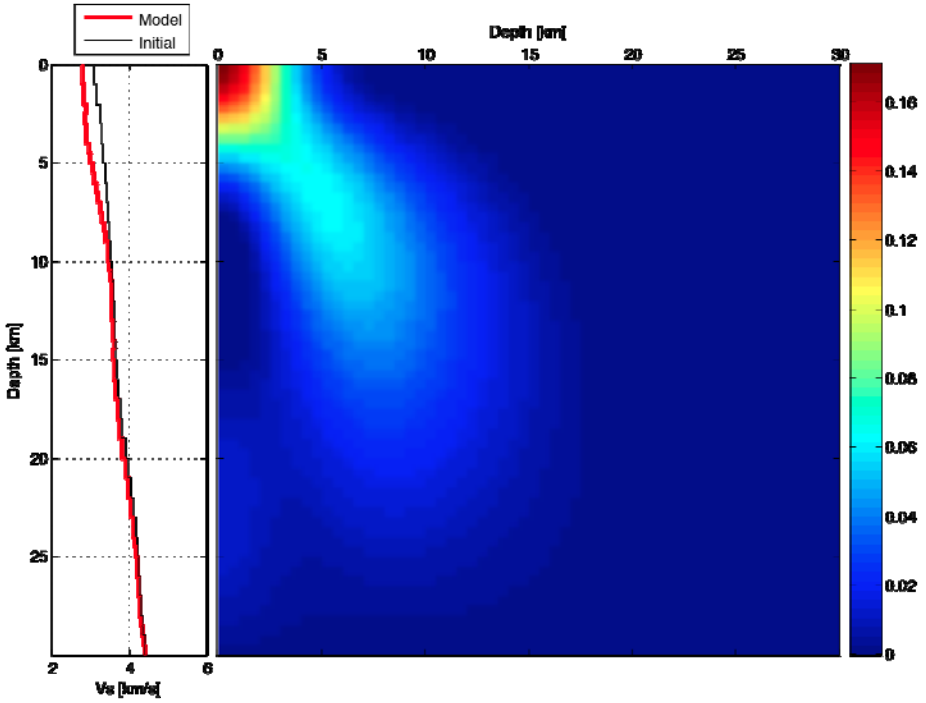

Comparison Rayleigh-Love (Average Model)

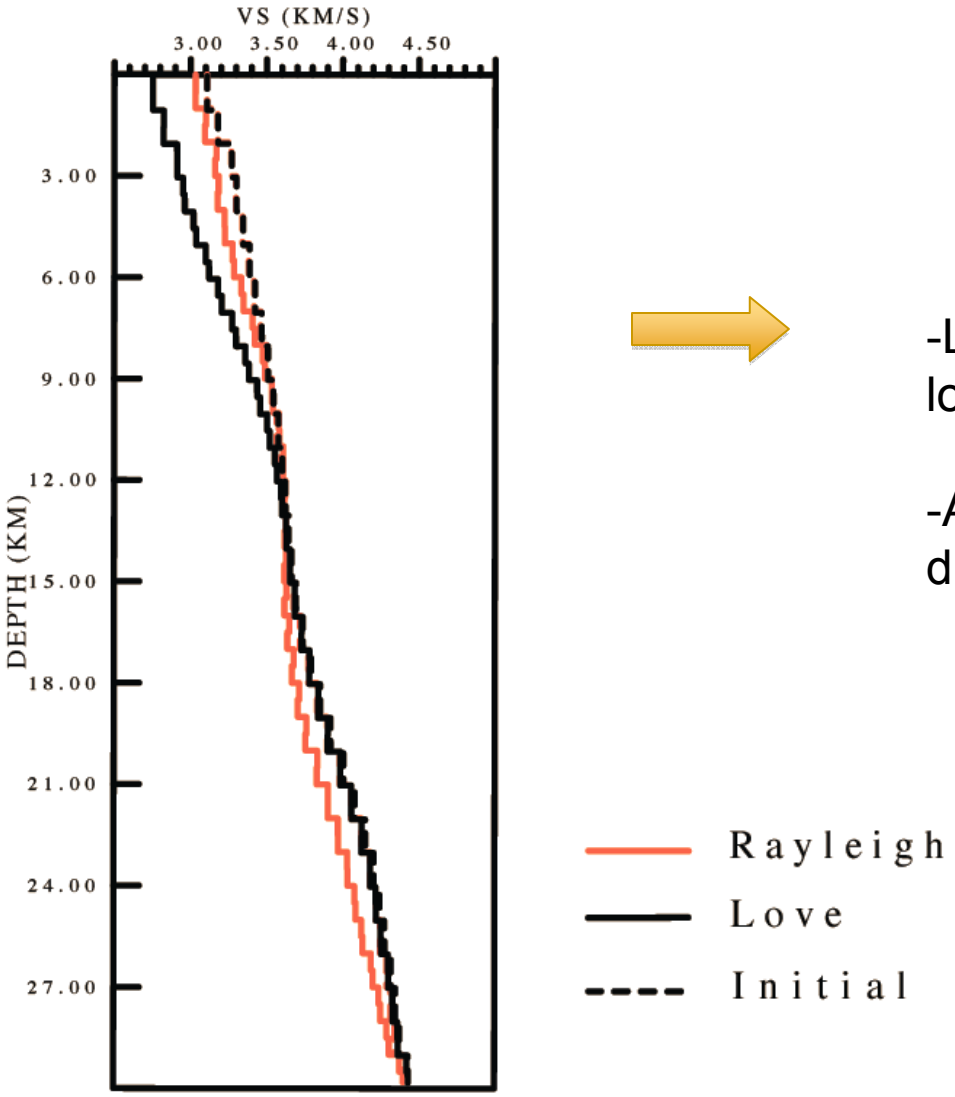

-Love waves have consistenly lower velocities

-Azimuthal Anisotropy due to the faults ?

Vs Maps

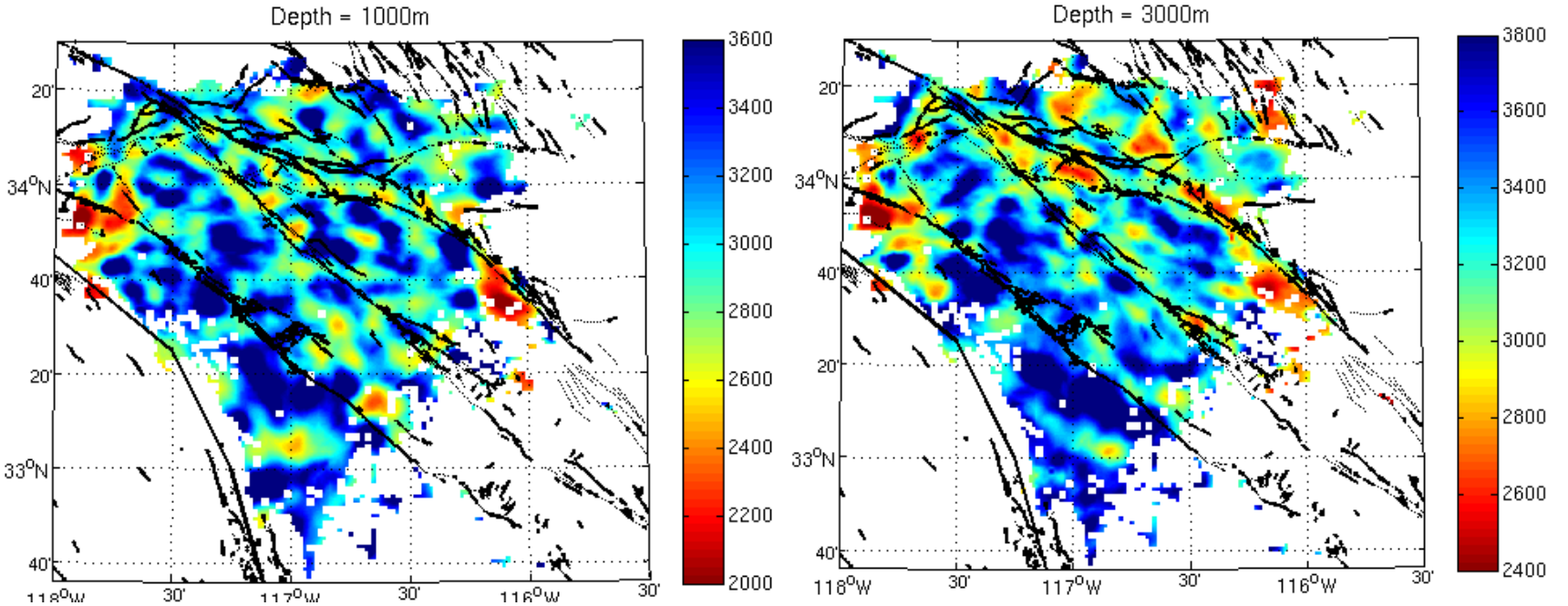

From Rayleigh waves

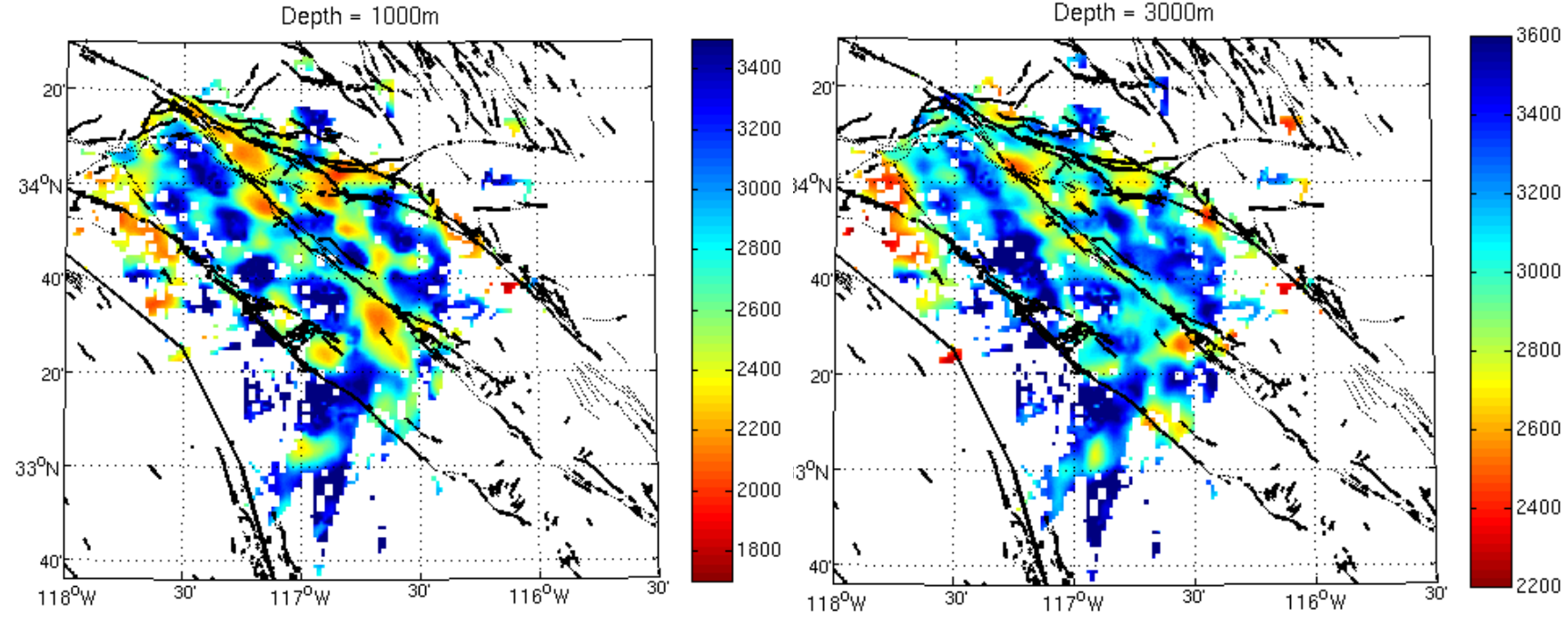

From Love waves

From Love waves

The results show flower-type damage structures in the top 3 km (connect to the deeper images of Allam & Ben-Zion 2012)

High-resolution results in the top 500-1000m can be obtained by cross correlating earthquake waveforms (work in progress with P. Roux)

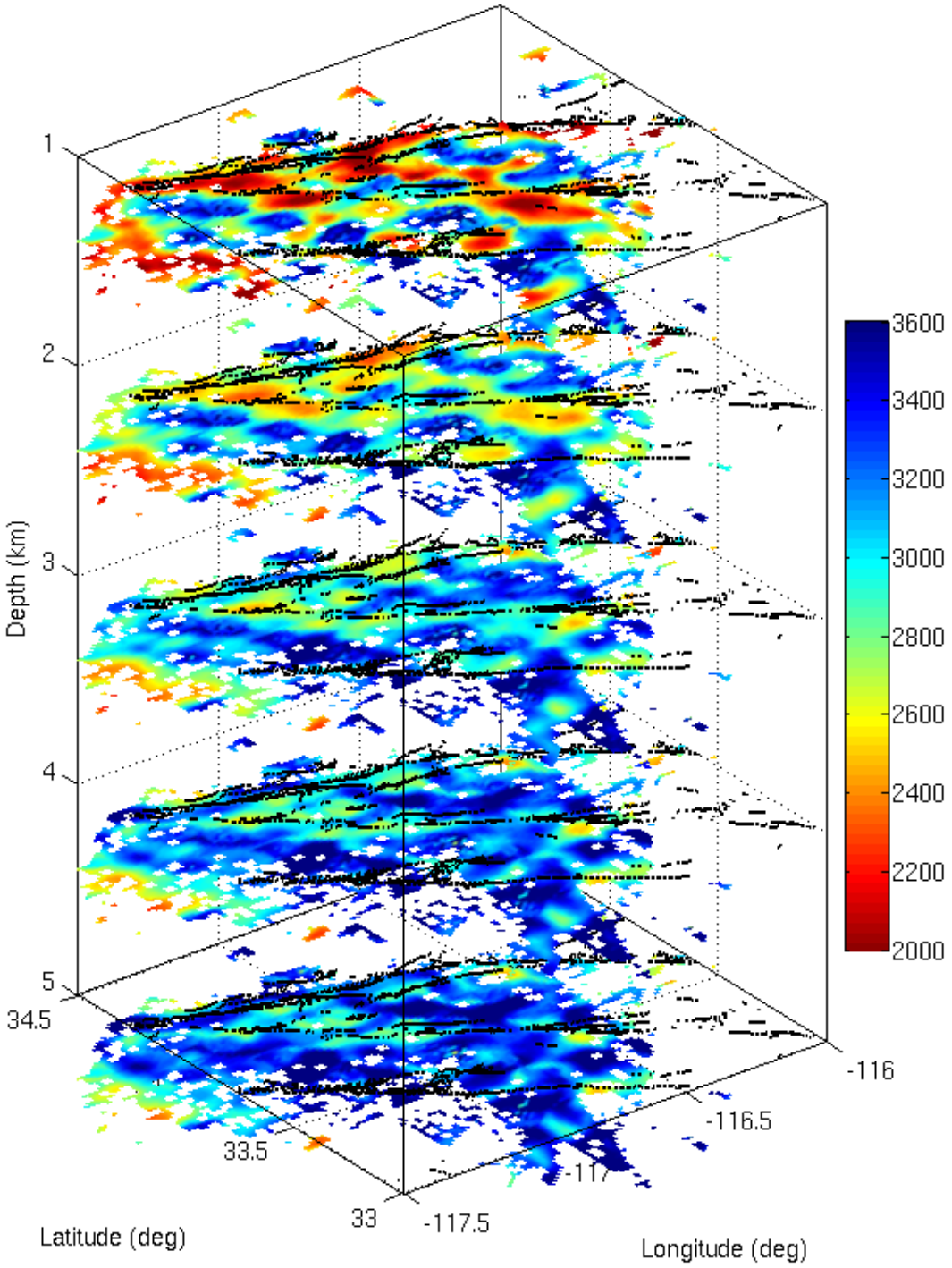

Imaging bimaterial fault interface with Head Waves

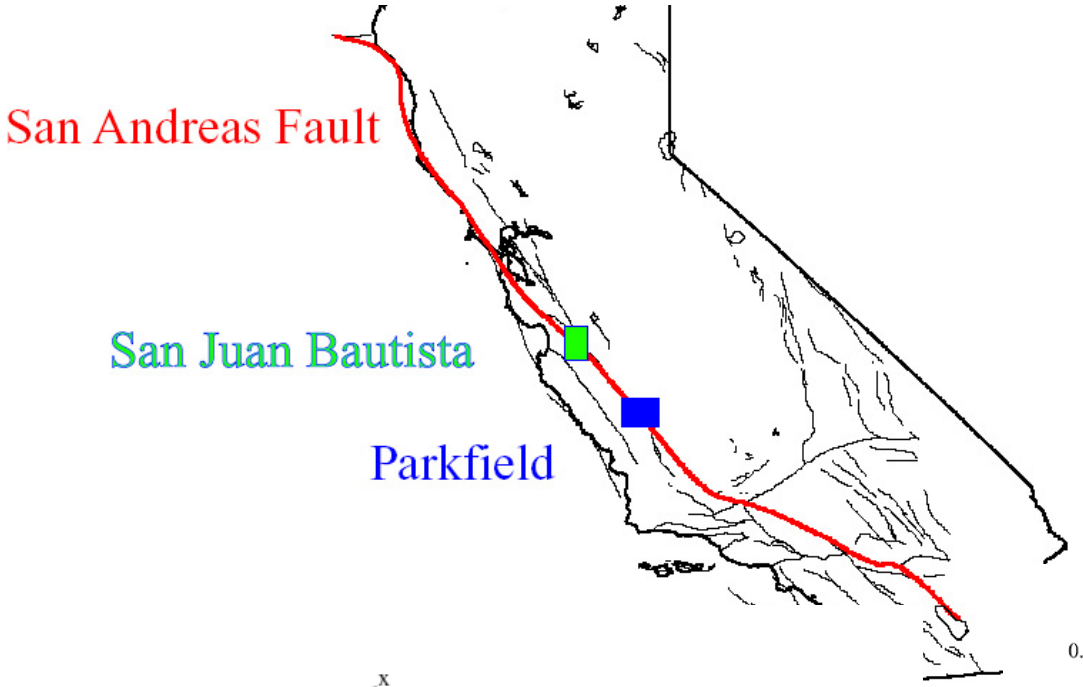

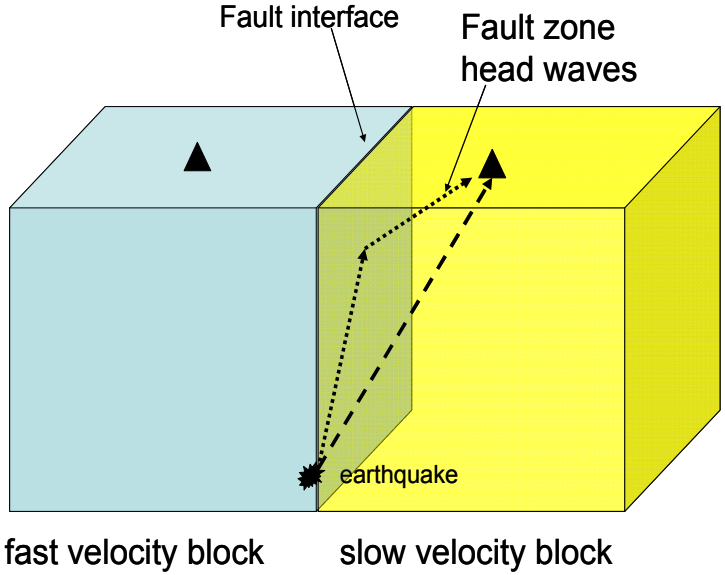

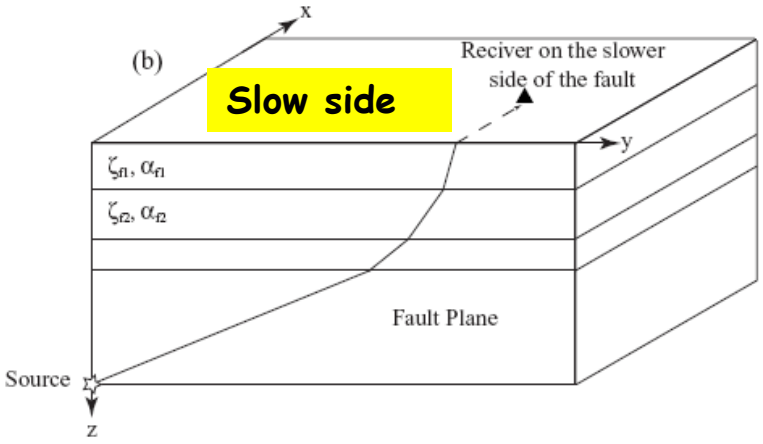

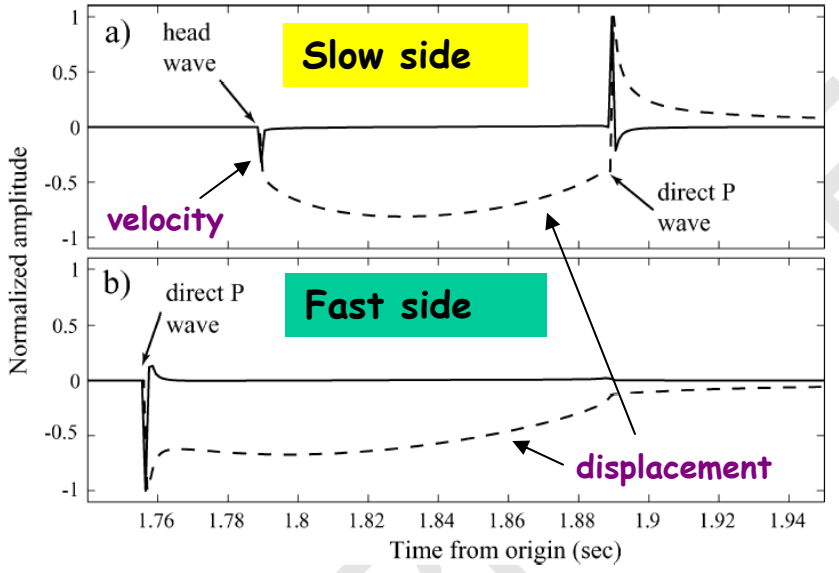

The head waves are <u>first arrivals</u> at stations on the slower side of the fault with normal distance $x < x_c = r \tan [\cos^{-1}(\alpha_2/\alpha_1)]$ and have <u>opposite polarity</u> than the direct *P* wave (Ben-Zion, 1989, 1990)

Imaging bimaterial fault interface with Head Waves

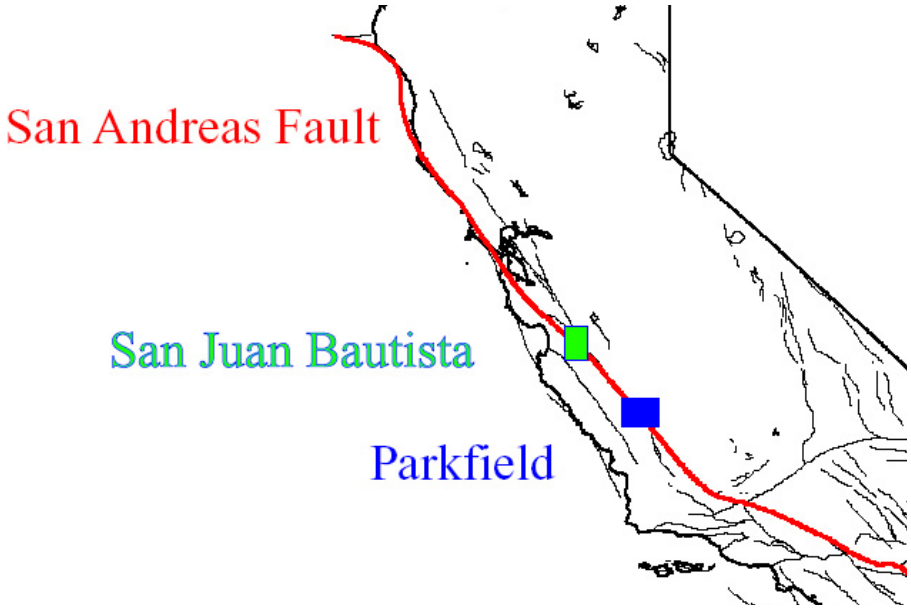

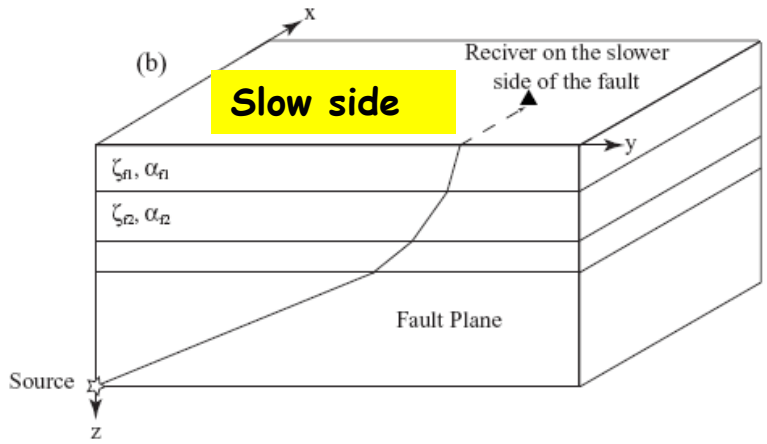

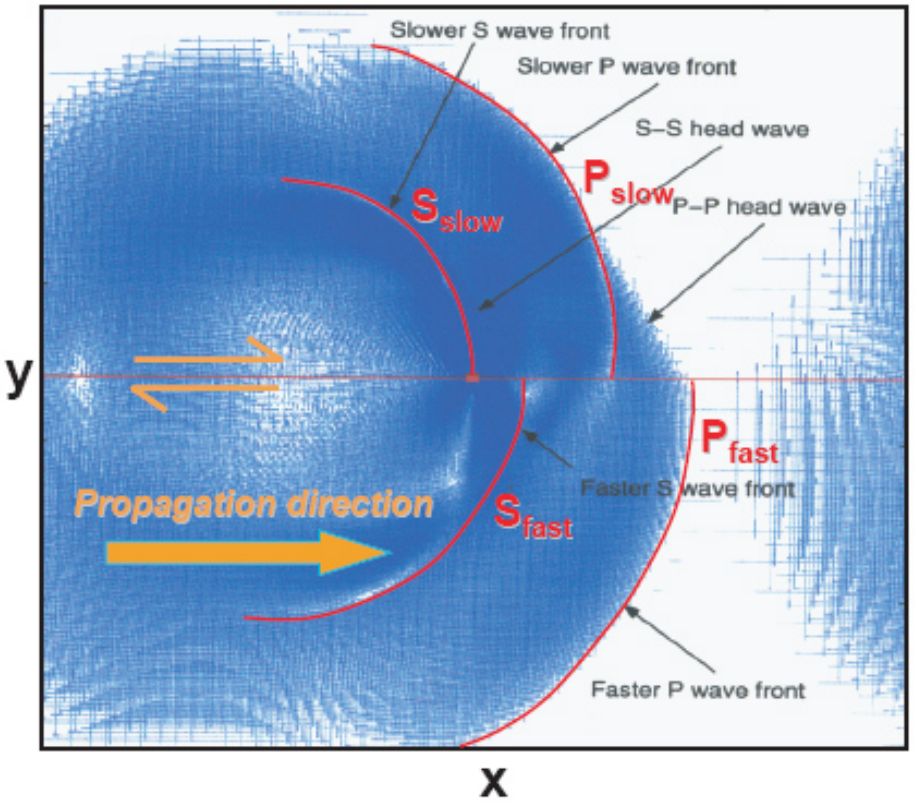

The head waves are <u>first arrivals</u> at stations on the slower side of the fault with normal distance $x < x_c = r \tan [\cos^{-1}(\alpha_2/\alpha_1)]$ and have <u>opposite polarity</u> than the direct *P* wave (Ben-Zion, 1989, 1990)

Ben-Zion and Malin (Sci., 1991)

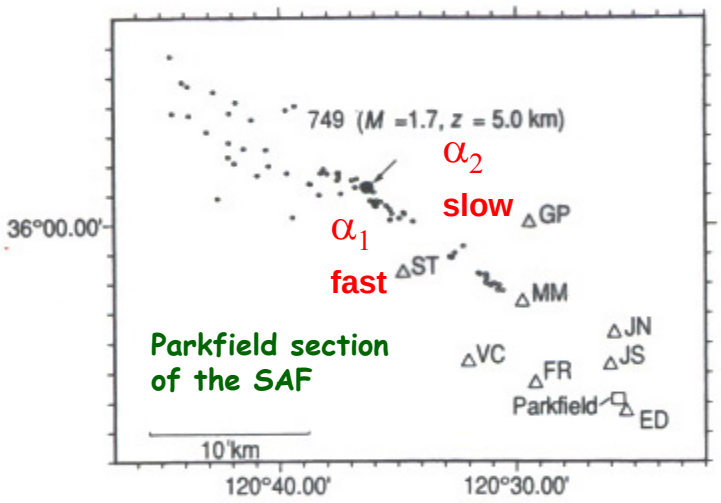

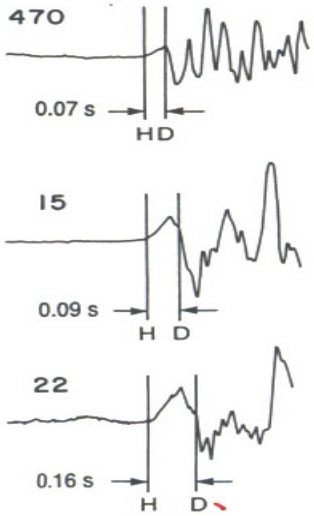

$\Delta t \sim r\,[1/\alpha_2 - 1/\alpha_1] \sim r\,(\Delta\alpha/\alpha^2)$

$X_c = r \tan[\cos^{-1}(\alpha_2/\alpha_1)]$

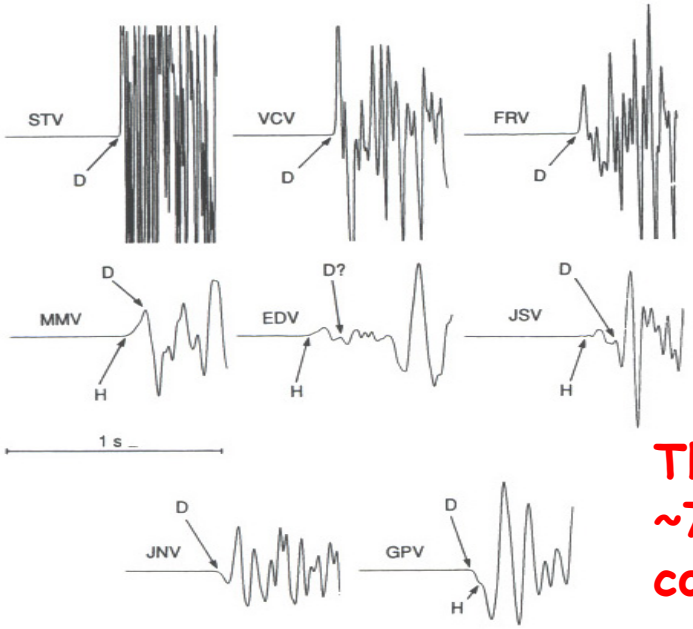

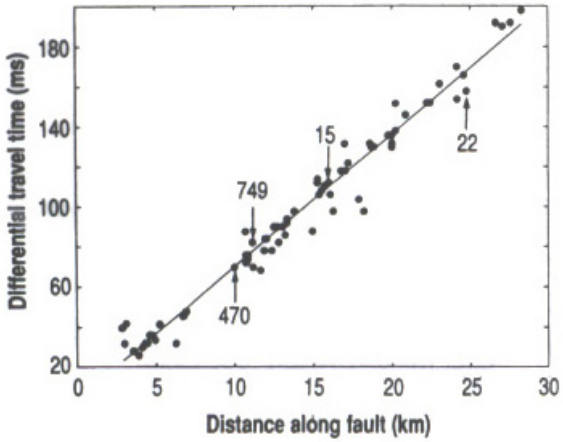

The SAF at Parkfield has a material contrast of ~7% that extends to a depth of ~10 km and is continuous along strike for 10's of km.

Fault Zone Head Waves south of Hollister
(McGuire and Ben-Zion, 2005)

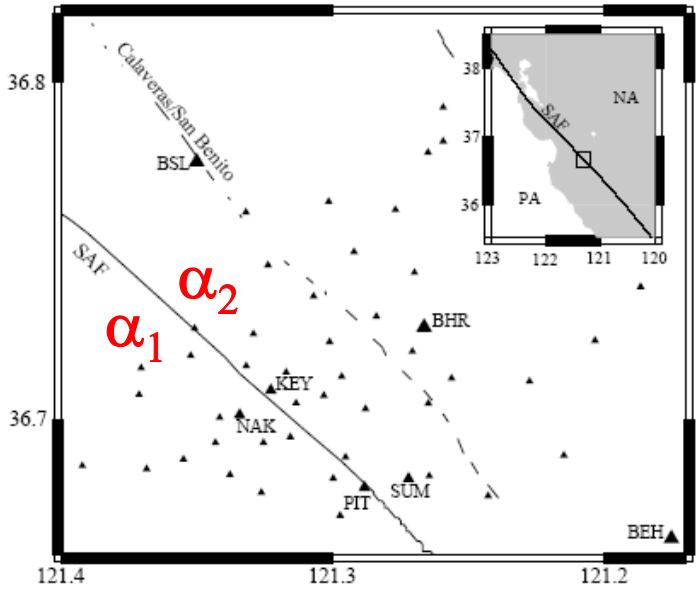

α_2

α_1

$X_c = r \tan [\cos^{-1}(\alpha_2/\alpha_1)]$

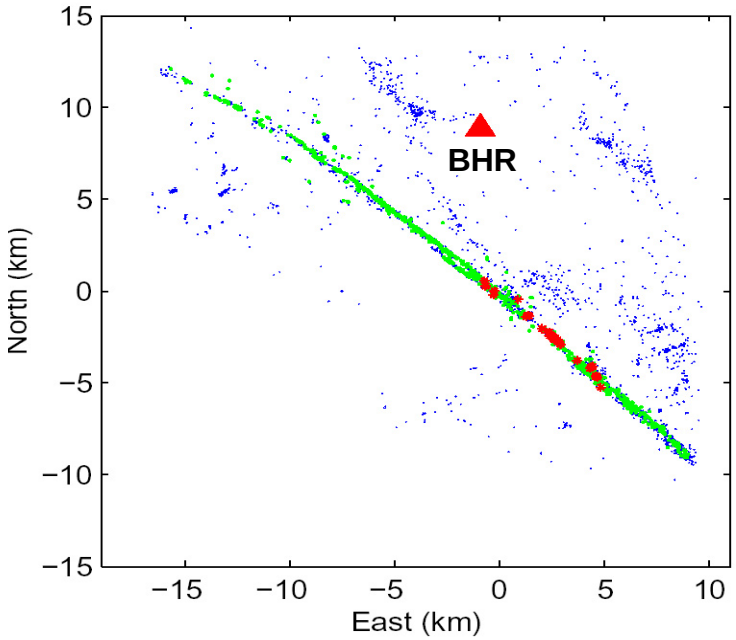

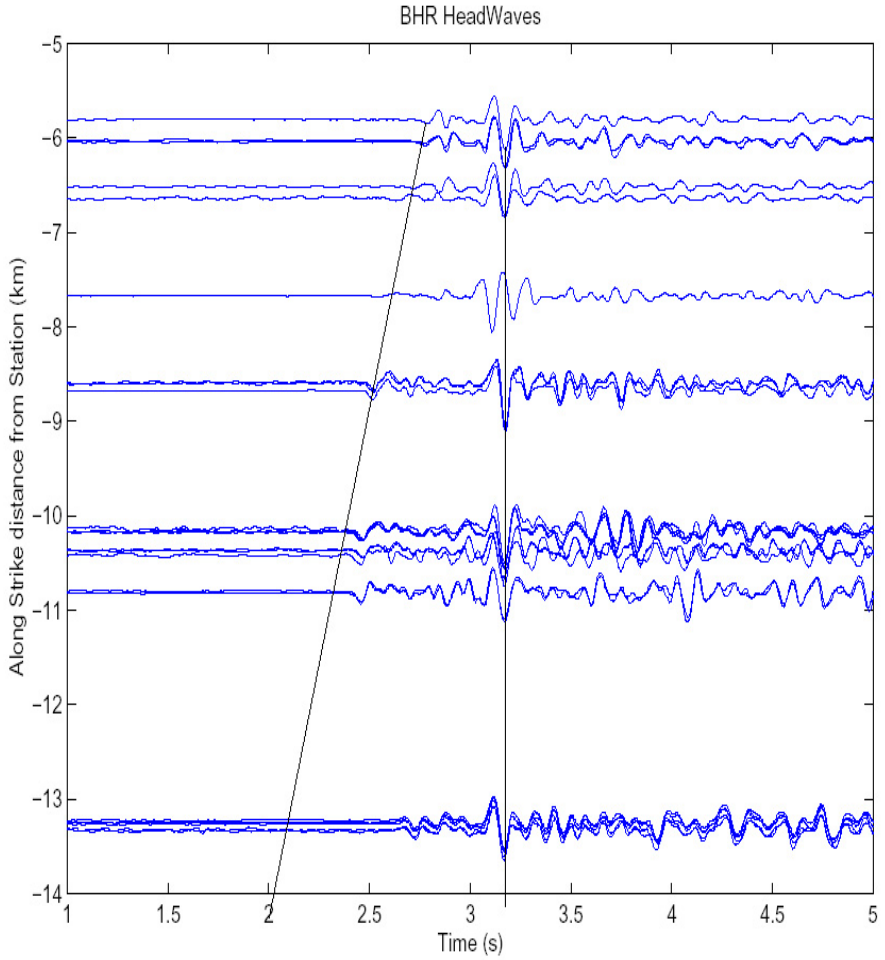

$\Delta t \sim r [1/\alpha_2 - 1/\alpha_1] \sim r (\Delta\alpha/\alpha^2)$

The SAF at this location has average velocity contrast of 10-20% to ~10 km depth

Local Tomography results

Eberhart-Phillips & Michael (1993)

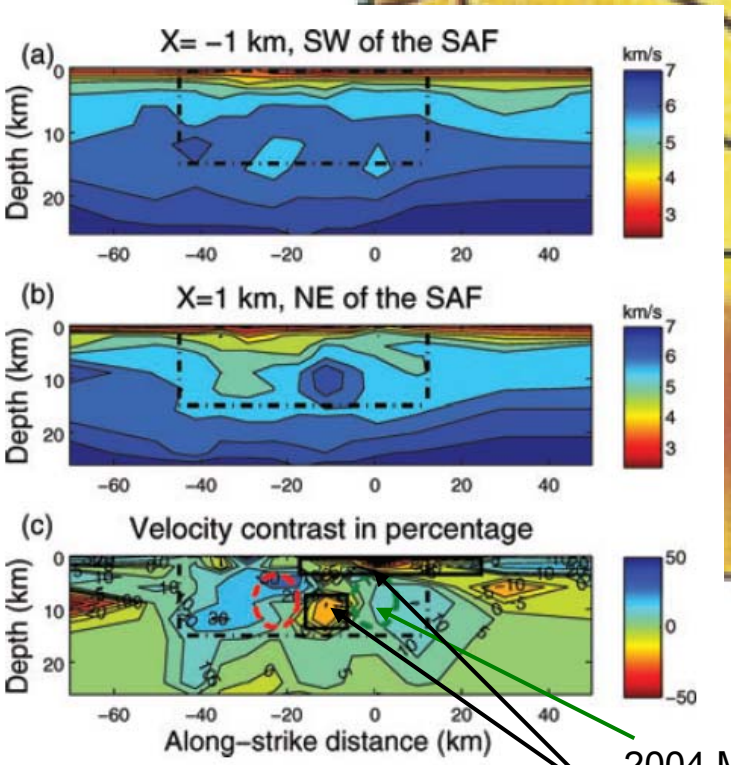

Thurber et al (2006)

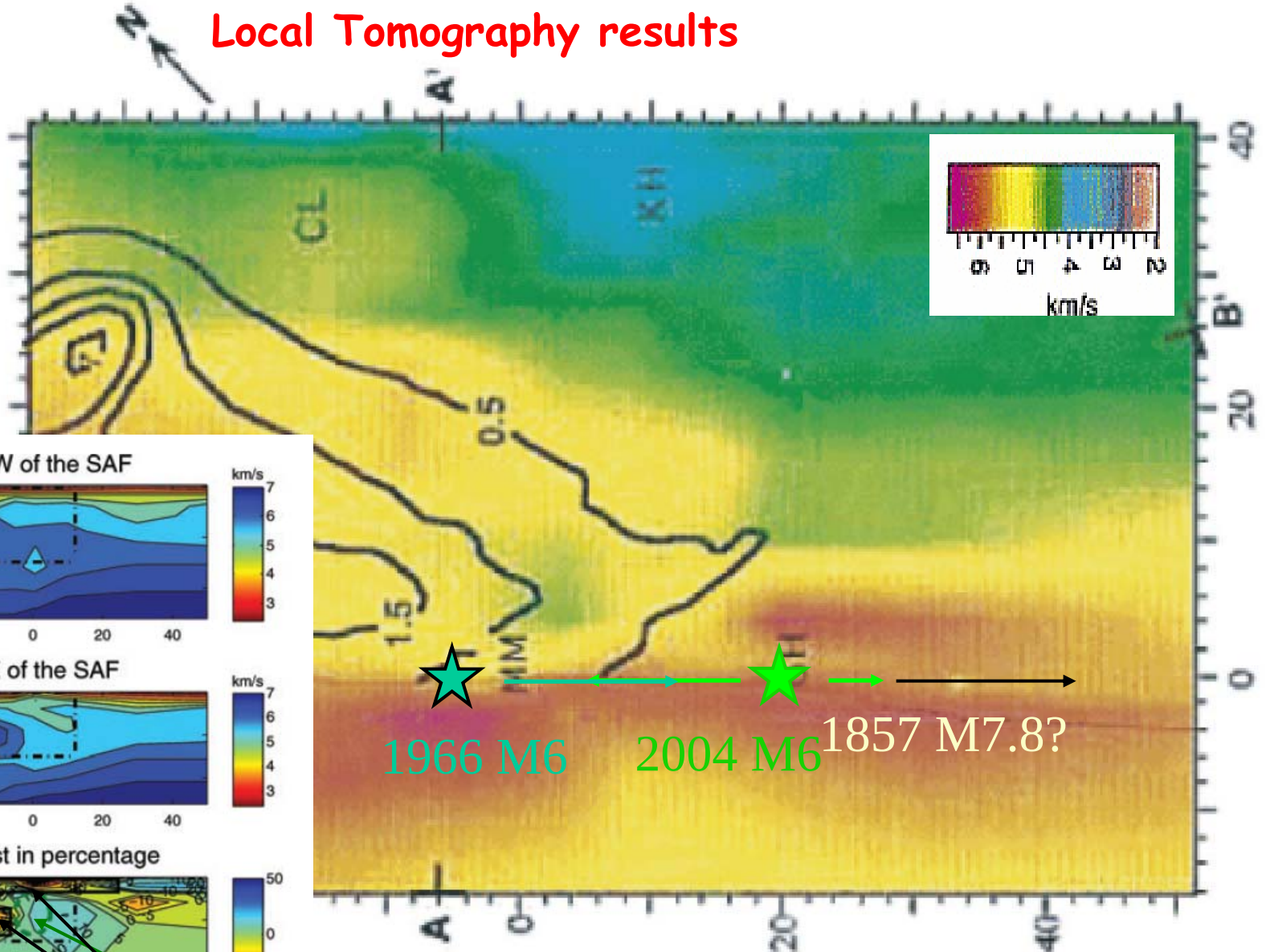

2004 M6 velocity contrast reversals

"The previously reported strong wavespeed contrast across the SAF (southwest side fast) is imaged in most places, with the primary exception being the general region of the 2004 Parkfield rupture zone, where a high Vp body is present northeast of the fault."

Zhao et al. (GJI, 2010)

Station to the north

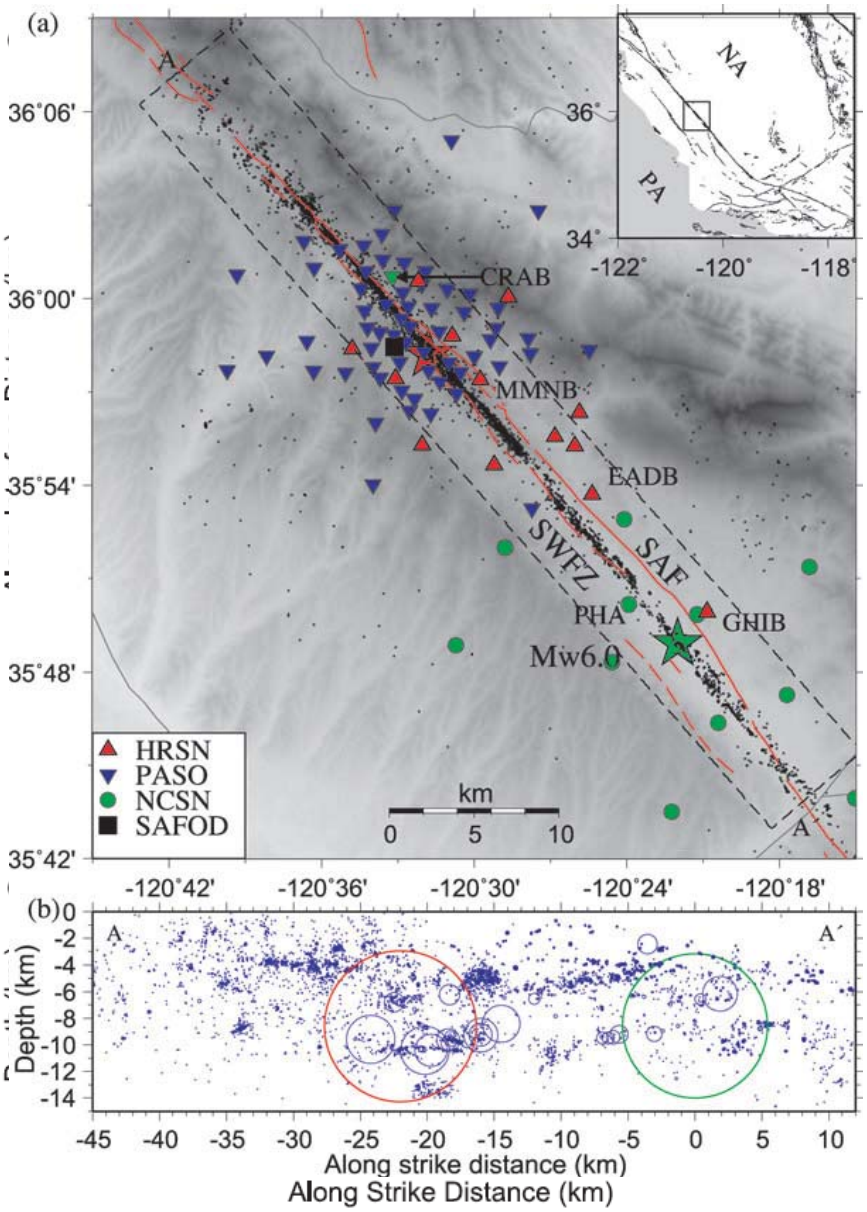

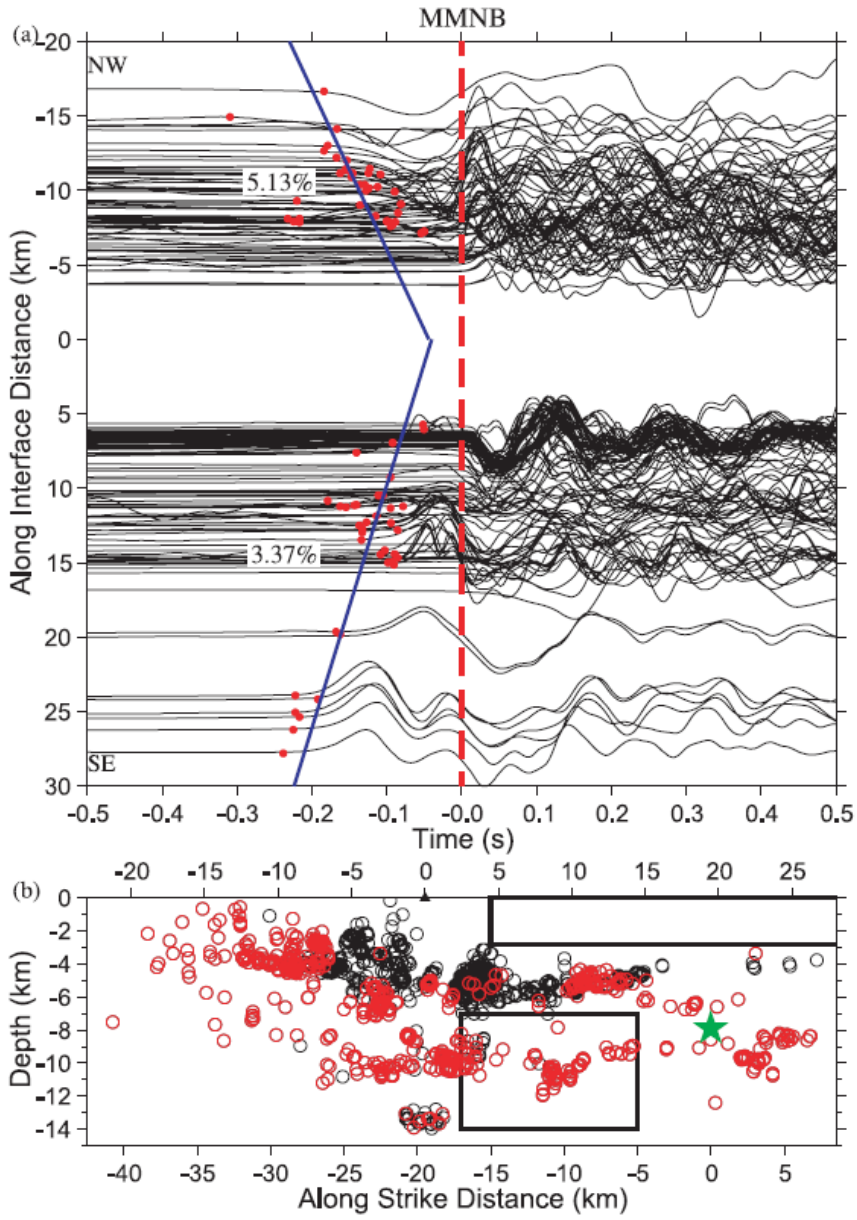

Stations to the south

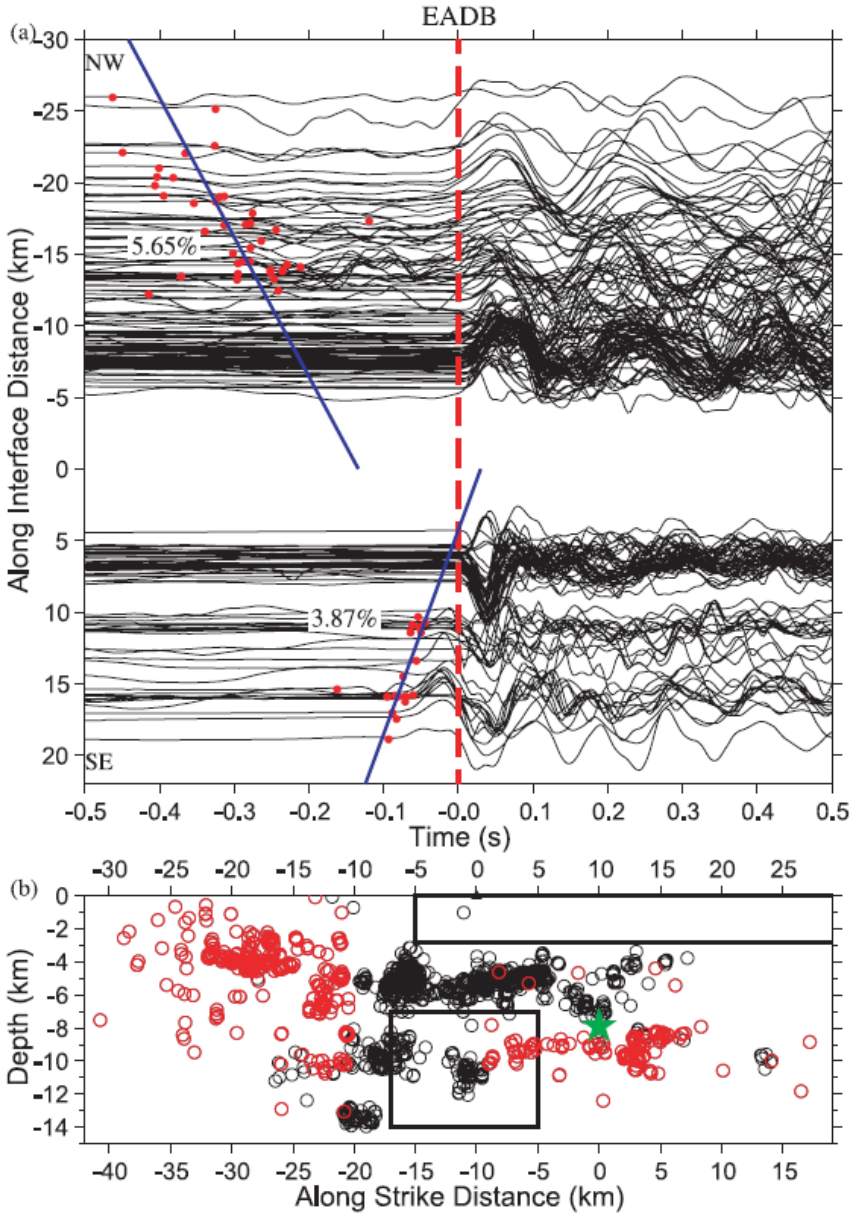

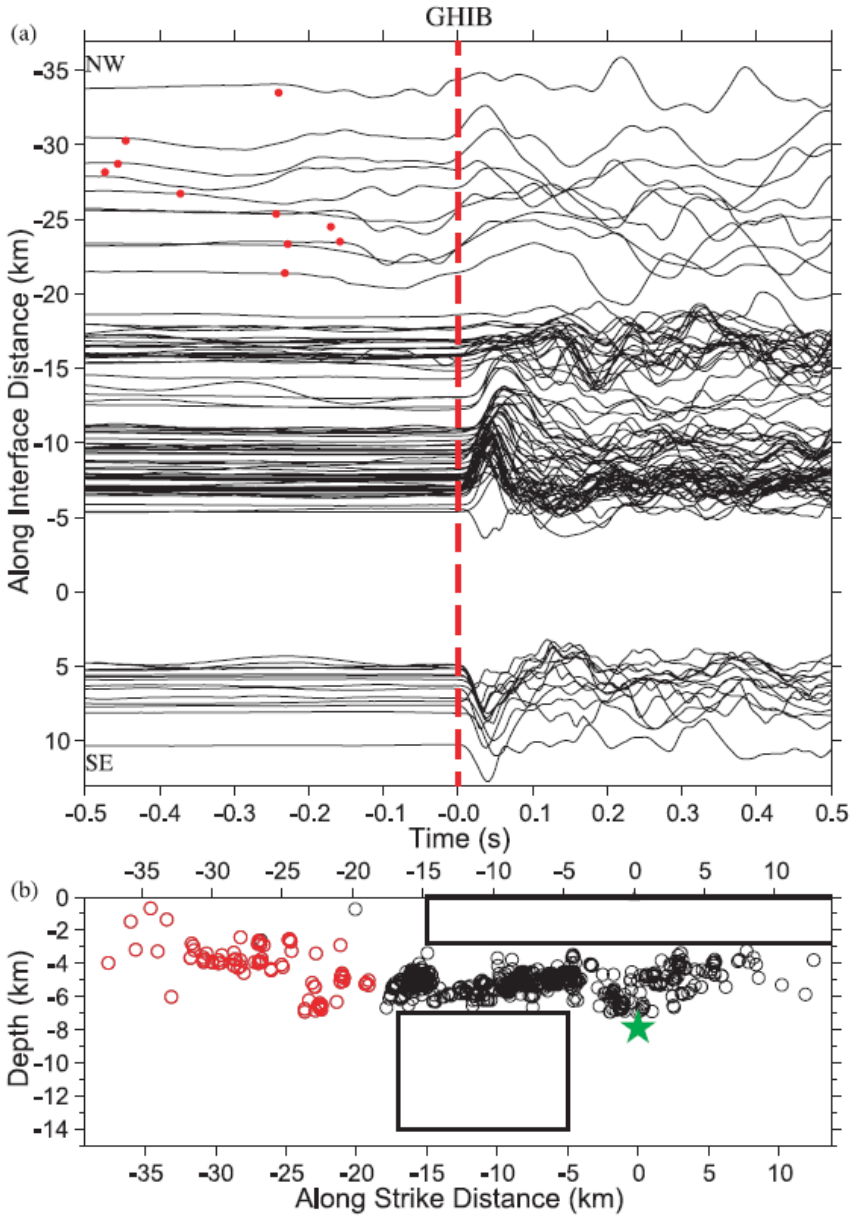

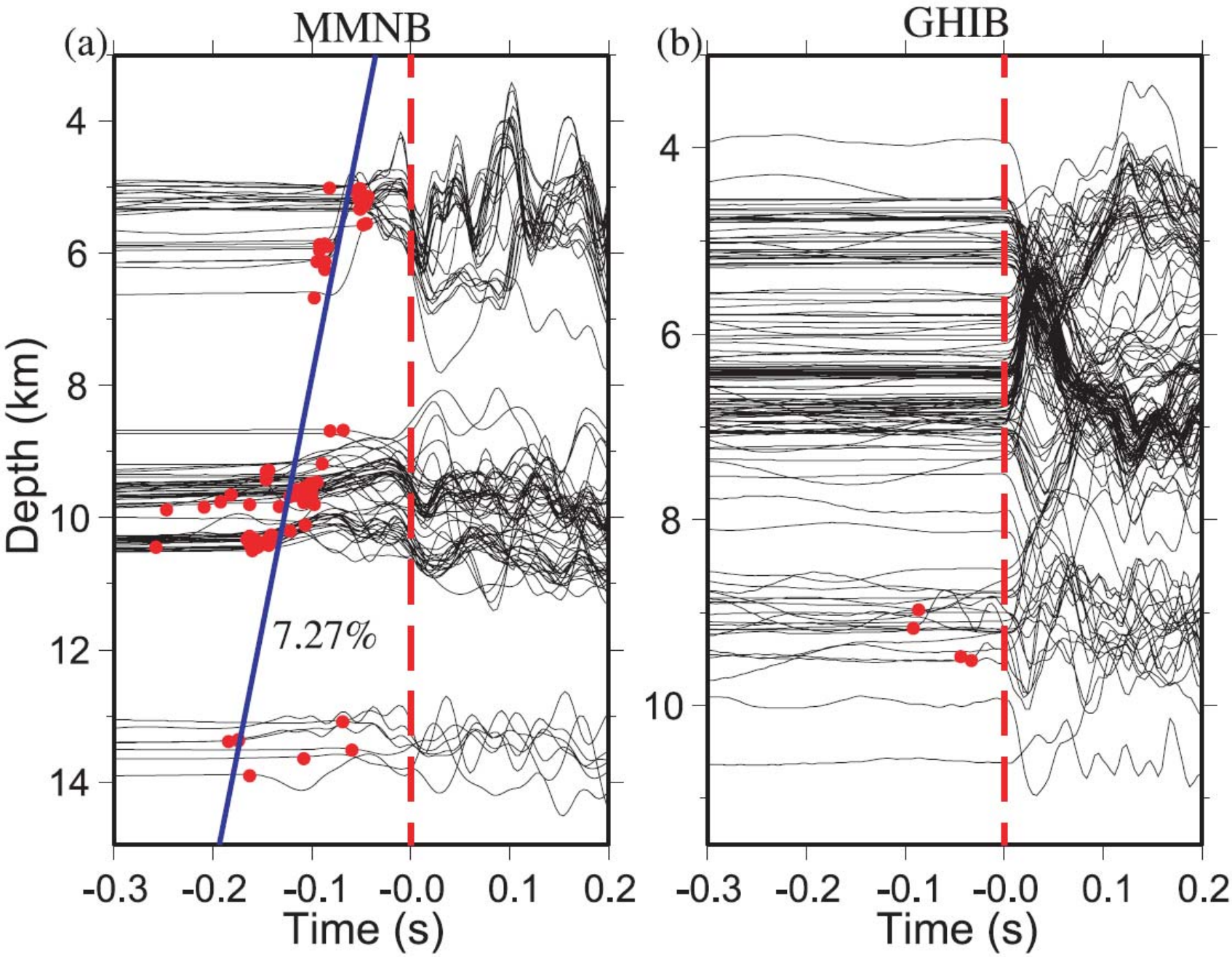
(a)
MMNB
(b)
GHIB
Depth (km)
4
6
8
10
12
14
7.27%
-0.3
-0.2
-0.1
-0.0
0.1
0.2
Time (s)

Evidence for a bimaterial interface along the Mudurnu segment of the North Anatolian Fault Zone from polarization analysis of P waves

Fatih Bulut, Yehuda Ben-Zion and Marco Bohnhoff (EPSL, 2012)

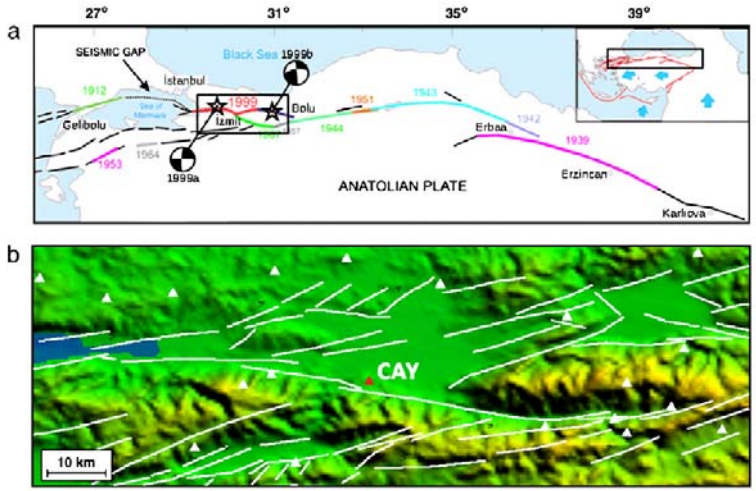

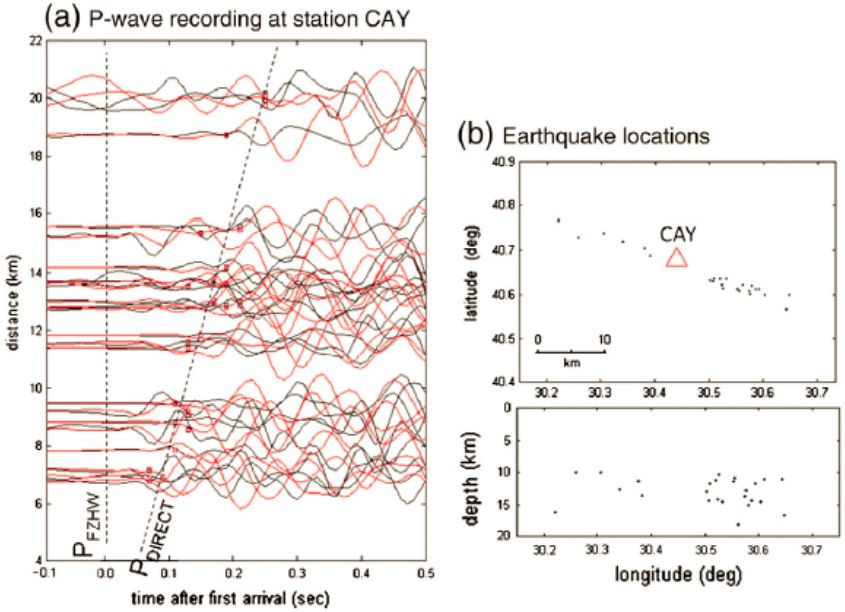

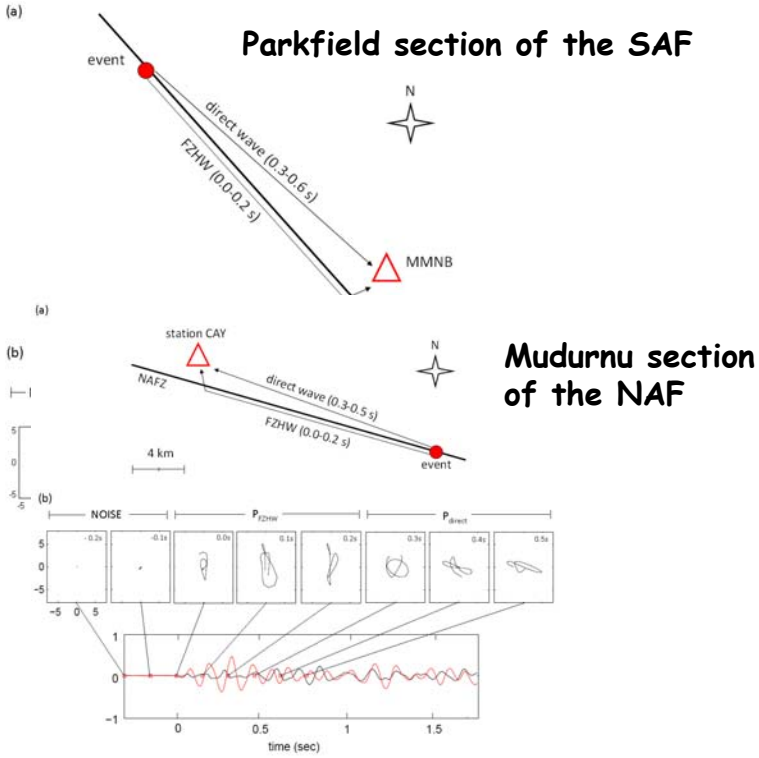

The moveout analysis indicates average velocity contrast of ~6% over the top 15 km of the Mudurnu segment of the NAFZ

Allam, Ben-Zion & Peng (2013)

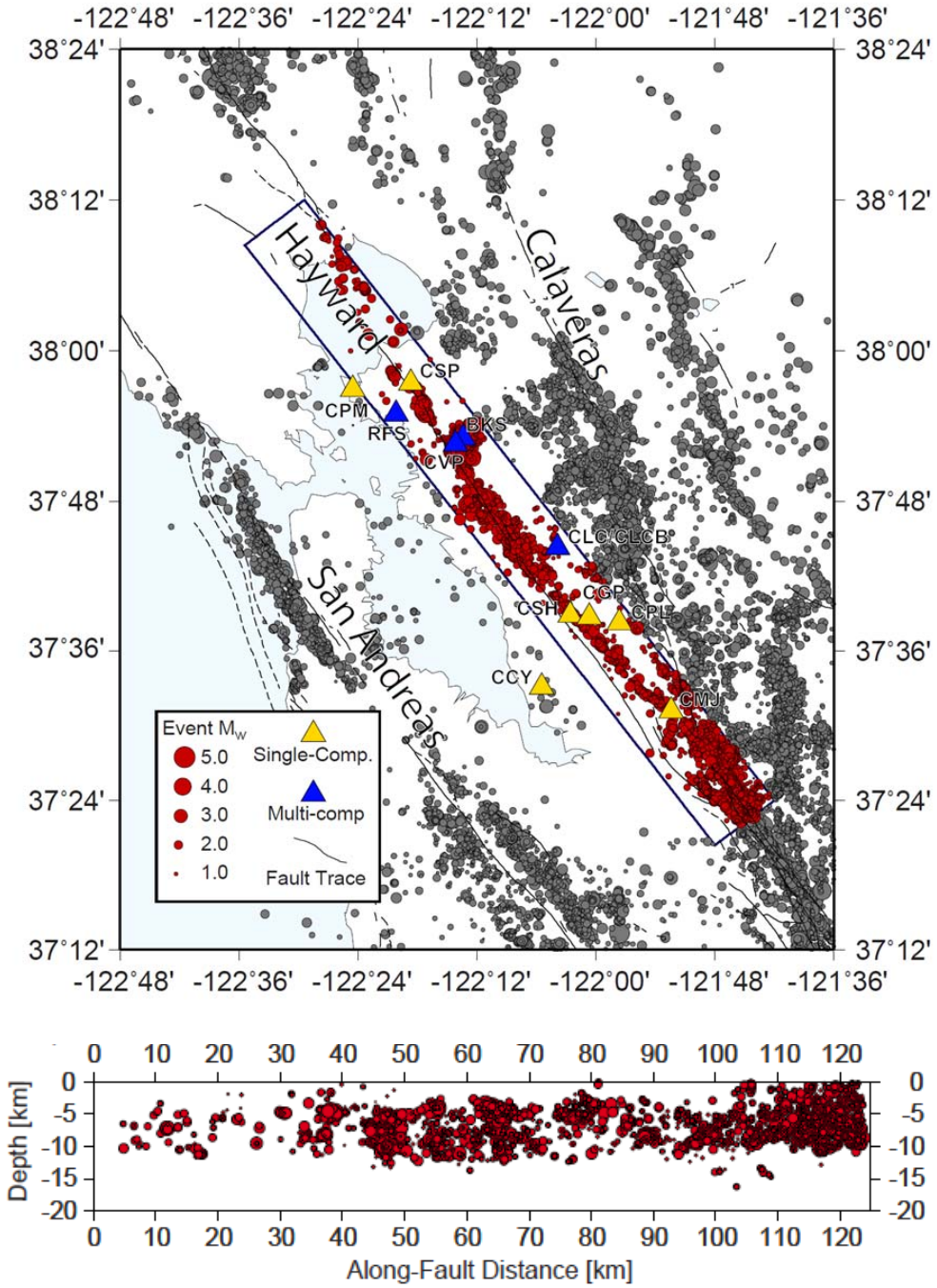

- 5834 Events > M_w 1.0
- DD relocated catalog (Waldhauser & Schaff, 2008)
- From 1984-2009
- 9 station on NE side
- 3 stations on SW side
- Wide variety of instruments (broadband, strong motion, single-component, etc…)
- Bandpass 1Hz < X < 15Hz

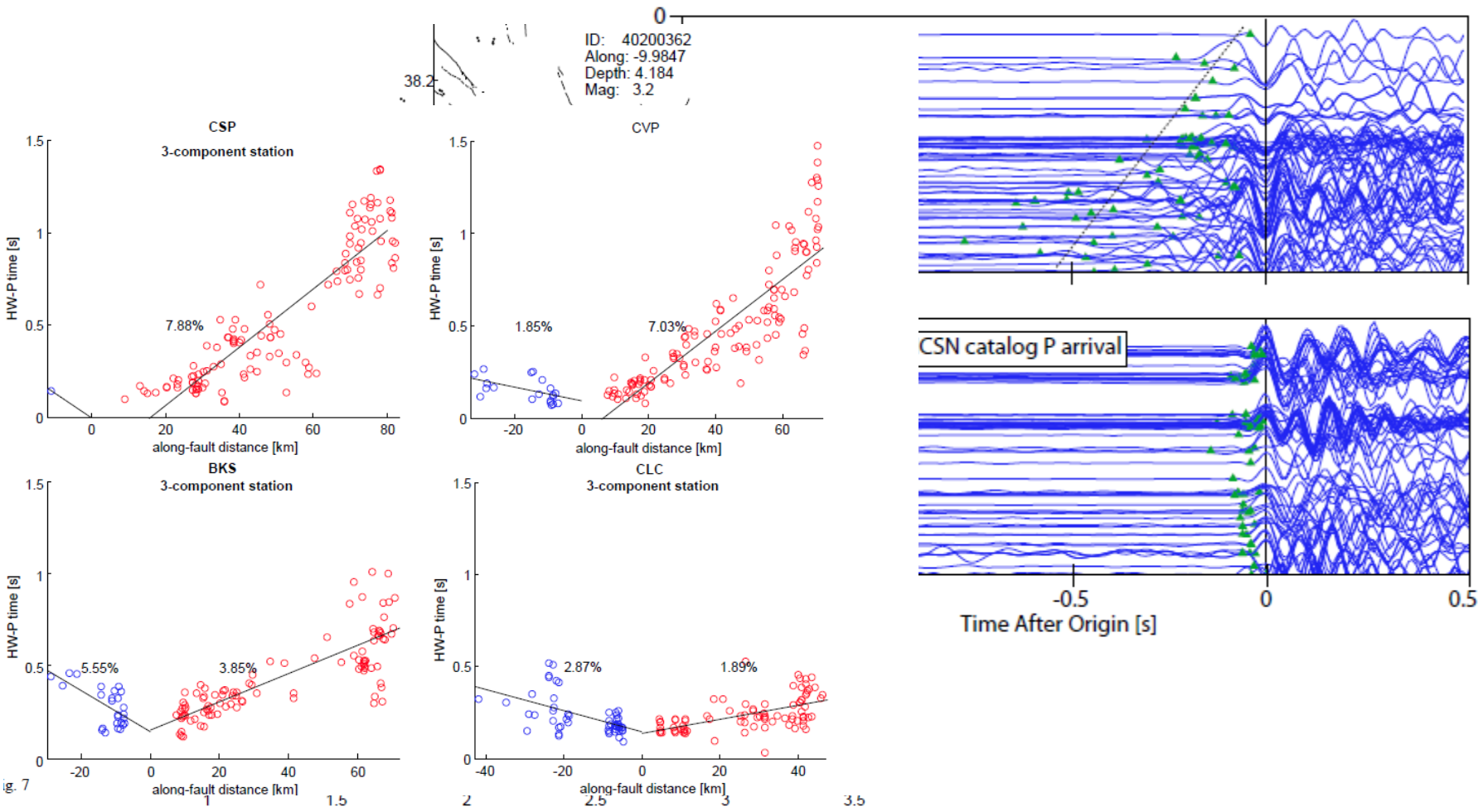

There is a continuous bimaterial interface for ~80km along the Hayward fault with variable velocity contrast

Analysis of fault zone trapped waves

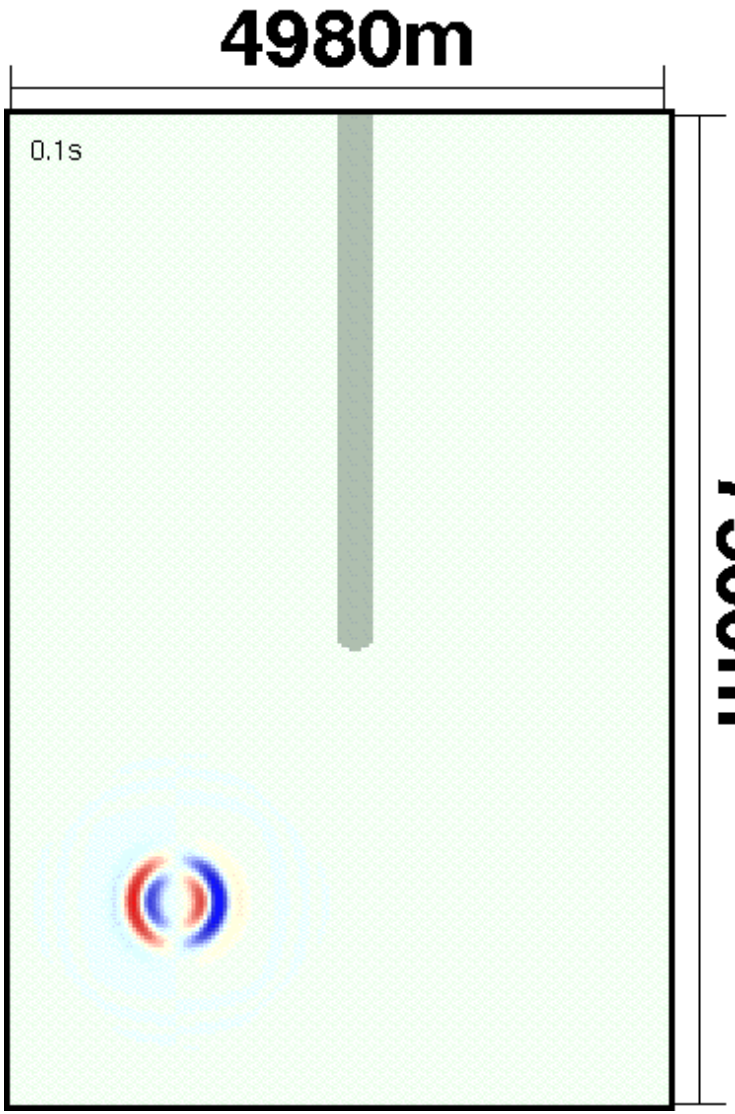

Jahnke, Igel and Ben-Zion (GJI, 2002)

Ben-Zion and Aki, 1990

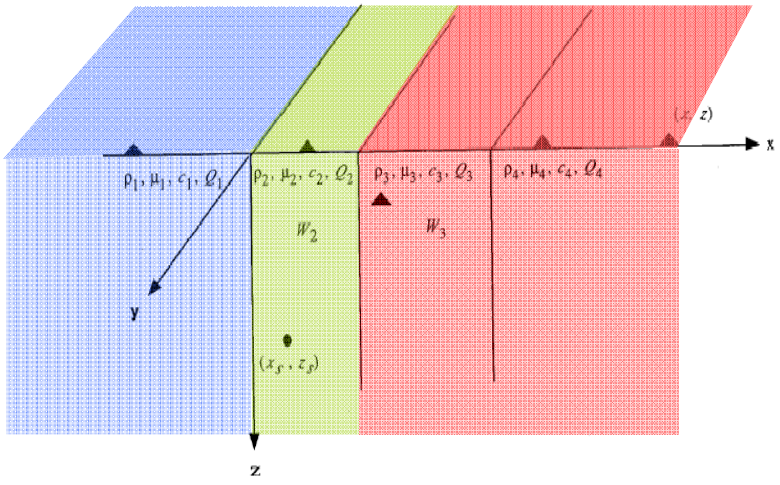

Direct body waves

Head waves

Trapped waves

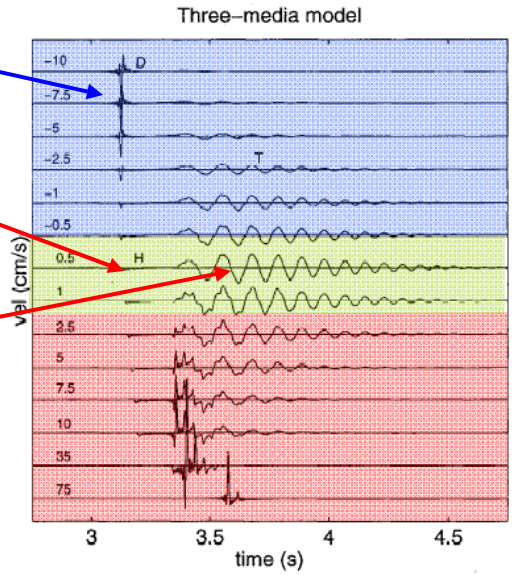

Trapped waves depends strongly on

$N = r/[W \tan(\theta_c)] = r/[W \tan(\sin^{-1}(\beta_2/\beta_1))]$

Seismic observations associated with damaged fault zone rocks

(Ben-Zion et al., 03; Peng and Ben-Zion, 04, 05, 06; Wu et al., 09, 10; Lewis & Ben-Zion, 10)

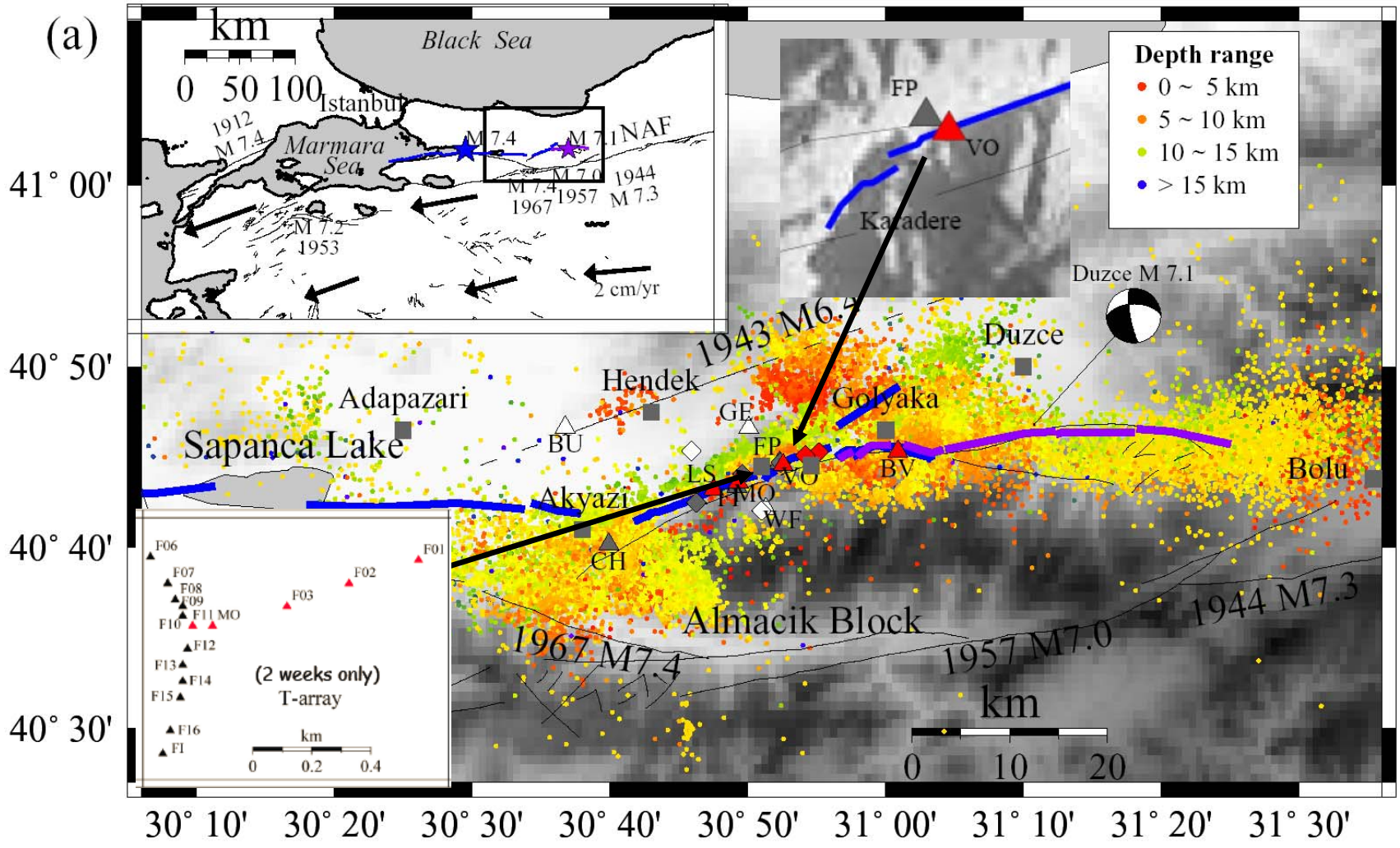

A PASSCAL network along the Karadere-Duzce branch of the NAF recorded ~26000 earthquakes in the 6-months following the 1999 Izmit earthquake

Fault zone trapped waves

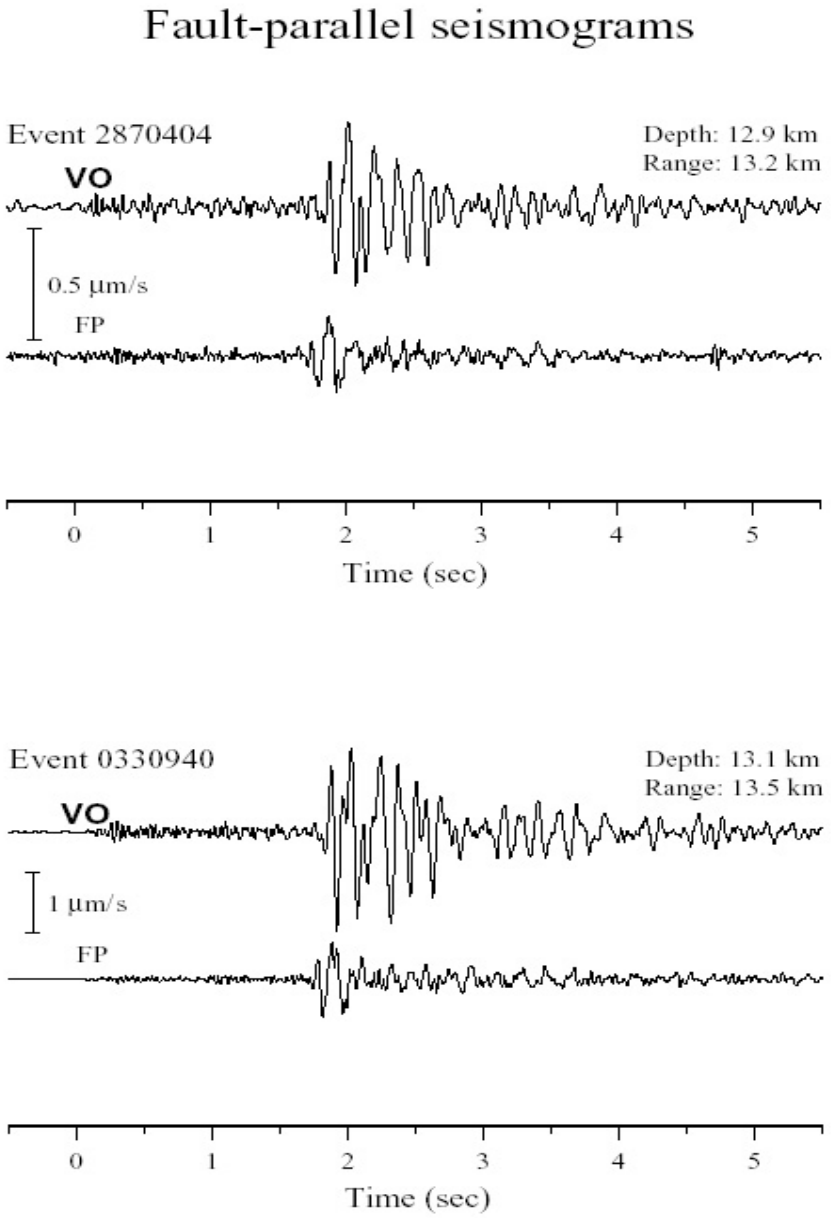

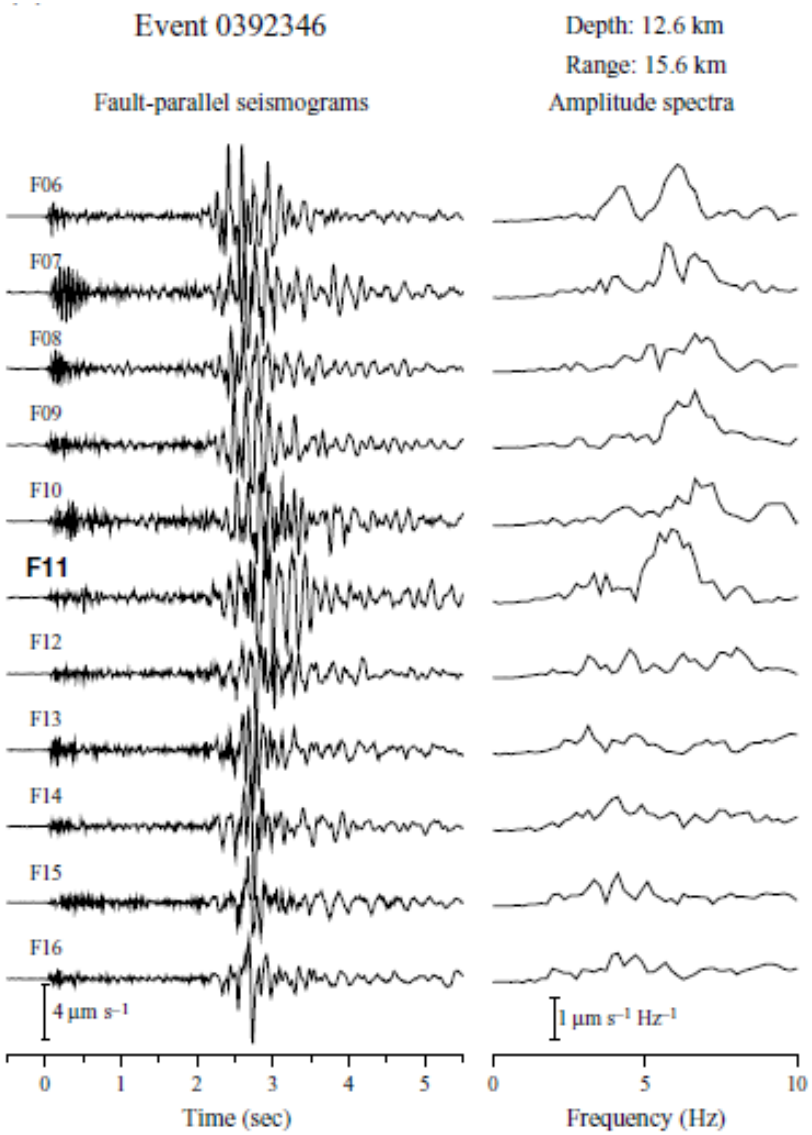

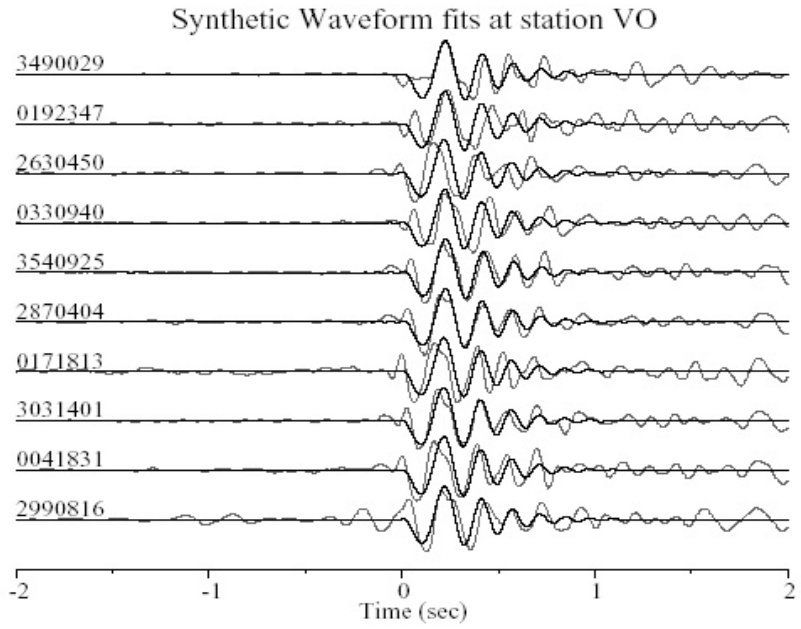

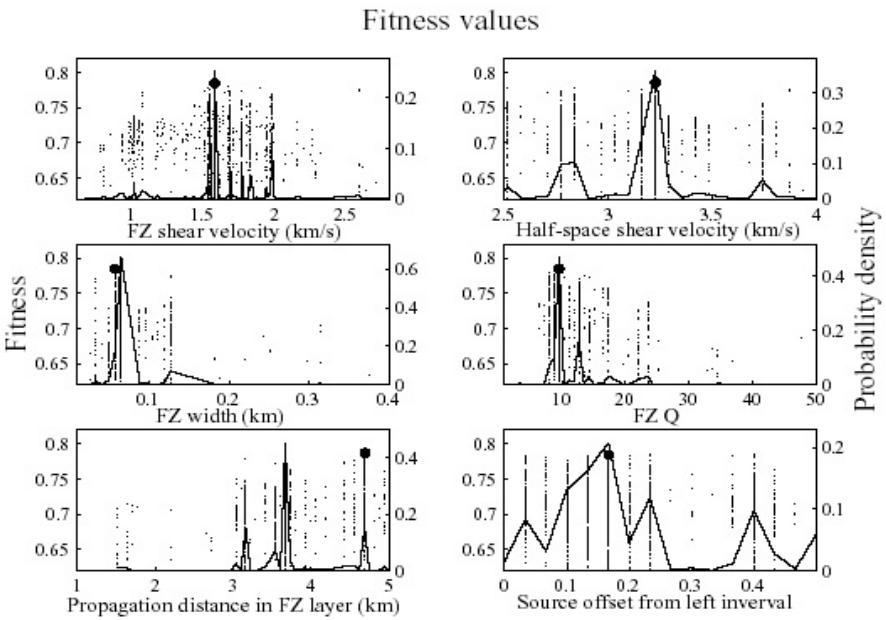

The damaged fault zone layer is most likely characterized by:

width ~75 m,
depth ~3.5 km,
S-wave velocity reduction ~50%,
Q-value ~10.

Similar results are obtained from analyses of trapped waves also at the:

- **Nocera Umbra fault in Italy** (Roveli et al., 2002)
- **Rupture zone of the 1992 Landers, CA, earthquake** (Peng et al., *GJI*, 2003)
- **Trifurcation area of the San Jacinto Fault** (Lewis et al., *GJI*, 2005; Yang and Zhu, 2010)
- **Parkfield section of the San Andreas Fault** (Lewis and Ben-Zion, *GJI*, 2010)
- **Calico fault, ECSZ, CA** (Yang et al., 2011)

Analyses of subsets of data imply strong along-strike variations and discontinuities of the trapping structures! (Lewis & Ben-Zion, GJI, 2010)

Rupture zone of the 1992 Landers, CA, earthquake (Peng et al., *GJI*, 2003)

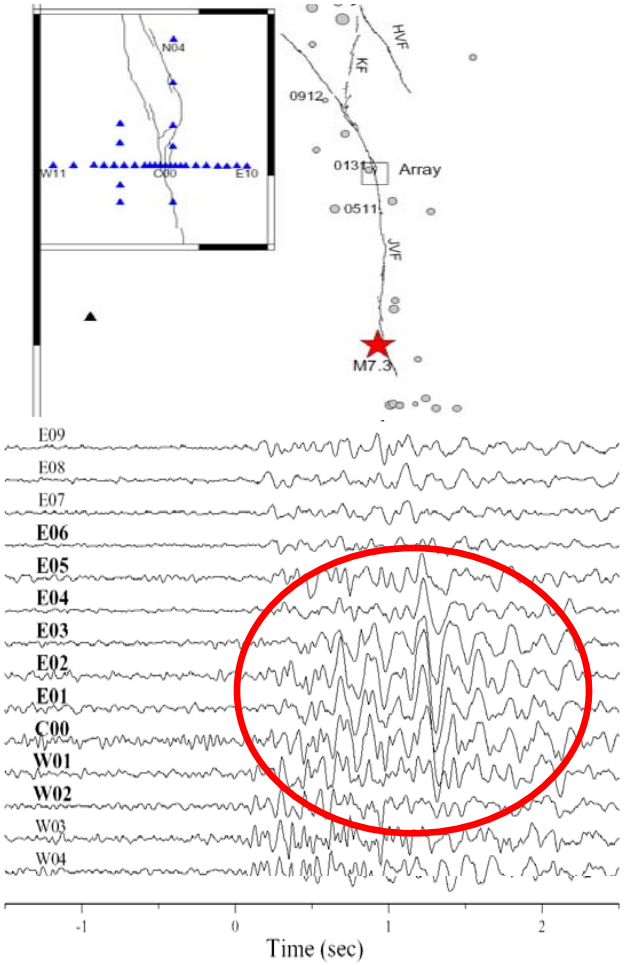

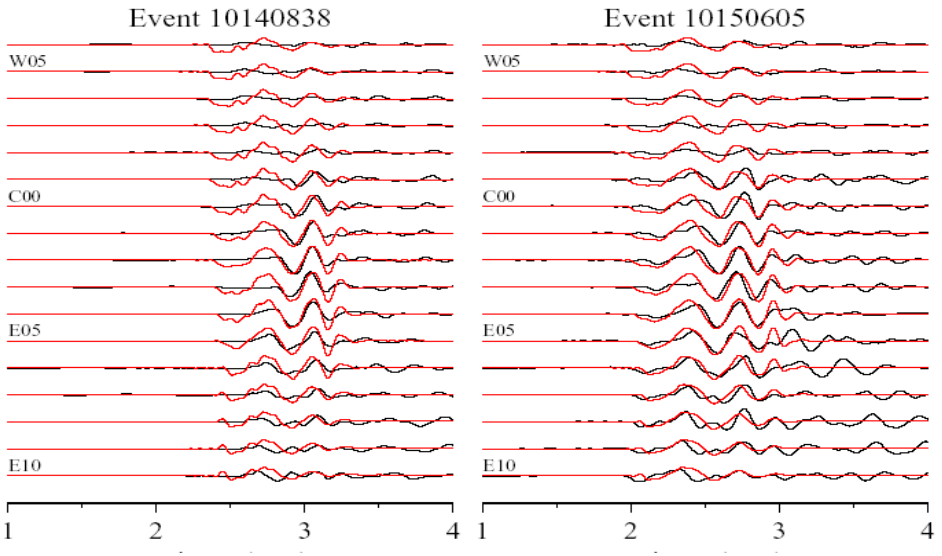

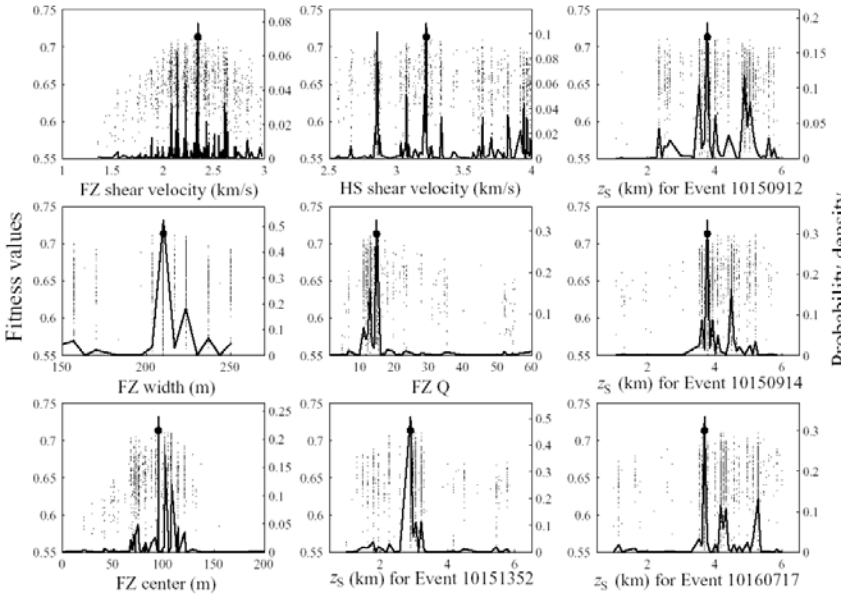

Most likely damage zone parameters:

width ~200 m,
depth ~3.5 km,
S velocity reduction ~50%,
Q-value ~15.

Parkfield section of the San Andreas fault (Lewis and Ben-Zion, *GJI*, 2010)

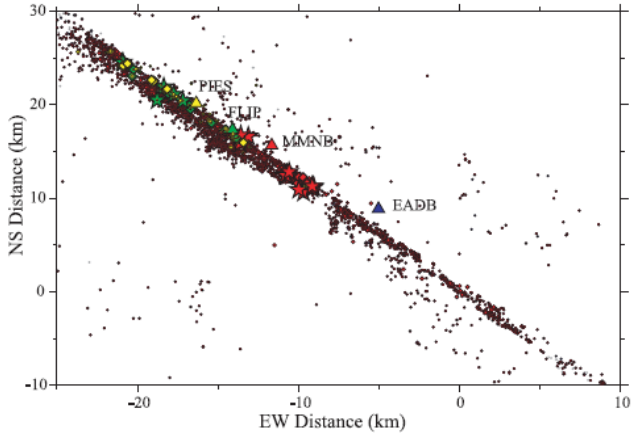

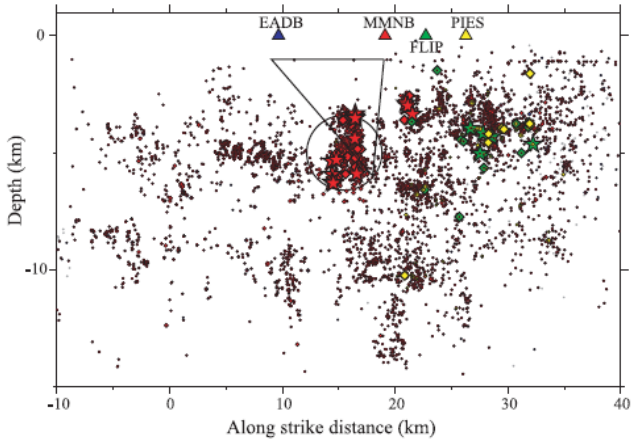

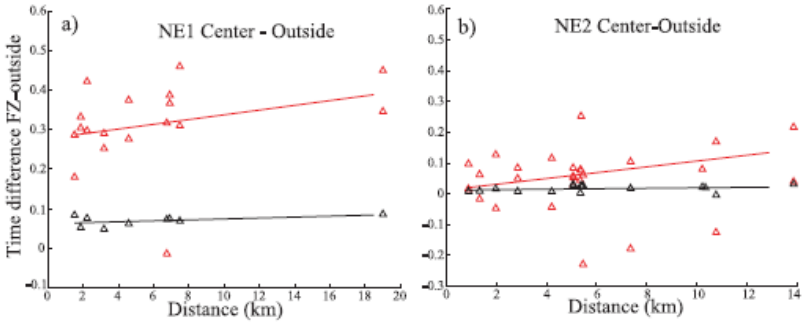

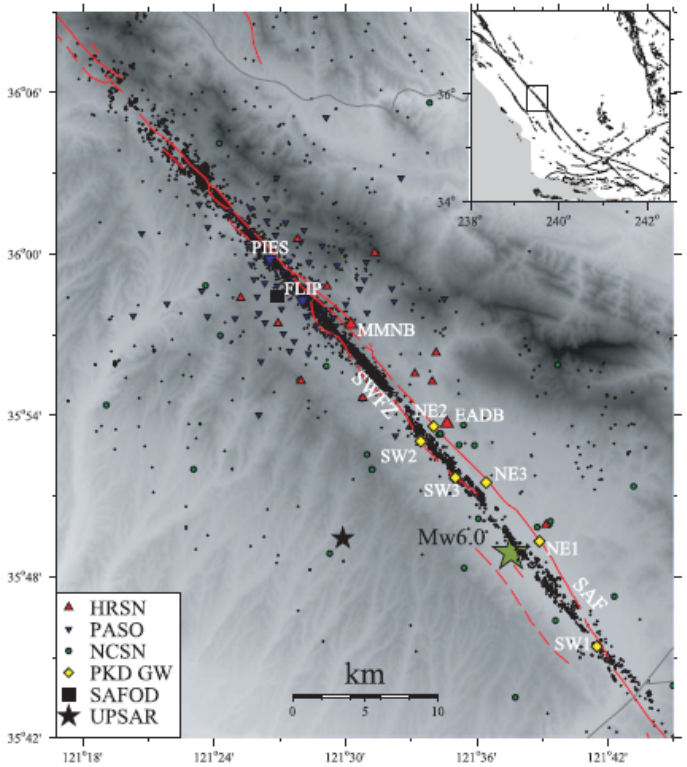

Most likely damage zone parameters:

width ~150 m,
depth ~3 km,
S velocity reduction ~40%,
Q-value ~20,
Coherent waveguide exists only over distances along-strike of 3-5 km.

Trifurcation area of the San Jacinto fault zone (Lewis et al., *GJI*, 2005)

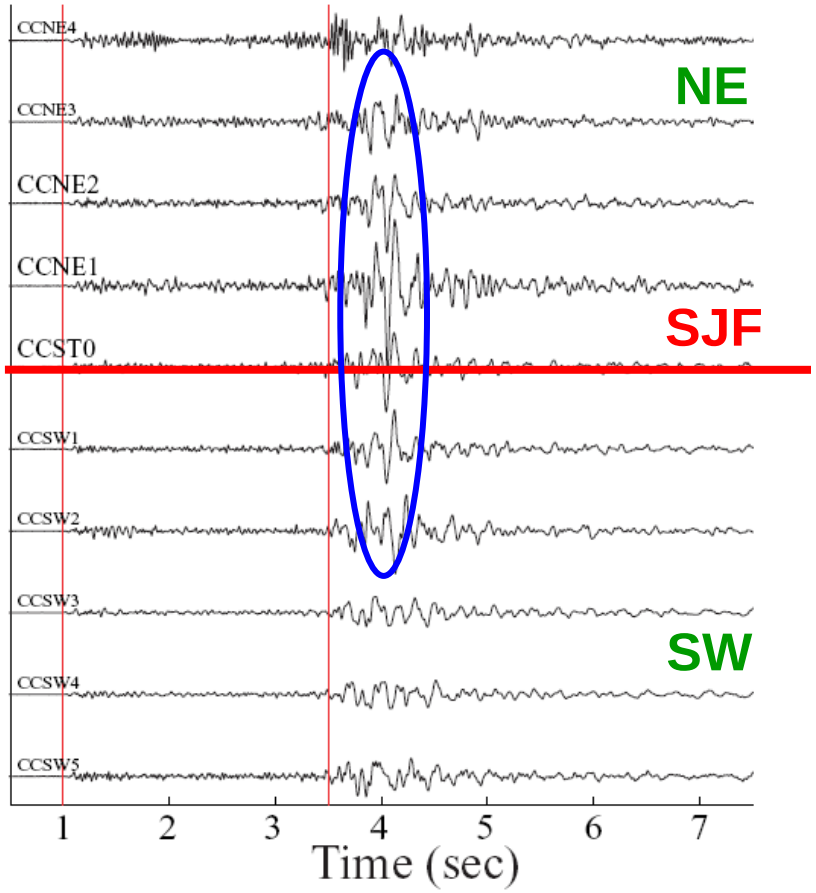

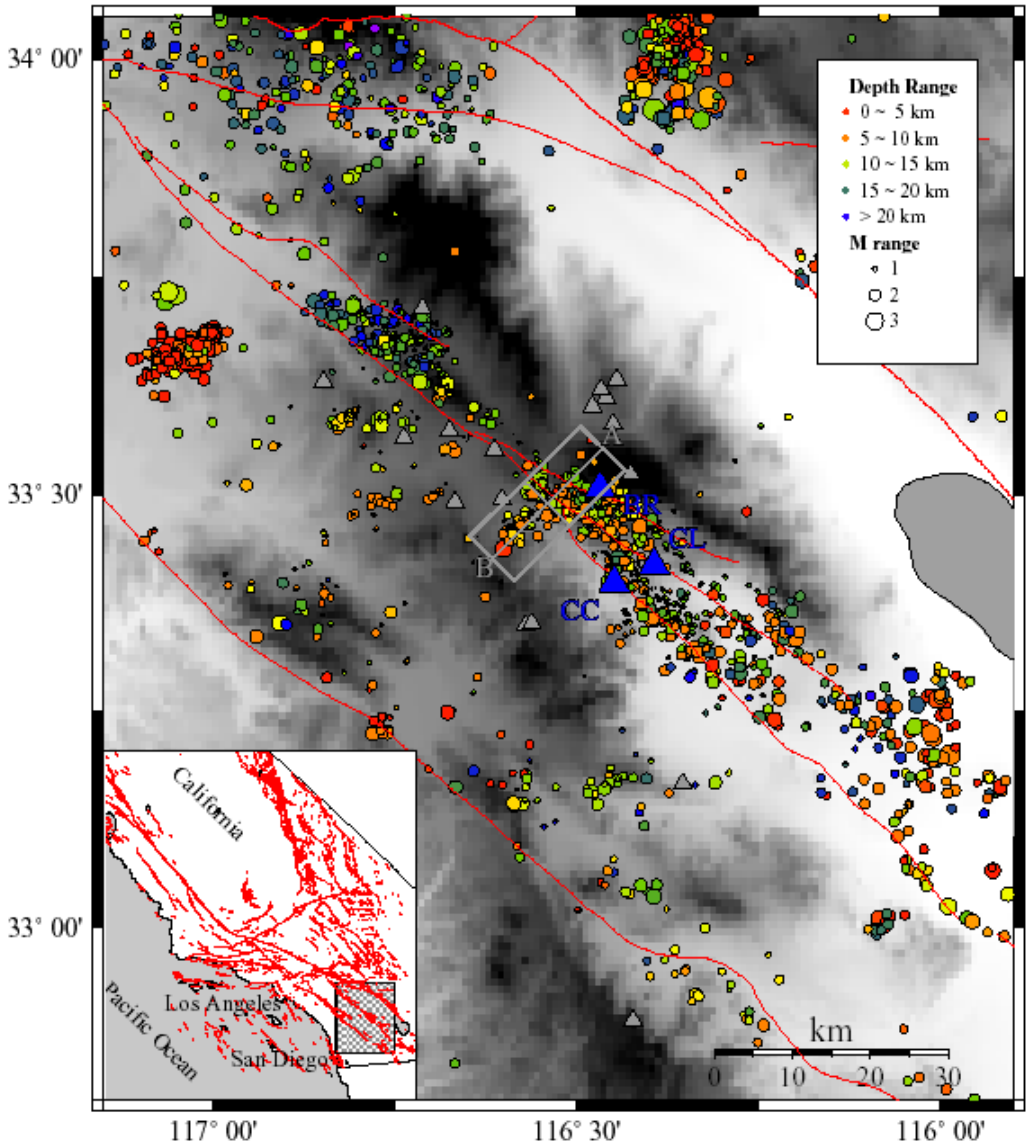

Most likely damage zone parameters:
width ~125 m,
depth ~3.5 km,
S velocity reduction ~40%,
Q-value ~30.

The da
seismic
direction of ruptures on a bimaterial interface in the core structure of the SJF.

Expected damage patterns generated by many earthquakes

Dynamic rupture on a frictional fault with off-fault plastic yielding

Homogenous solid

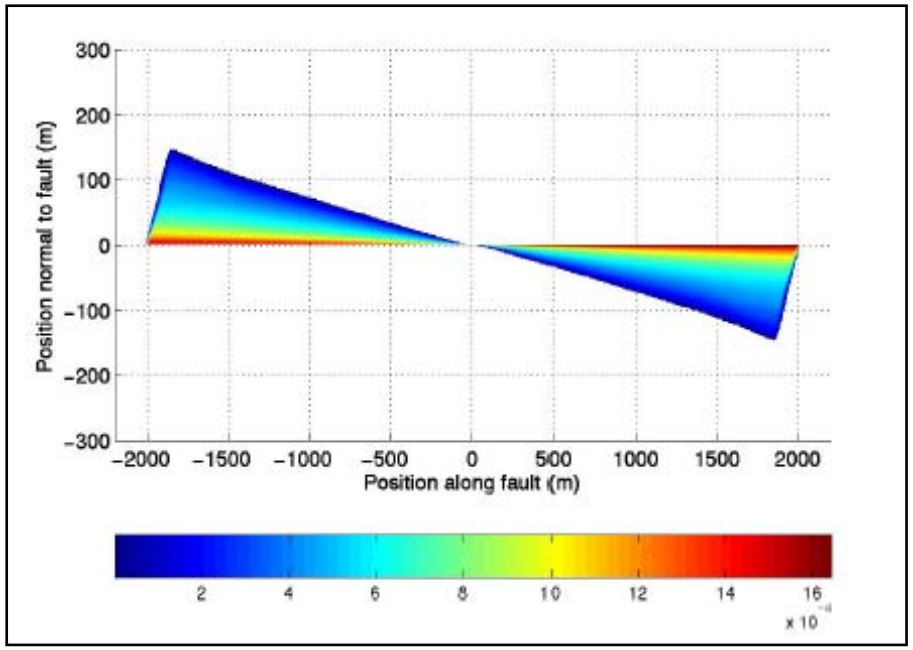

Andrews, 2005

Bimaterial

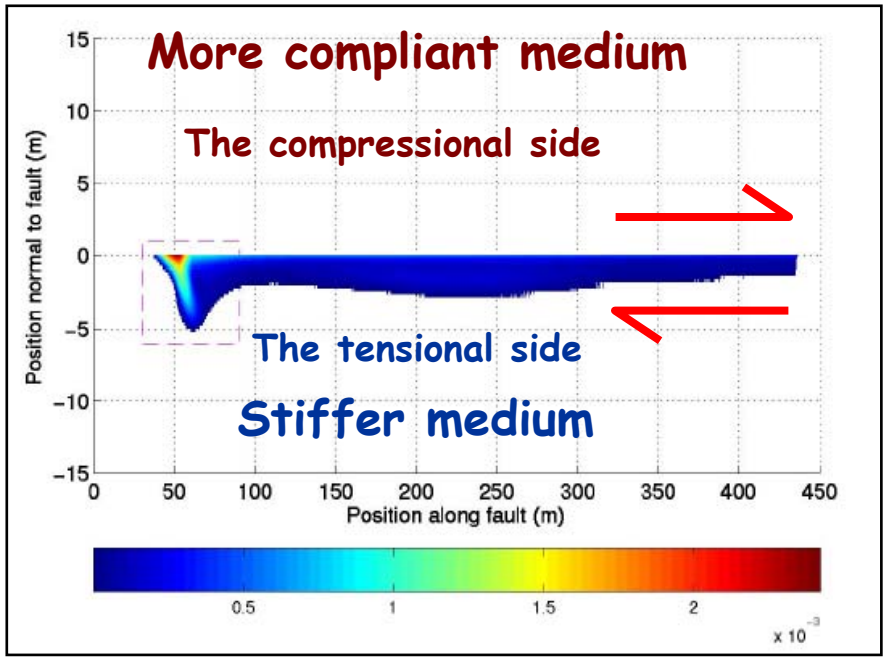

Ben-Zion and Shi, 2005

Analyses of seismic fault zone waves and geological data in several large structures show strongly asymmetric damage zones, as expected for ruptures along a bimaterial interface (Lewis et al. 05, 07; Dor et al. 06, 08; Wechsler et al. 09; Mitchell et al. 11)

SJF near Anza

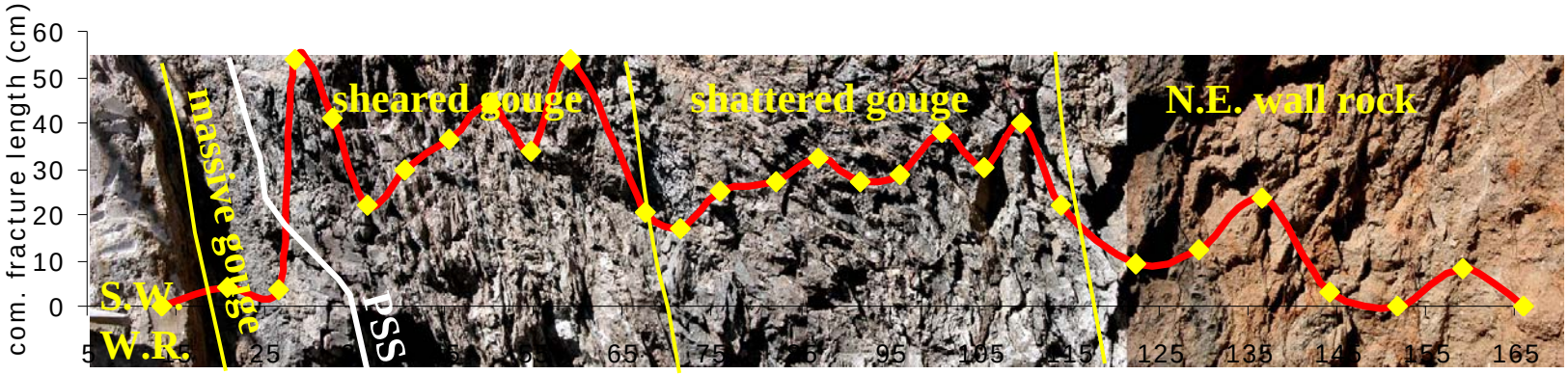

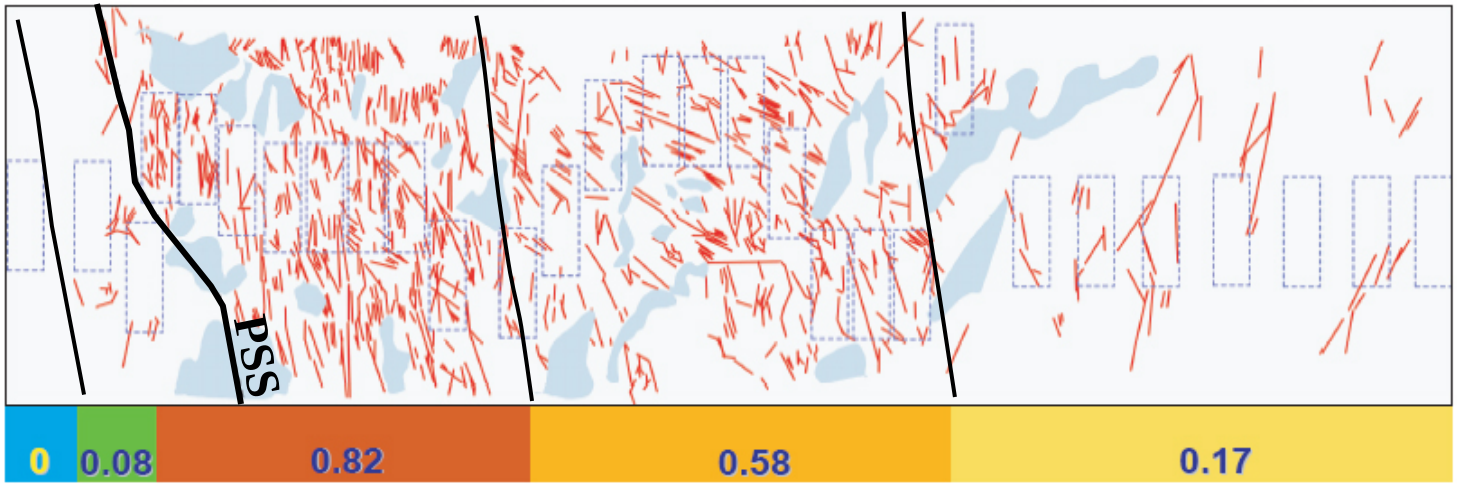

Gouge scale ~1m

Dor et al. (PAGEOPH, 2006)

Pulverized Fault Rocks and Damage Asymmetry along the Arima-Takatsuki Tectonic Line, Japan

Tom Mitchell, Yehuda Ben-Zion and Toshi Shimamoto (EPSL, 2011)

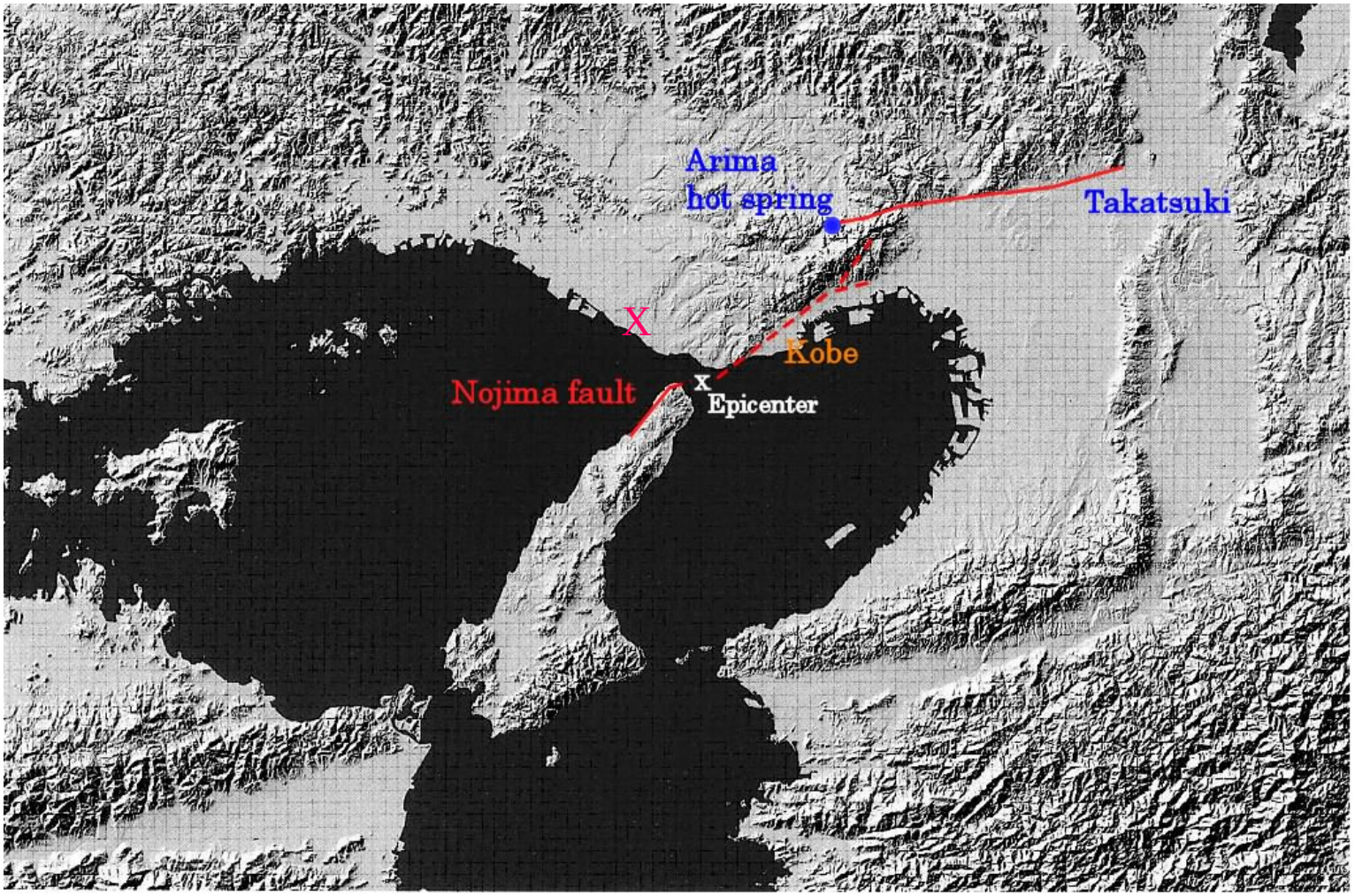

Arima-Takatsuki Tectonic Line

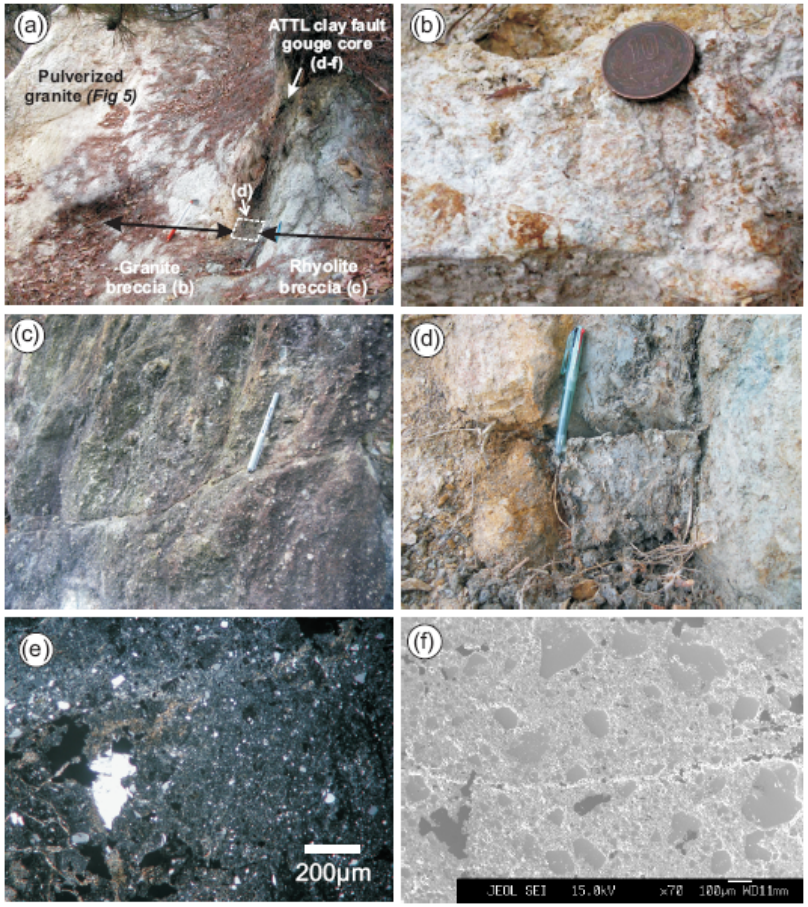

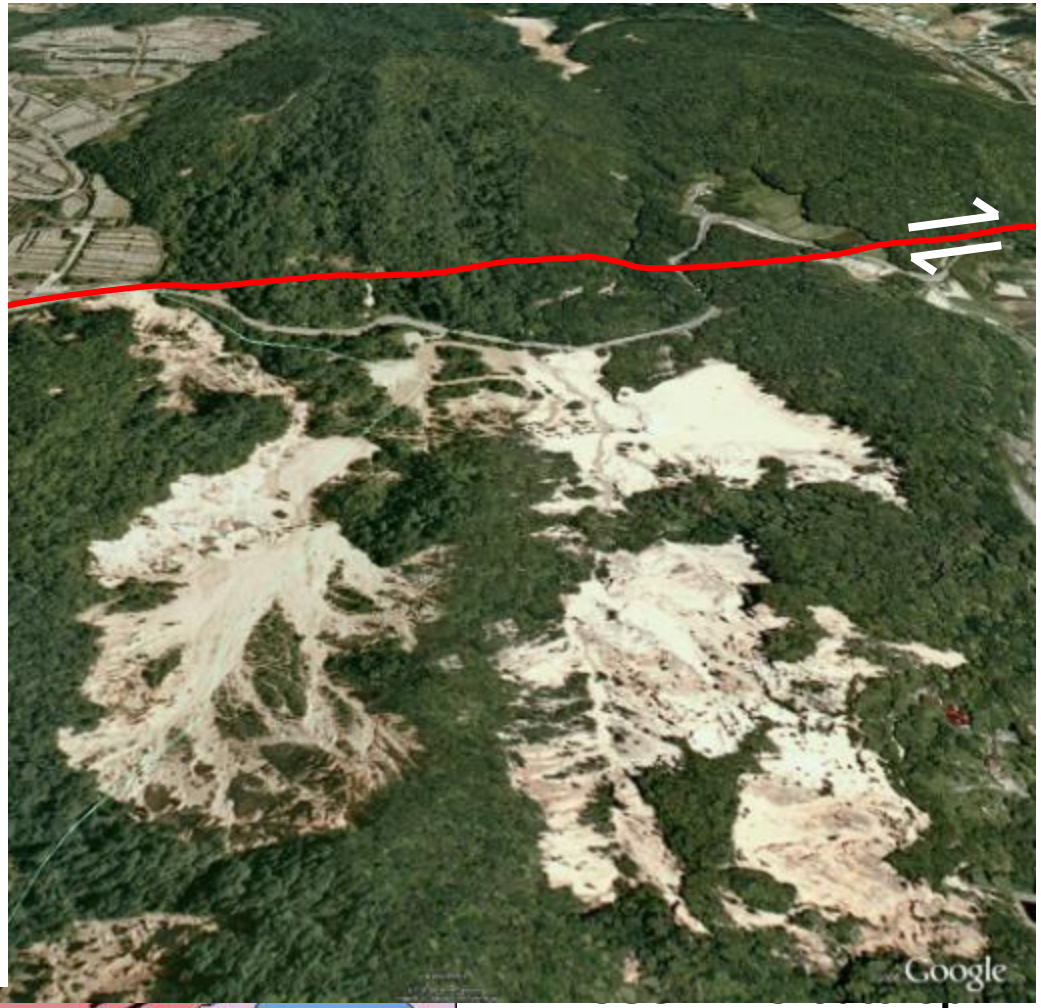

2 km east of Arima hot spring.

after H. Matsuura (graduation thesis).

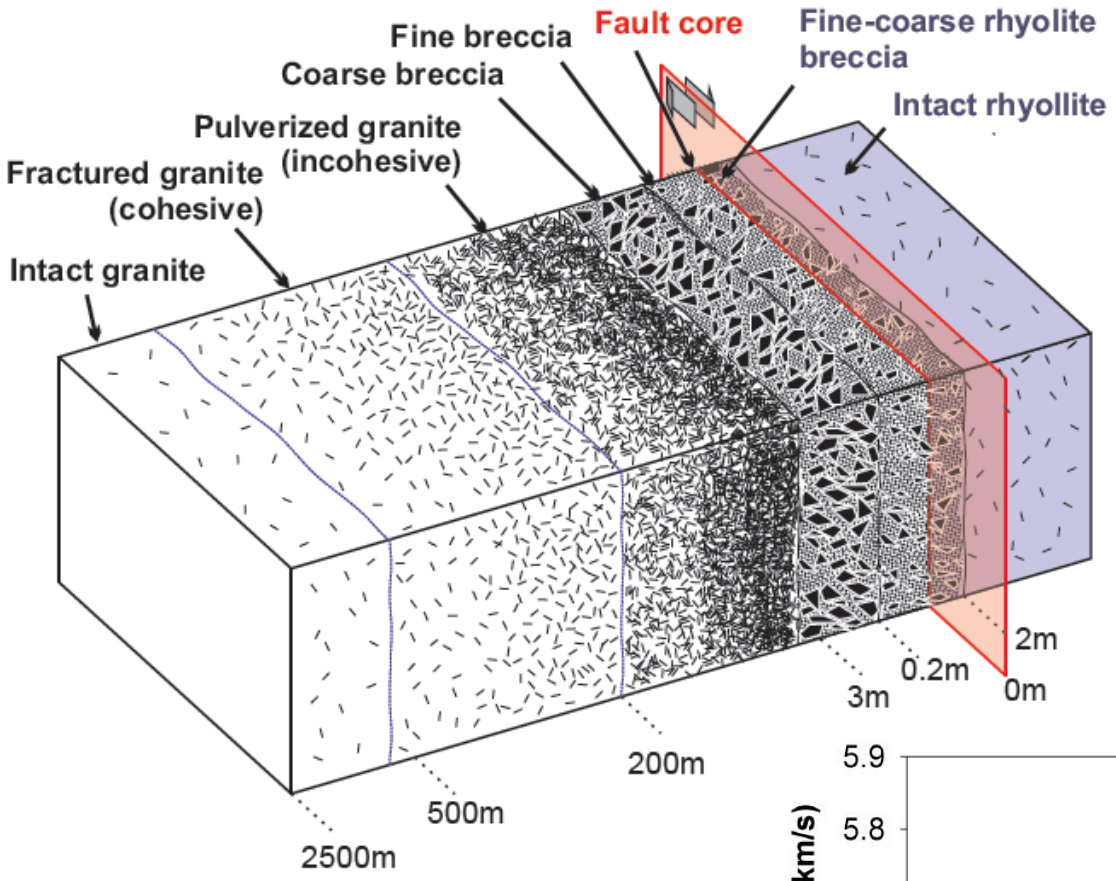

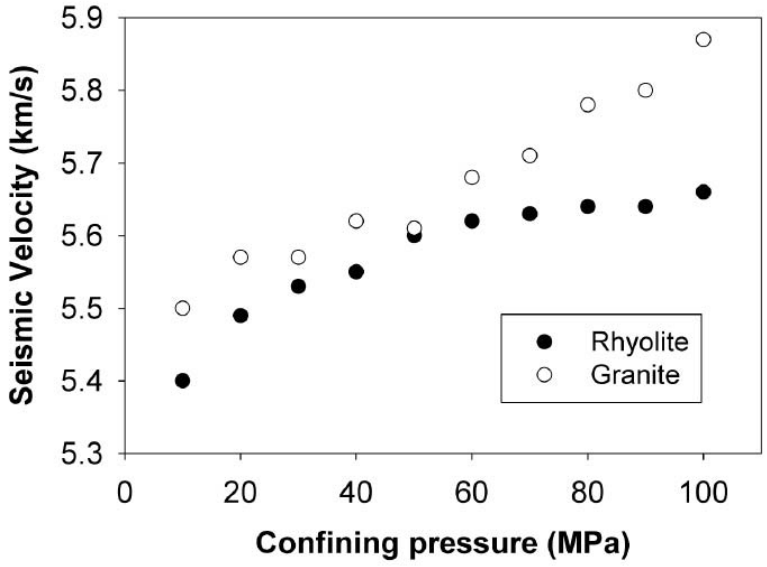

Strongly asymmetric structure

More damage and pulverization on the side with higher seismic velocity at depth

4D analysis of anisotropy and scattering along the Karadere-Duzce branch of the NAF (Peng and Ben-Zion, 2004, 2005, 2006)

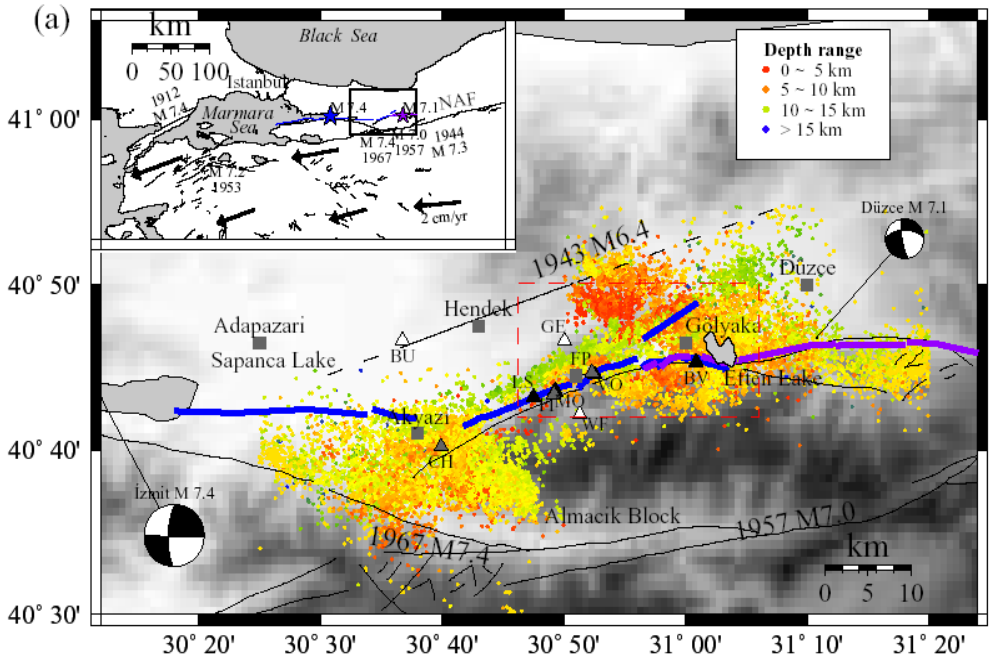

cluster C04, station FP

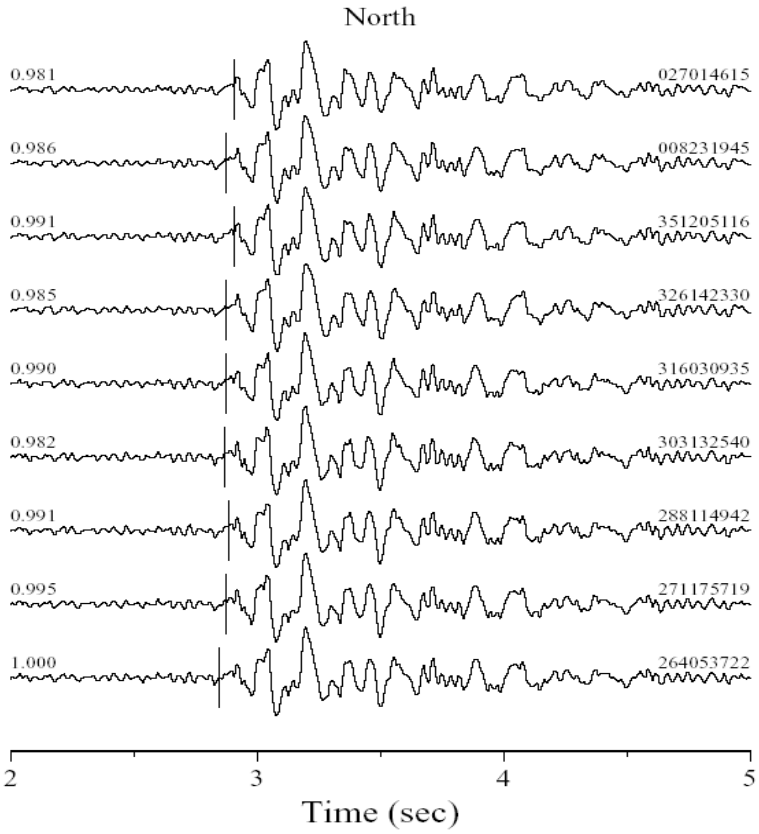

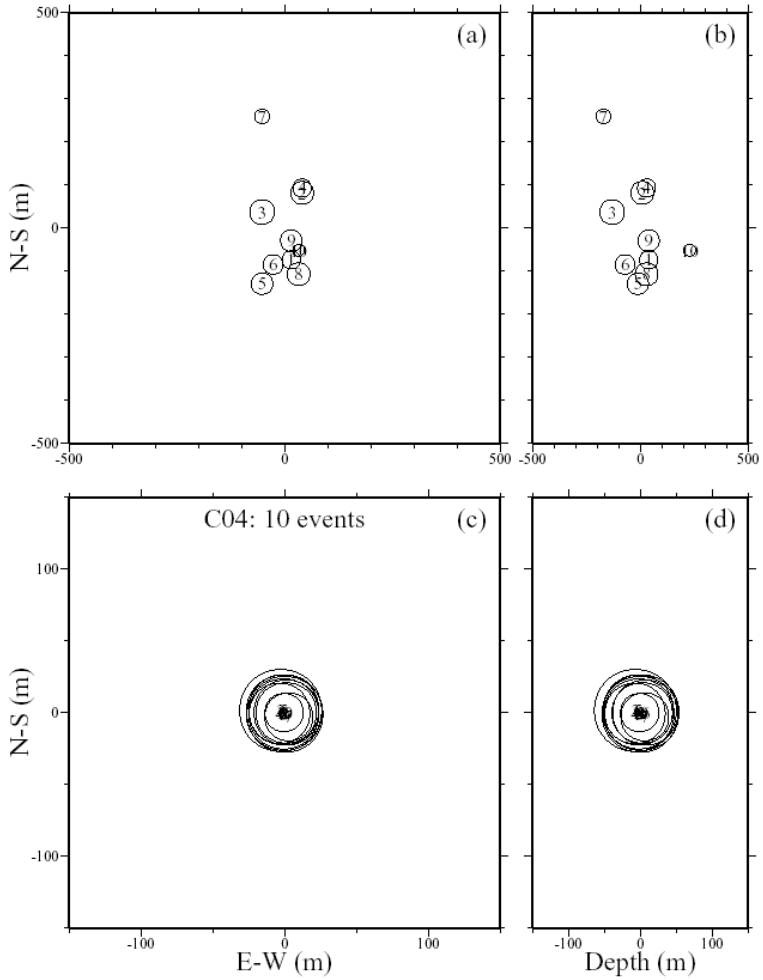

Estimate source areas with

$$r^3 = (7/16)(P_0 / \Delta\varepsilon)$$

$$\log P_0 = 1.00M - 4.72$$

with $\Delta\varepsilon$ = 10^{-4}

Keep only events with at least 50% overlap of rupture area

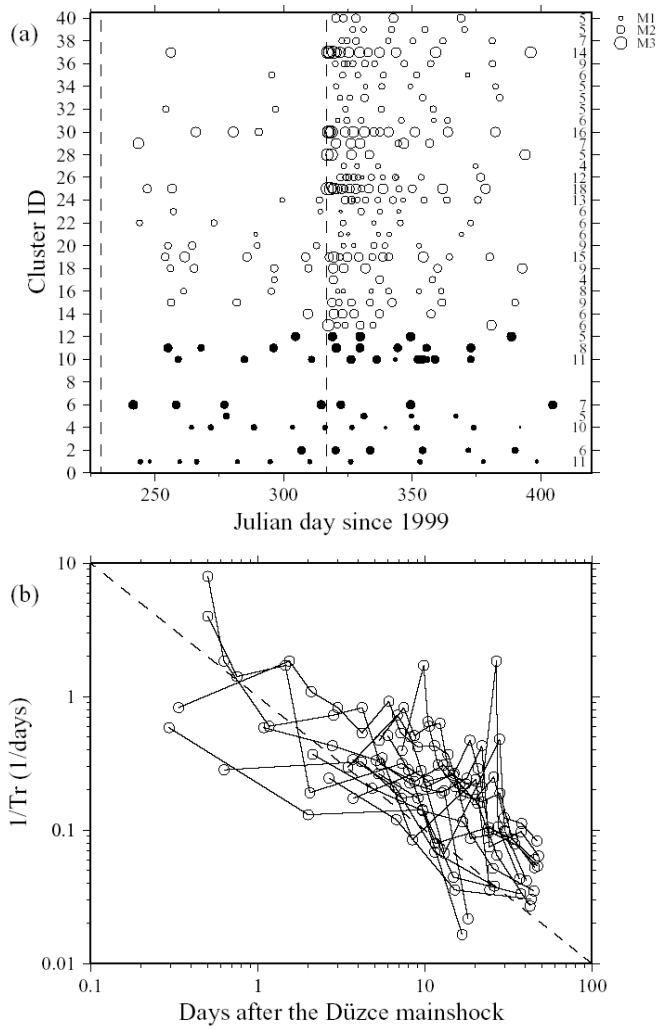

The temporal evolution of events in repeating earthquake clusters follows approximately the Omori law of regional aftershocks

Anisotropy analysis

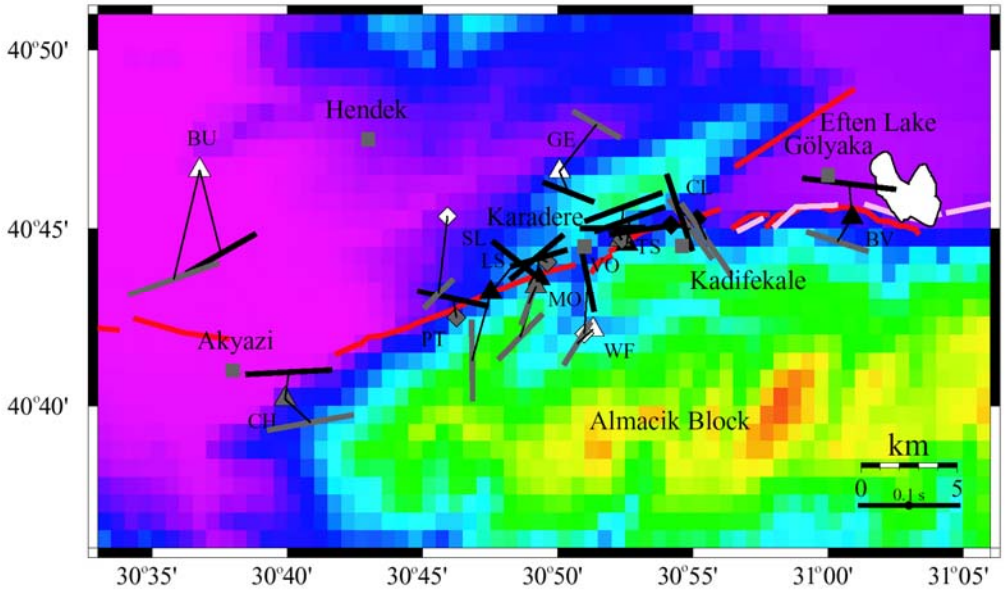

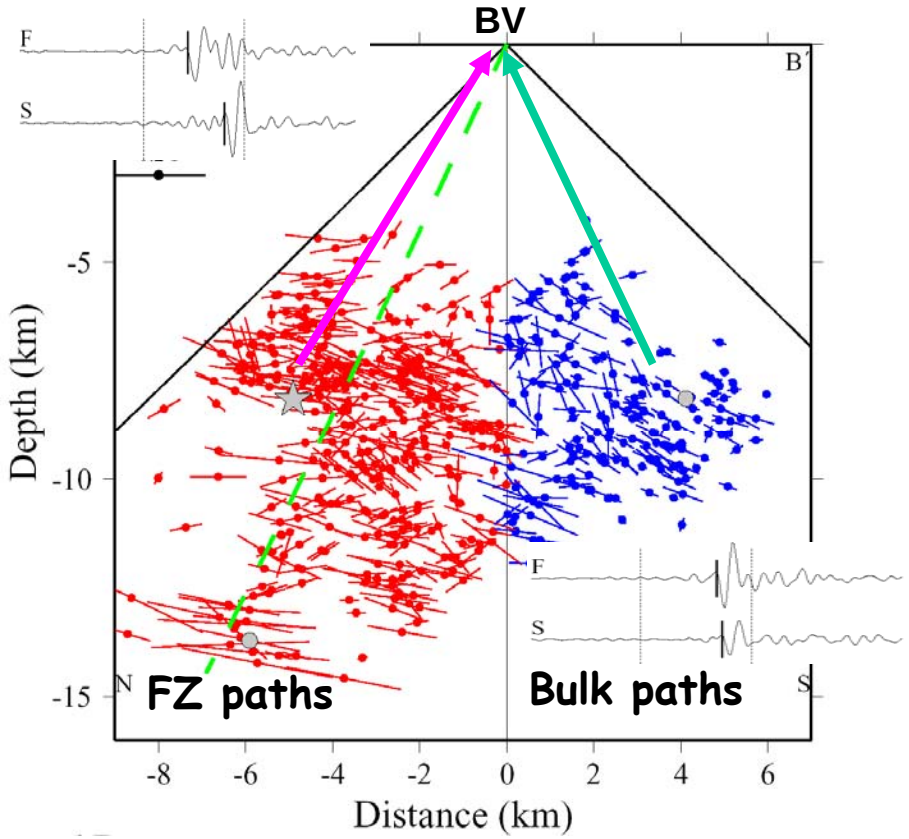

-Construct 2 × 2 covariance matrix from the horizontal seismograms (Silver & Chan 1991). Ideally, eigenvector associated with λ_1 points to initial polarization direction and λ_2 is zero).

-Perform grid search over $\varphi - \delta t$ space (fast polarization direction and time delay) to find solution that minimizes λ_2 and produces most singular covariance matrix and linear particle motion.

Automatic quality determination based on several criteria (e.g. SNR > 3, CCC of fast & slow waves > 0.7, λ_2 < 0.3, SD δt < 0.1 sec).

Analyze further high quality results.

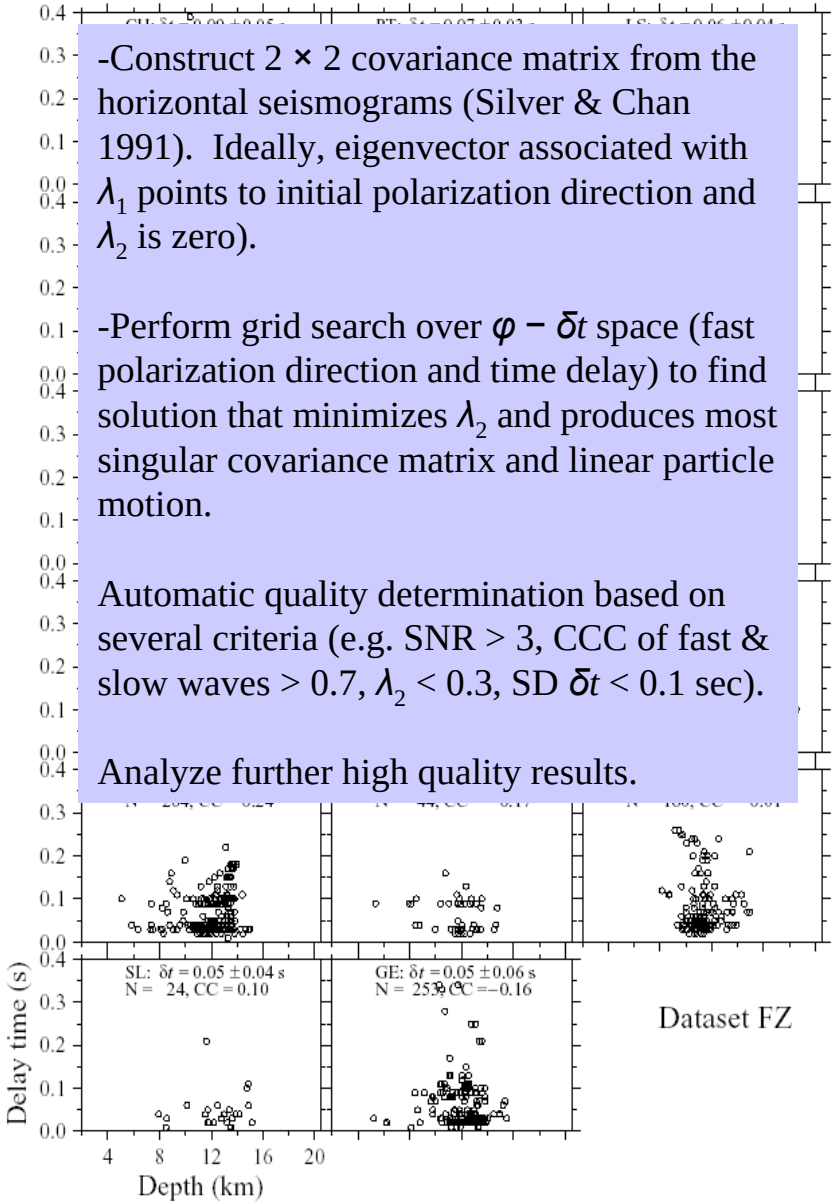

No systematic depth changes

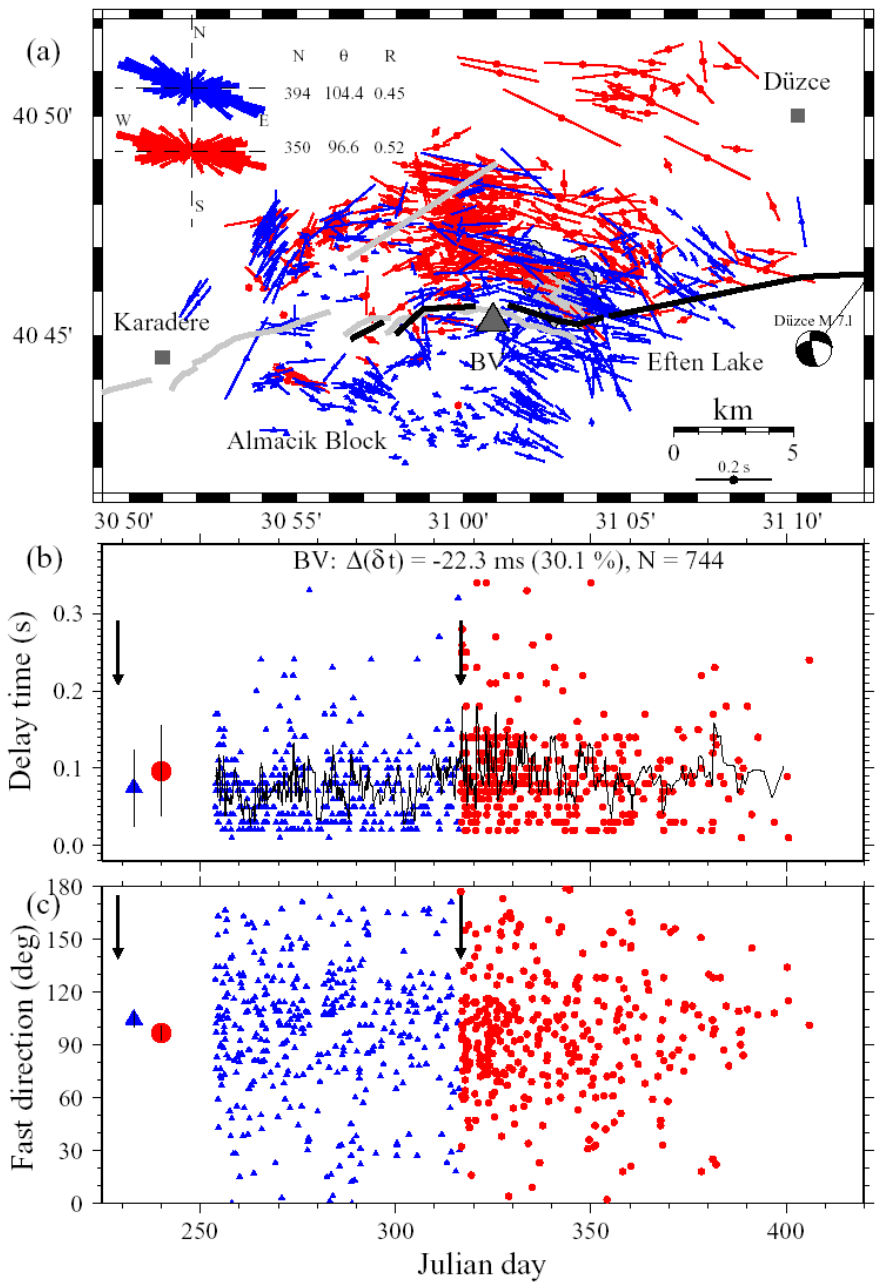

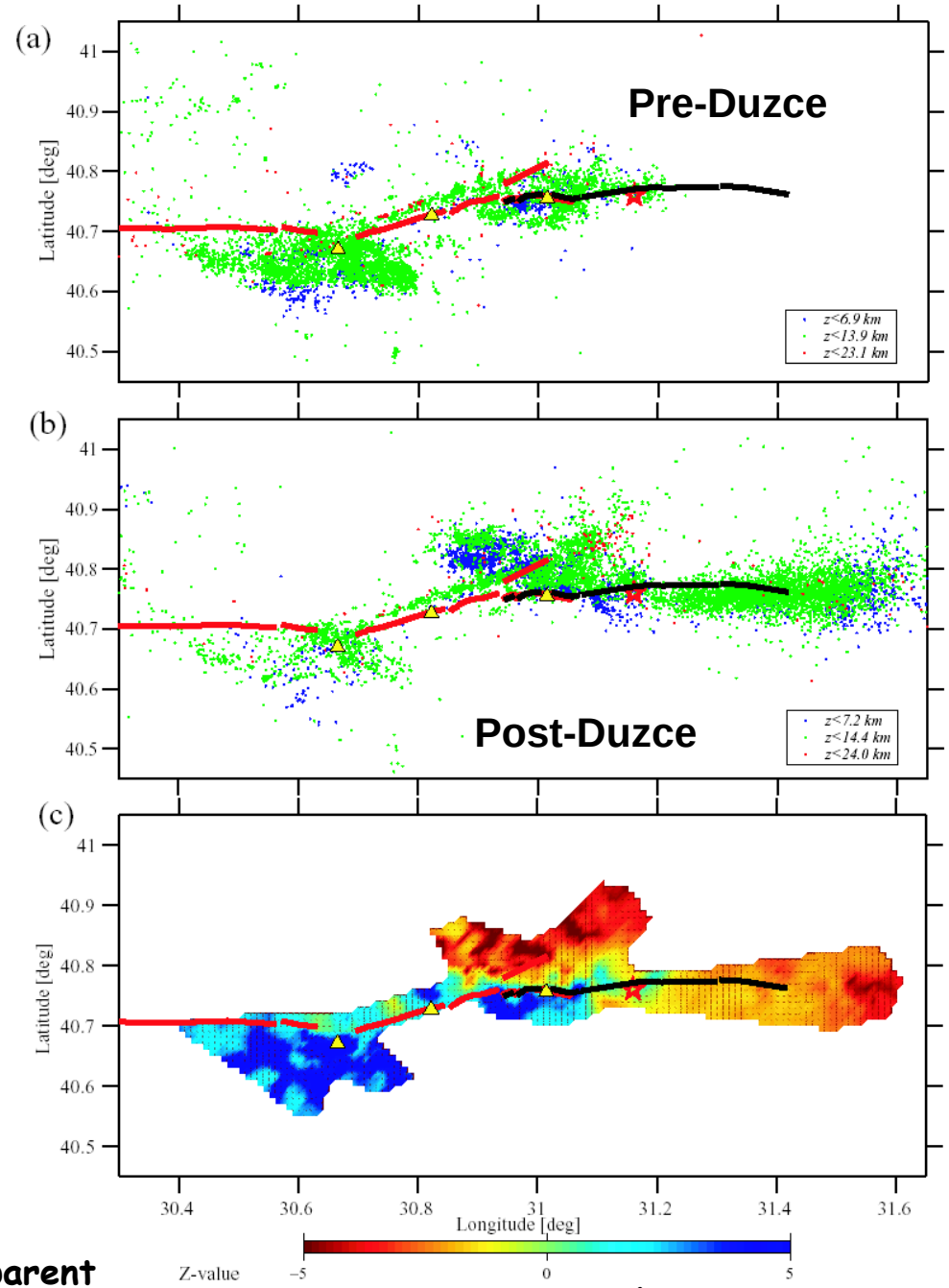

Regular analysis mixing space-time indicates apparent 30% delay time change across the Duzce event

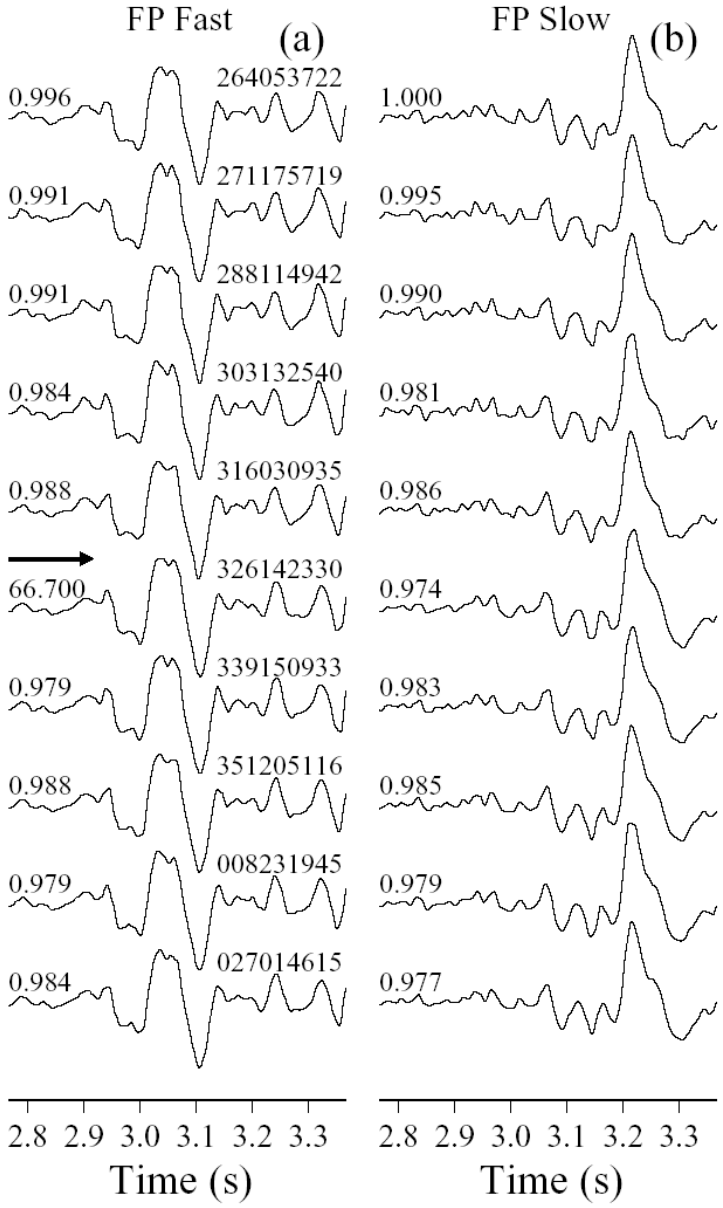

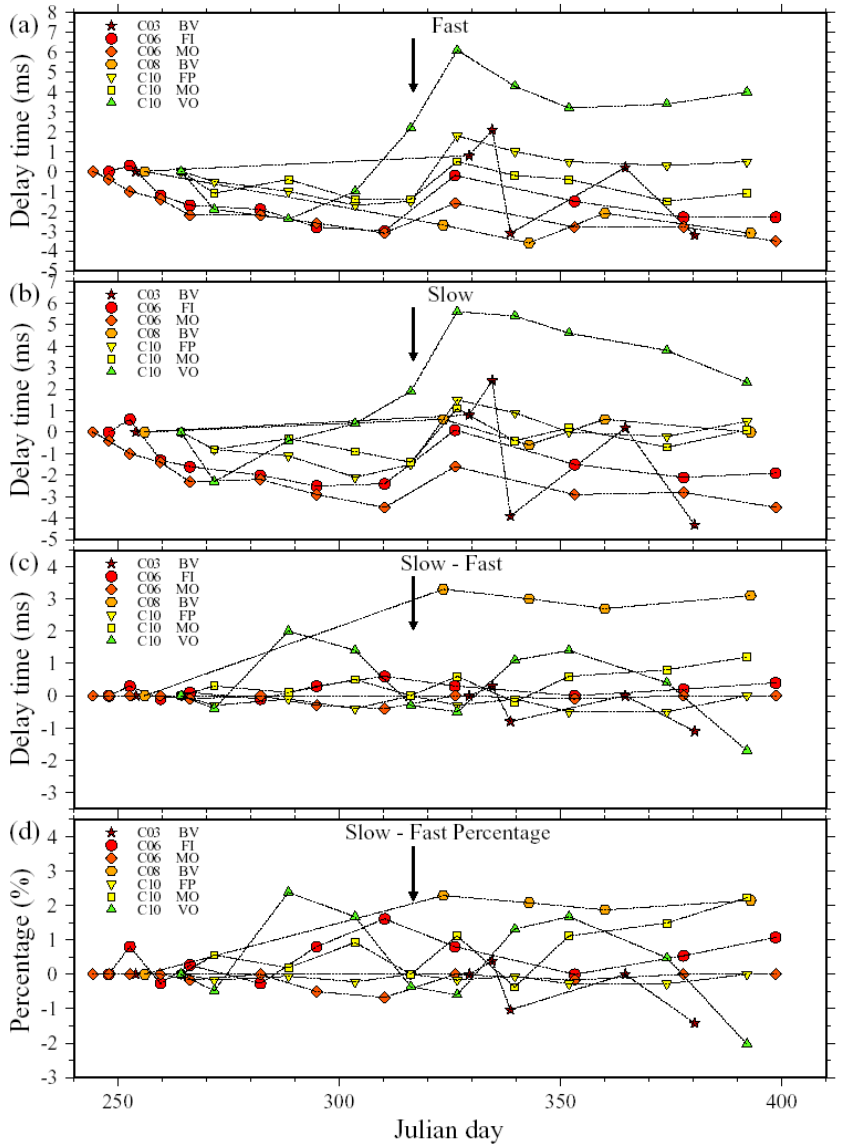

Analysis of repeating earthquakes with similar propagation paths indicates at most 2% co-Duzce mainshock change; no precursory effect

Temporal changes of delay times based on evolving de-correlation analysis

(Peng and Ben-Zion, 2006)

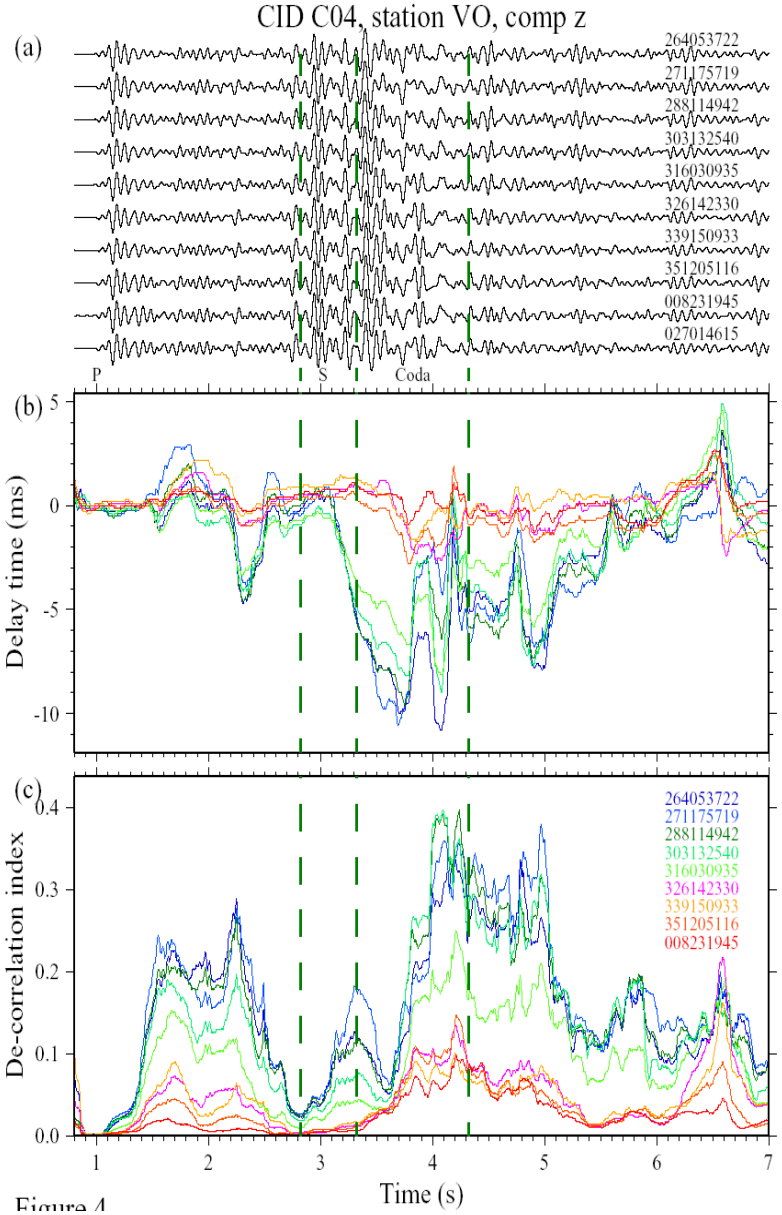

Figure 4

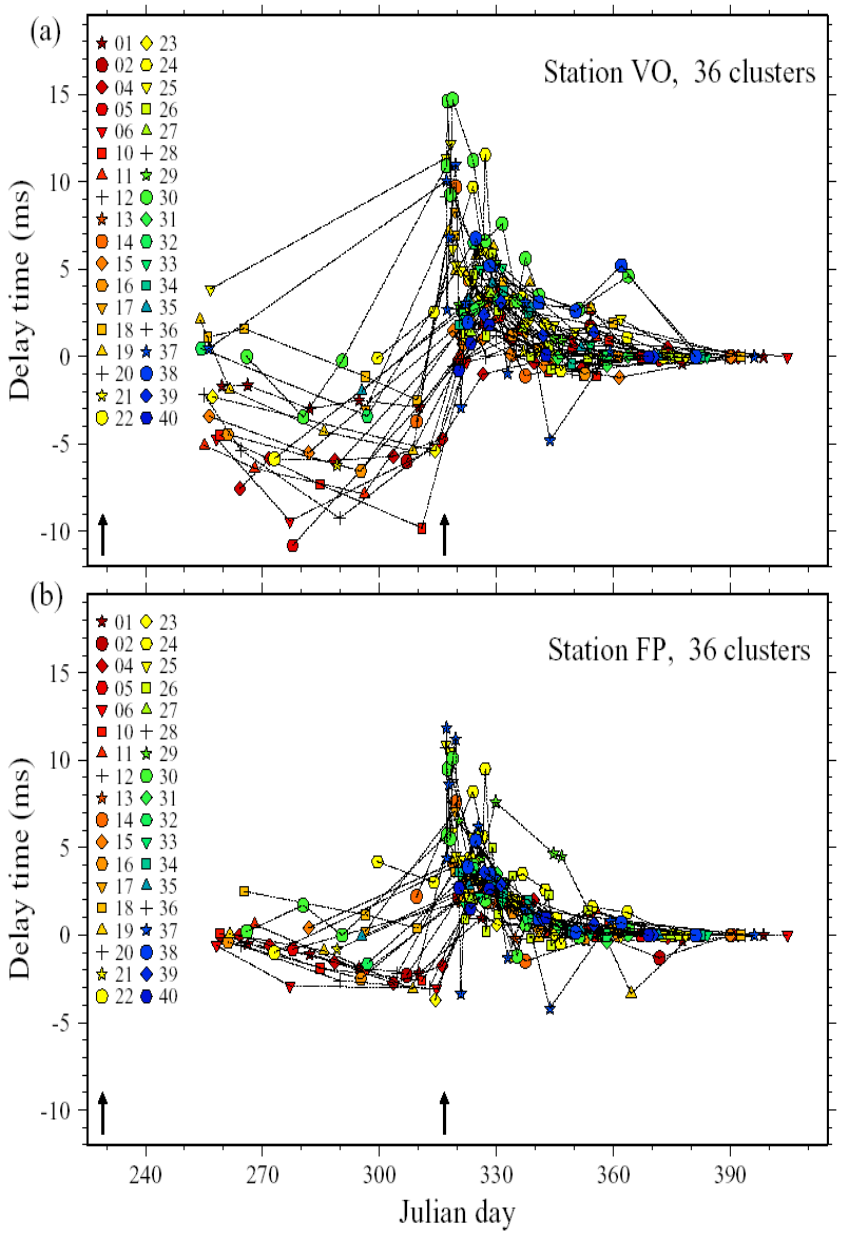

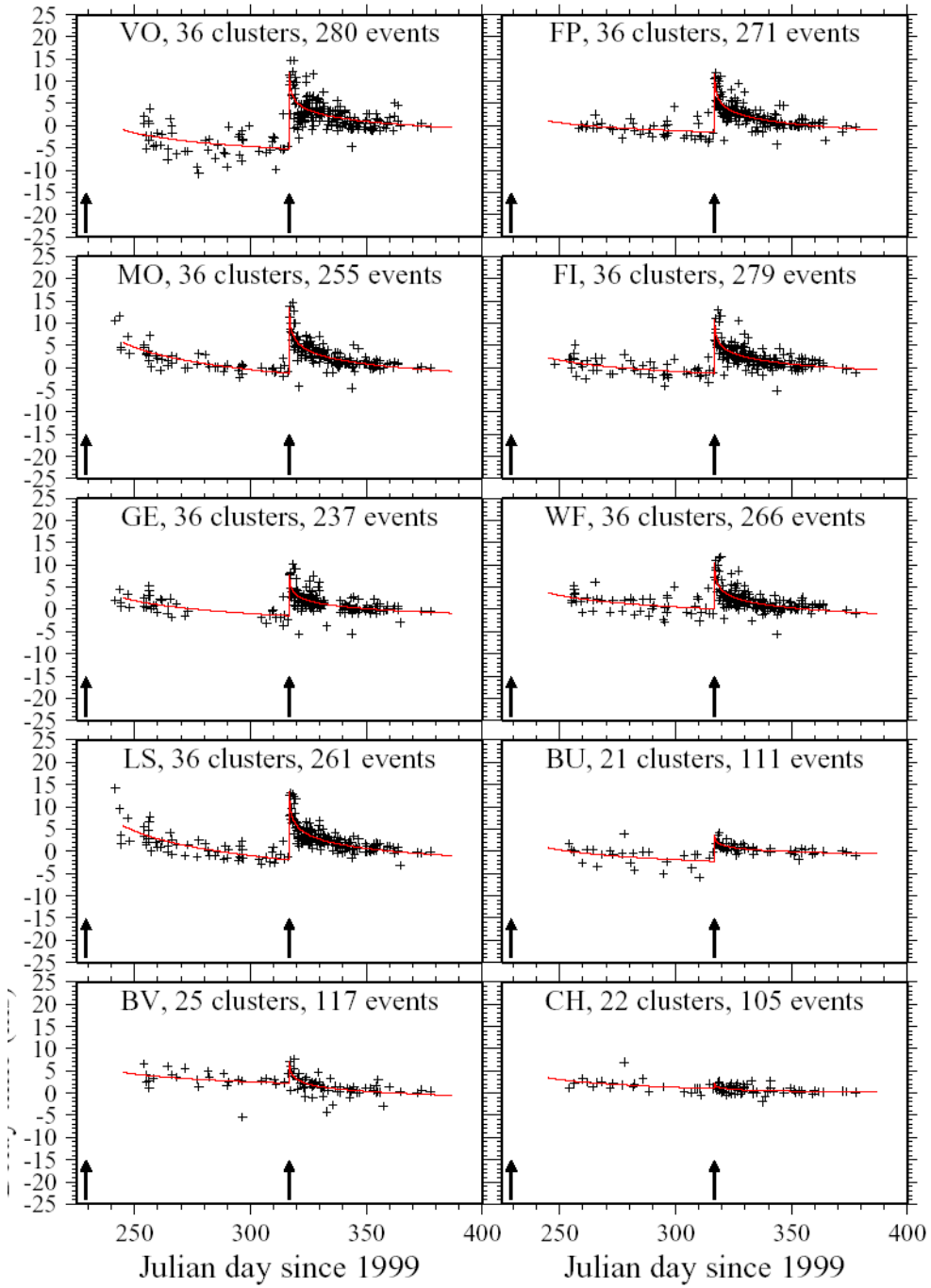

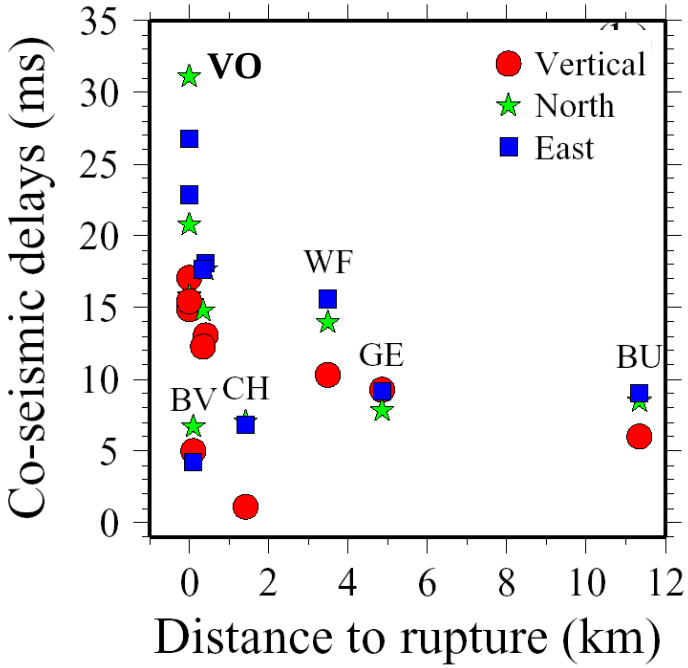

- The changes are strongest in the vicinity of the damaged FZ rock, but exist at all stations and do not change with source location (including depth).

- The effects reflect changes in the top damaged surface layer and shallow FZ damaged rock (e.g., 200-500 m)

- Similar results were obtained by others (e.g., Rubenstein and Beroza, 04, 05) for earthquakes in California and Japan.

Non-linearity and temporal changes of fault zone site response

(Wu, Peng and Ben-Zion, GJI, 2009, 2010)

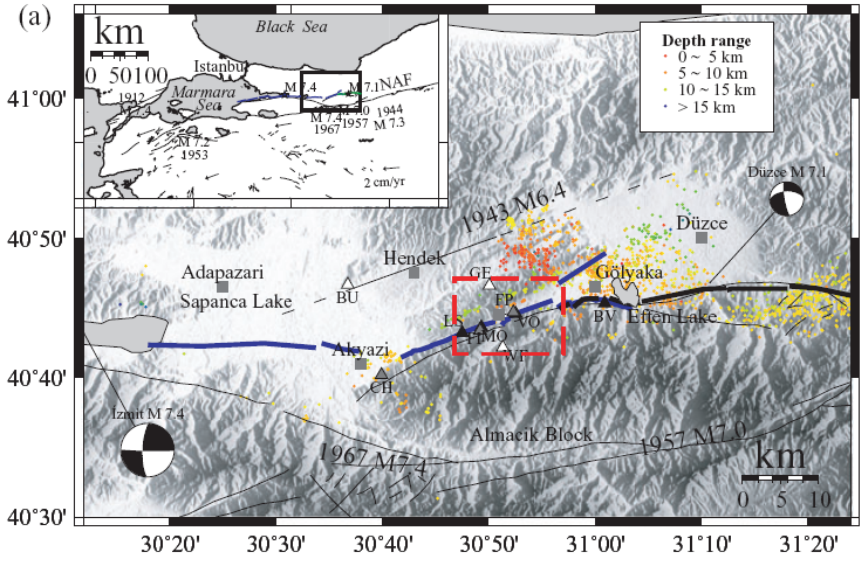

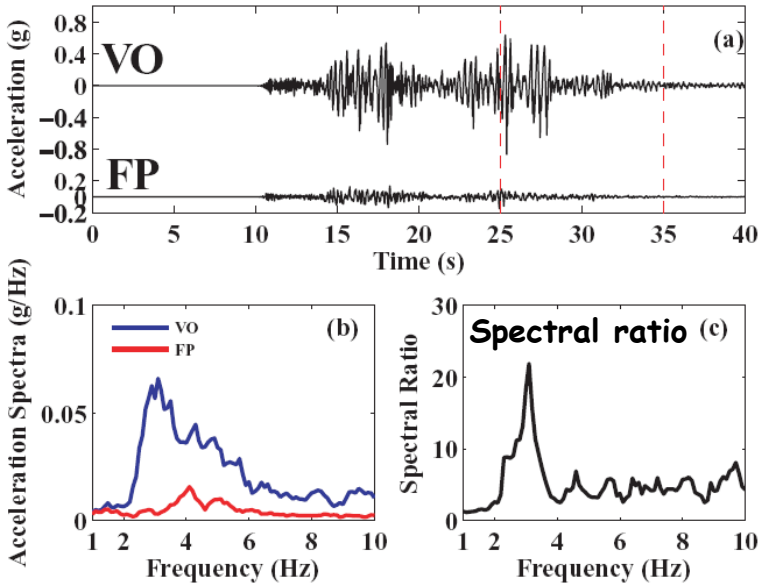

Spectral ratios of 15 events

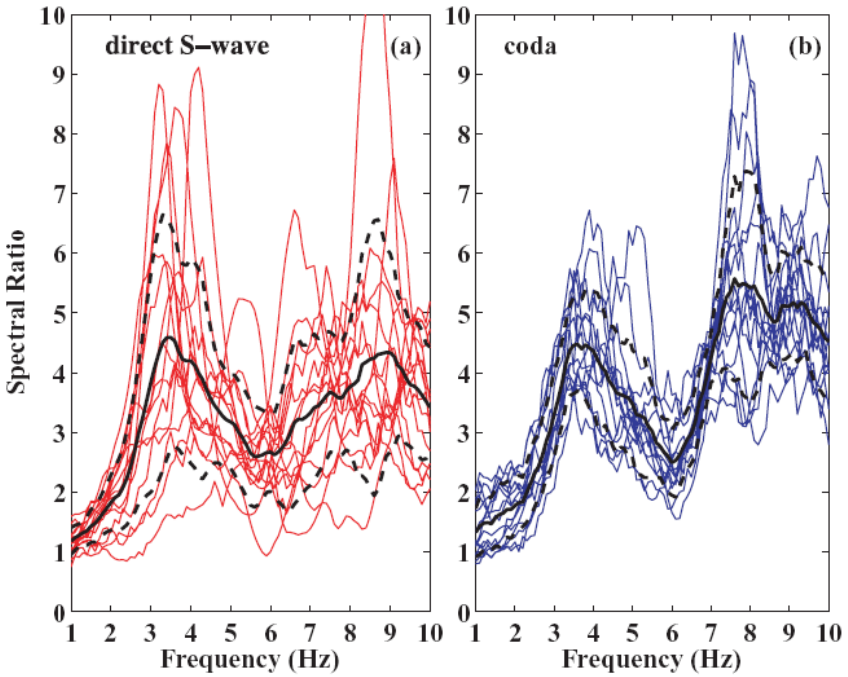

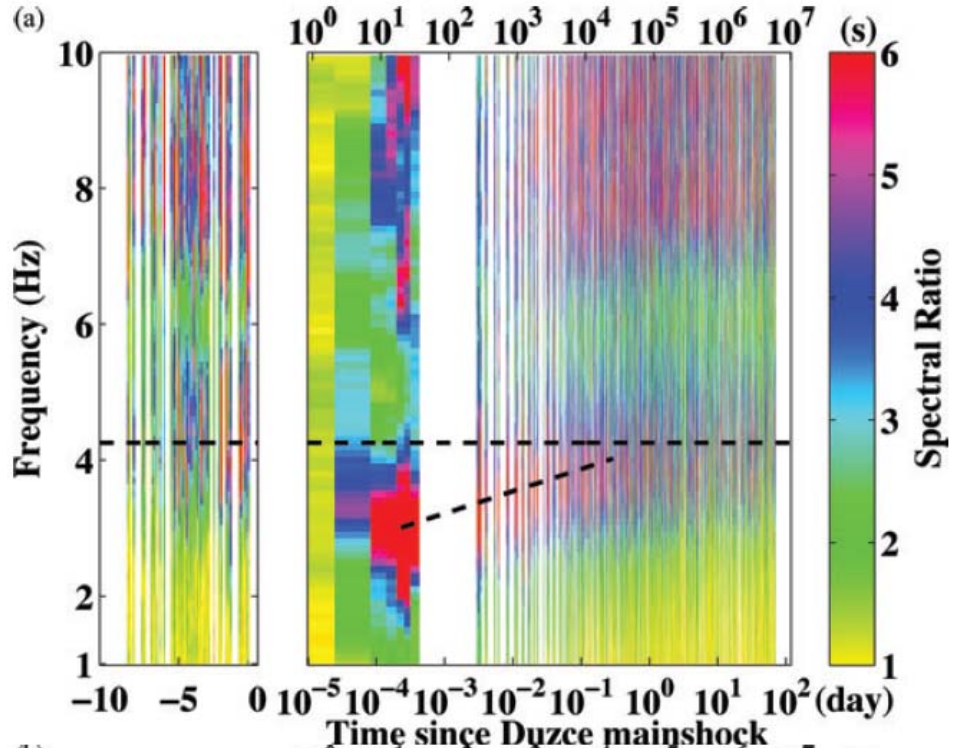

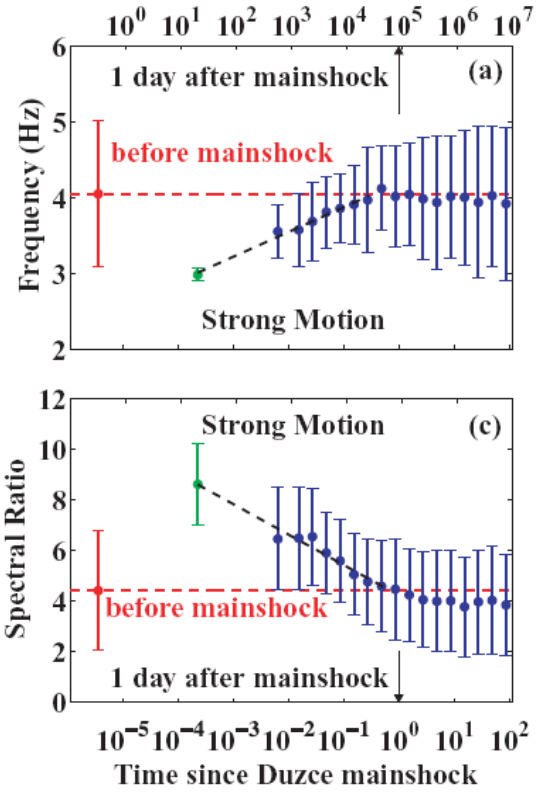

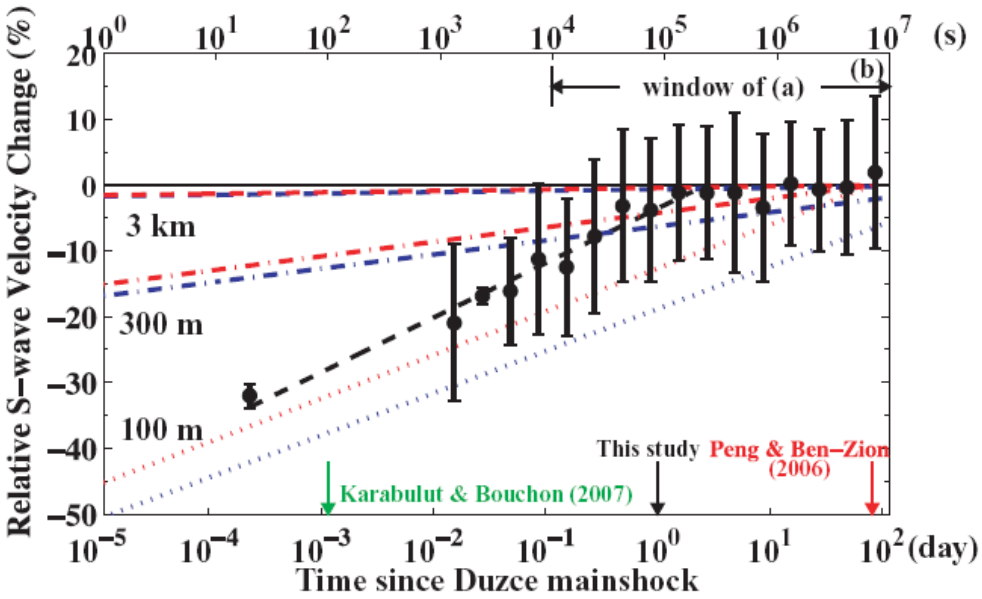

·The results suggest 30-50% S velocity reduction in the top 100-300 m, and logarithmic healing with strong effects over ~1 day but ~3 months or longer duration.

·Similar results were obtained by Karabulut and Bouchon (07), Rubenstein et al. (04, 05, 07), Sawazaki et al. (06, 08), and others for earthquakes in the US and Japan.

Schematic Summary

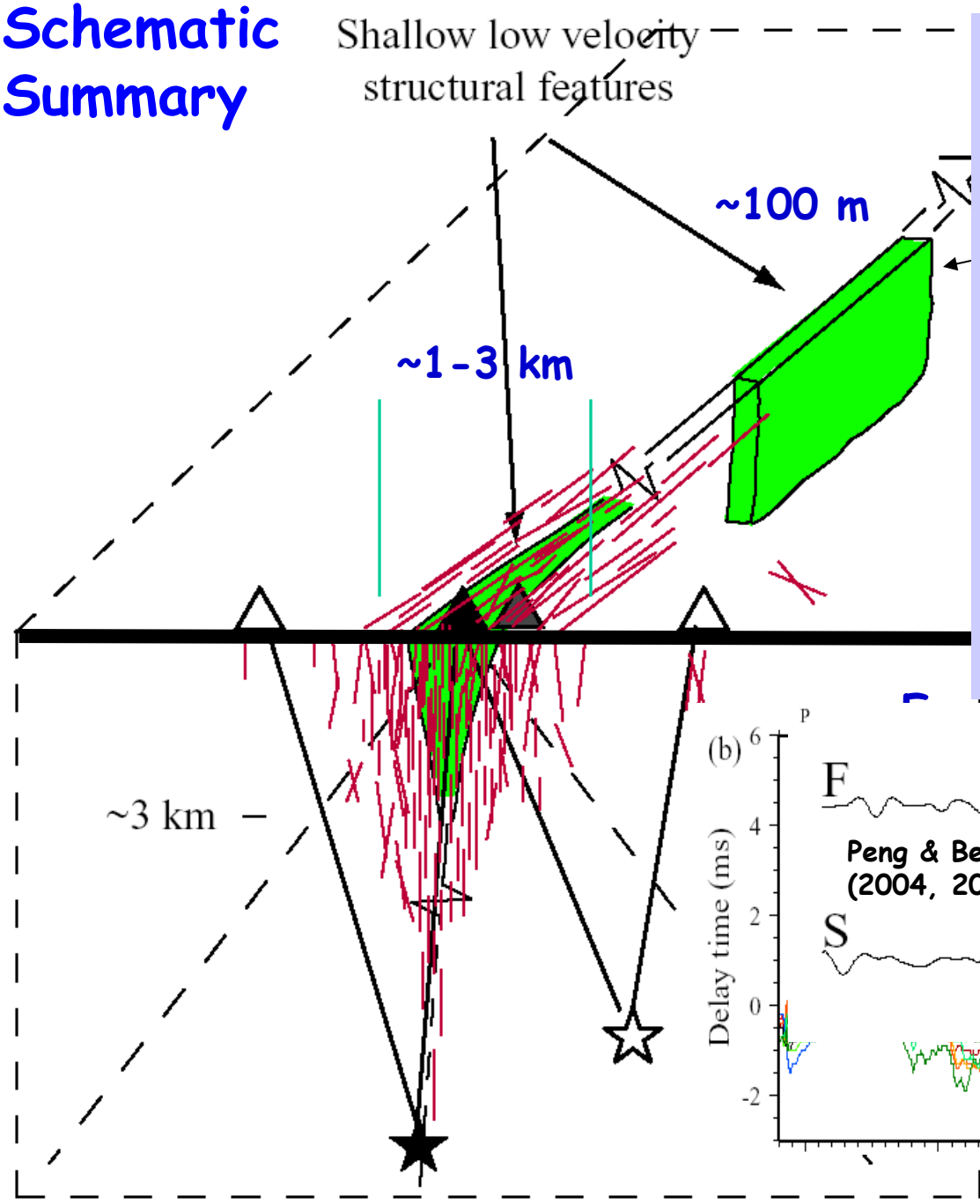

The trapping structures are ~100 m wide, have ~50% reduction of S-wave velocity, extend generally over the top 3 km, and show considerable along-strike variability.

The waveguides are surrounded by broader damage zones, also limited primarily to the top 3 km, producing seismic anisotropy and scattering

Analyses of repeating earthquakes and spectral ratios show strong co-seismic velocity reductions (~30-50% in the fault zone) followed by logarithmic recovery with time.

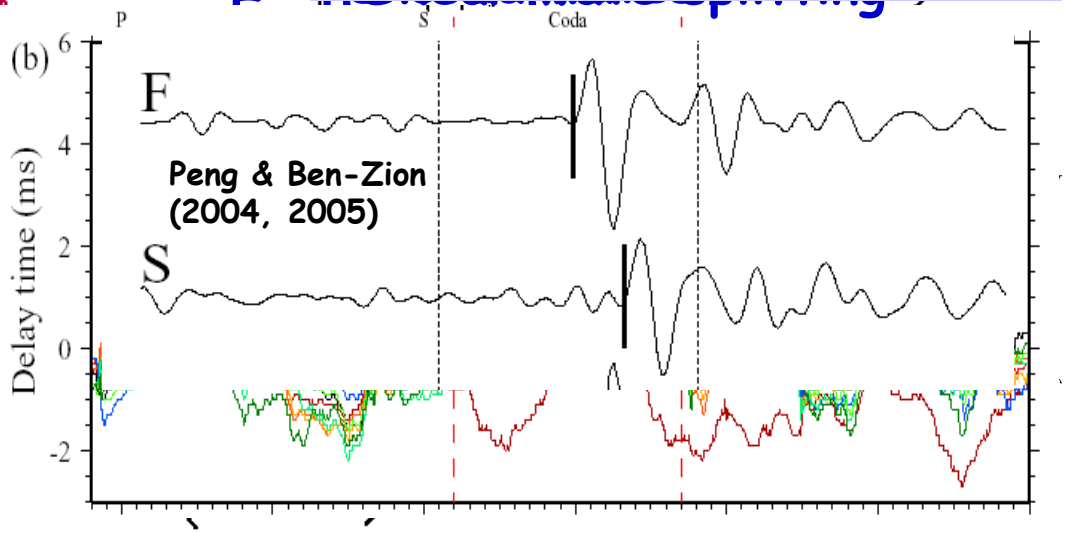

Conclusions

- High resolution imaging of fault zone environments requires using different signals (body waves, head and trapped waves, scattered waves, surface waves, …) and techniques (travel time and waveform tomography, noise correlations, …).
- Earthquake data provide detailed information on the seismogenic sections (depth 3-15 km).
- Ambient noise data provide detailed information on the shallower structure.

- Fault zones have hierarchical flower-type damaged zones and bimaterial interfaces.
- The damage zones have ~100m wide cores with intense damage (e.g. $\Delta\beta$ ~ 30-50%, Q ~ 10-30) that act as seismic trapping structures. They have considerable along-strike variability & discontinuities over length scales of ~5 km and are surrounded by ~3 km zones of lower damage that produce fault-related anisotropy and scattering.
- The bimaterial interfaces extend to the bottom of the seismogenic zone and are continuous over 10s to 100 km.
- The damage zones get re-activated during earthquakes (strong co-seismic velocity reduction of 30-40 % in the top few 100's of m of the crust) followed by log(t) healing.
- The damage zones are often asymmetric w.r.t. the principle slip zone that may reflect preferred propagation direction of earthquake ruptures.

Additional works in progress:

- Correlation of earthquake waveform for high-resolution imaging of the top 500-1000m (with P. Roux)
- Correlation of ambient noise for constructing trapped noise (with G. Hillers, M. Campillo, P. Roux)
- Attenuation imaging (with Xin Liu)
- Receiver function for sub-horizontal structures (with Liu, Schulte-Pelkum, Ozakin, Zignoe, others)
- Adjoint waveform tomography that includes body waves, surface waves, head waves and trapped waves (with Amir Allam and Carl Tape)

Thank you